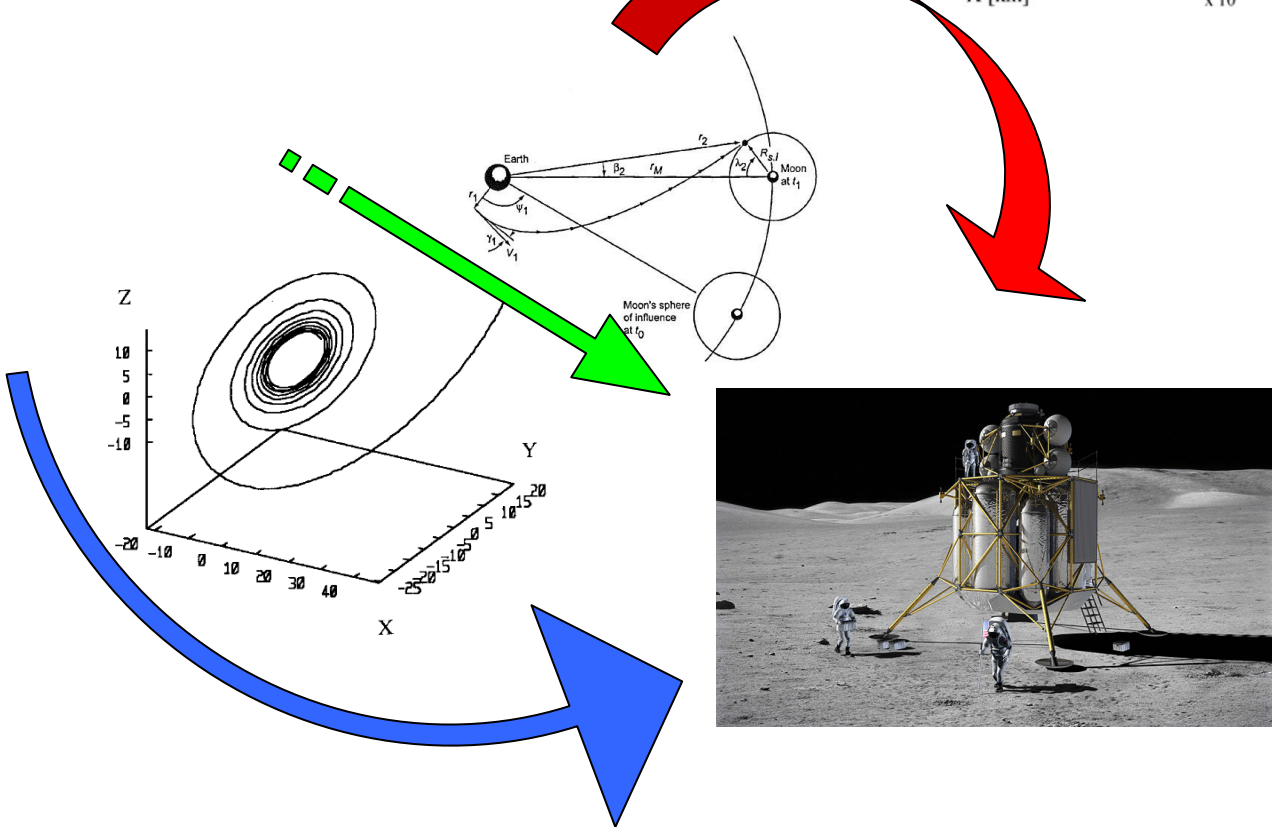
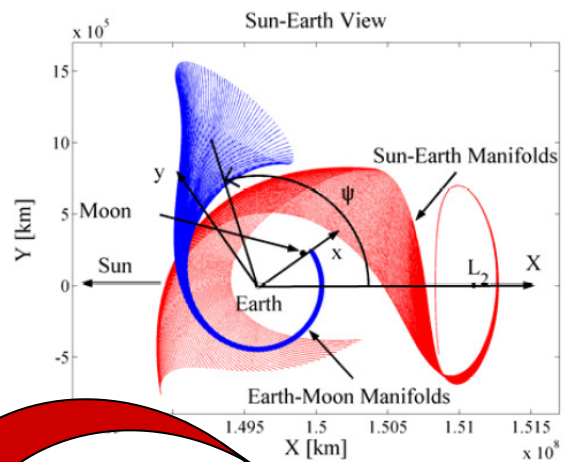


Earth-Moon Transfer Orbits

Master of Science Thesis



Valentino Zuccarelli

December 14, 2009

TU Delft

Earth-Moon Transfer Orbits

Master of Science Thesis

Valentino Zuccarelli

December 14, 2009

Astrodynamic & Satellite Systems
Faculty of Aerospace Engineering
Delft University of Technology
Kluyverweg 1, 2629 HS Delft
The Netherlands



**Astrodynamic &
Satellite systems**

Delft University of Technology
Department of
Astrodynamics and Satellite Systems

Members of the graduation commission:

Head of Department:

prof. ir. B.A.C. Ambrosius
Delft University of Technology

Supervisor:

ir. R. Noomen
Delft University of Technology

Member:

dr. ir. E. Mooij
Delft University of Technology

Member:

dr. ir. S. O. Erb
ESA, ESTEC (TEC-ECM)

PREFACE

In this page, I want to say thanks to many people, that have been next to me helping in the last tough year of my life. Let me do that in their own language.

Il primo pensiero va alla mia famiglia, e come potrebbe non essere per loro. Un profondo grazie va a mio fratello, è grazie a te e al tuo essere stato vicino a mamma, che sono potuto venire qui in Olanda, studiando, lavorando e combattendo per raggiungere i miei traguardi e i miei sogni... il tutto mai da solo, perchè dietro di me avevo voi.

Un affettuoso e immenso grazie va quindi ai miei genitori, che mi hanno sempre su(o)portato e aiutato, ciascuno a suo modo, con il proprio carattere e con i propri mezzi. Un grazie particolare va alla donna più forte che conosca, che mi ha trasmesso la testardaggine e la caparbietà di andare avanti superando ogni difficoltà, grazie mamma.

Then a thanks to my colleagues from the 9th floor, even though I've been rarely there in the last period, but meeting you has been a pleasure.

A thanks to my colleagues of TEC-ECM, I've shared with you four intense months and I'm sure we'll meet there very soon.

Graag wil ik ook mijn begeleider Ron Noomen bedanken, hij heeft mij uitstekend geholpen tijdens mijn afstuderen. Je bent altijd aardig en hulpvaardig geweest, daar wil ik je voor bedanken.

Chcę podziękować mojej dziewczynie Agnieszce. Pracowałem nad pracą magisterską głównie w Twoim domu (w moim trochę też...) i nie mogłem wybrać lepszego miejsca. Na koniec chcę powiedzieć : kocham Cię kochanie moje.

ABSTRACT

This work is part of the ESA-project, that wants a preliminary study about the feasibility of building a permanent base on the south pole of the Moon, before July 1st 2020. Moreover after having completed the building phase, the maintenance has to be guaranteed for at least another ten years during the operational phase. The problem is tackled considering only the orbit design point of view. The Space Trajectory Analysis (STA) software has to be used to perform the entire mission, which is a requirement imposed by ESA.

Actually this is a thesis group work, that has been split in three different parts, one per student: ascent (since the launch until the parking orbit is reached), transfer (until a lunar parking orbit is obtained) and landing phase. In this thesis the central part is investigated.

Since the best transfer orbit has to be found, all the possible options to go from the Earth to the Moon have been studied and analyzed: two-body problem, three-body problem and low-thrust trajectories.

Therefore the Lambert's problem has been tackled by using impulsive manoeuvres and low-accelerations arcs (modelled by the Exposins theory). In both cases a global optimizer has been used to find the best orbit transfer. For these two kinds of trajectories the STA Interplanetary Module and the STA Interplanetary Low-thrust Module have been used respectively.

The third option is represented by heteroclinic manifolds trajectories, able to connect the Sun-Earth and the Earth-Moon 3-body systems. To that purpose the STA 3-Body Module has been developed to compute trajectories exploiting this model. Also in this case a global optimizer has been used to get the best solution.

In all cases the total ΔV has been the objective function. Actually to build a lunar base the most relevant parameter is the payload mass that can be delivered into a lunar orbit per each launch. The TOF has been strongly considered only for the trajectory design of manned missions, and, in case of similar performance, for cargo missions too.

The computations turned out that the Ares V launcher is the only one able to transfer enough mass per launch in order to build the lunar base, and both high-thrust and 3-body trajectories can be selected. Actually 3-body trajectories allow to transfer circa 4 tons more per launch, for this reason they have been widely used for the building phase. Furthermore the Ares V is the only launcher that can accomplish successfully manned missions. In this case only high-thrust trajectories have been considered, since the TOF becomes an important factor to take into account.

Low-acceleration trajectories seemed to be well-promising, but a numerical integration of the trajectory (not included in the STA Interplanetary Low-thrust Module) is required in order to better evaluate this kind of orbit. This was outside the scope of this particular study.

LIST OF ACRONYMS AND ABBREVIATIONS

| | |
|-------|---|
| 2BP | 2-Body Problem |
| 3BM | 3-Body Module |
| 3BP | 3-Body Problem |
| CEV | Crew Exploration Vehicle |
| CR3BP | Circular Restricted 3-Body Problem |
| EDS | Earth Departure Stage |
| EL2 | Lagrange point 2 within the Sun-Earth system |
| EM | Earth-Moon 3-body system |
| ESA | European Space Agency |
| ESAS | Exploration System Architecture Study |
| GA | Genetic Algorithm |
| GUI | Graphical User Interface |
| GTO | Geostationary Transfer Orbit |
| ISS | International Space Station |
| LEO | Low Earth Orbit |
| LOI | Lunar Orbit Insertion |
| LL2 | Lagrange point 2 within the Earth-Moon system |
| LLO | Lunar Low Orbit |
| M | Manned missions |
| NASA | National Aeronautics and Space Administration |
| RAAN | Right Ascension of the Ascending Node |
| RCS | Reaction Control System |
| RF | Reference Frame |
| S/C | Spacecraft |
| SE | Sun-Earth 3-body system |
| STA | Space Trajectory Analysis |
| STK | Satellite Tool Kit |
| TLI | Translunar Injection |
| TOF | Time Of Flight |
| U | Unmanned missions |
| WSB | Weak Stability Boundary |

CONTENTS

| | |
|---|------|
| PREFACE | VII |
| ABSTRACT | IX |
| LIST OF ACRONYMS AND ABBREVIATIONS | XI |
| CONTENTS | XII |
| LIST OF FIGURES | XV |
| LIST OF TABLES | XVII |
| CHAPTER 1 | 1 |
| 1. Introduction | 1 |
| CHAPTER 2 | 4 |
| 2. Moon Mission: Scenario and Logistic Aspects | 4 |
| 2.1 Mission Requirements | 4 |
| 2.2 Mission Scenario | 5 |
| 2.3 Masses Naming Convention | 6 |
| 2.4 Base and Spaceport Architecture | 8 |
| 2.5 Launch Capability | 10 |
| 2.6 Preliminary Launches Sequence | 13 |
| CHAPTER 3 | 16 |
| 3. Earth-Moon Transfer Orbits: Options | 16 |
| 3.1 Transfer Orbits | 16 |
| 3.1.1 High-Thrust Orbits | 16 |
| 3.1.2 3-Body Orbits | 18 |
| 3.1.3 Low-Acceleration Orbits | 19 |
| 3.2 Parking Orbits | 20 |
| 3.2.1 Initial Parking Orbits | 20 |
| 3.2.2 Lunar Parking Orbit | 22 |
| CHAPTER 4 | 24 |
| 4. High-Thrust Trajectories: Theory | 24 |
| 4.1 N-Body Problem | 24 |
| 4.2 2-Body Problem | 25 |
| 4.3 Orbital Coordinates | 26 |
| 4.4 Sphere of Influence | 29 |
| 4.5 Perturbations | 30 |
| 4.6 Manoeuvres | 31 |
| 4.6.1 Change of Inclination | 32 |
| 4.6.2 Change of Altitude | 32 |
| 4.6.3 Combined Change of Inclination and Altitude | 33 |

| | | |
|-----------------------|--|-----------|
| 4.6.4 | "Given" Manoeuvre | 34 |
| 4.6.5 | Tsiolkovsky Law | 35 |
| 4.6.6 | High-Thrust Motor | 35 |
| 4.7 | Lambert's Problem | 35 |
| CHAPTER 5..... | | 37 |
| 5. | High-Thrust Trajectories: Results | 37 |
| 5.1 | STA Interplanetary Module | 37 |
| 5.2 | Launch Window Mode..... | 38 |
| 5.3 | Numerical Targeting Mode | 41 |
| 5.4 | Numerical Simulation Mode | 45 |
| CHAPTER 6..... | | 47 |
| 6. | Three-Body Trajectories: Theory | 47 |
| 6.1 | Introduction to 3BP and 3BM | 47 |
| 6.2 | Mode 1: Trajectory Propagator | 49 |
| 6.2.1 | Circular Restricted 3-Body Problem | 49 |
| 6.2.2 | Reference Frames..... | 49 |
| 6.2.3 | Circular Restricted 3-Body Problem: Equations of Motion..... | 52 |
| 6.2.4 | Jacobi's Integral and Hill's Surfaces..... | 52 |
| 6.2.5 | Mode 1 Implementation | 54 |
| 6.3 | Mode 2: Halo Orbit and Manifolds Computation | 55 |
| 6.3.1 | Numerical Approach for Halo orbits..... | 55 |
| 6.3.2 | Stability of Halo orbits | 57 |
| 6.3.3 | Manifolds | 58 |
| 6.4 | Mode 3: Transfer Orbit Optimization | 59 |
| 6.5 | Mode 4: Earth-Moon Transfer Orbit Theory | 60 |
| 6.5.1 | Heteroclinic Connection..... | 60 |
| 6.5.2 | Technique to Guarantee Heteroclinic Connection | 62 |
| CHAPTER 7..... | | 65 |
| 7. | Three-Body Trajectories: Results..... | 65 |
| 7.1 | 3BM Implementation and Validation..... | 65 |
| 7.2 | Halo orbits computations | 67 |
| 7.3 | Earth-Moon Transfer Orbit | 69 |
| 7.3.1 | Earth Parking Orbit-SE Halo Orbit | 72 |
| 7.3.2 | SE Halo Orbit-Patching Section..... | 75 |
| 7.3.3 | Patching Section-EM Halo Orbit | 75 |
| 7.3.4 | EM Halo Orbit-Lunar Parking Orbit..... | 76 |
| 7.3.5 | Total ΔV and payload delivered..... | 77 |
| 7.4 | Halo orbits for Communication Satellites | 78 |
| CHAPTER 8..... | | 81 |
| 8. | Low-Acceleration Trajectories: Theory | 81 |
| 8.1 | Introduction to low-acceleration trajectories..... | 81 |
| 8.2 | Exposins Theory..... | 82 |
| 8.3 | Low-Thrust Engines | 86 |
| 8.4 | Electric Input Power..... | 87 |

| | |
|--|-----|
| CHAPTER 9..... | 90 |
| 9. Low-Acceleration Trajectories: Results..... | 90 |
| 9.1 STA Interplanetary Low-Thrust Module | 90 |
| 9.2 Simulation A | 92 |
| 9.3 Simulation B..... | 94 |
| 9.4 Simulation C..... | 95 |
| CHAPTER 10..... | 97 |
| 10. Conclusions and Recommendations..... | 97 |
| 10.1 Conclusions | 97 |
| 10.1.1 Definition of the Minimum LEO Mass | 97 |
| 10.1.2 Selection of the Launchers and Trajectories Available..... | 98 |
| 10.1.3 Design of the Launch Sequence for the Building Phase | 100 |
| 10.1.4 Design of the Launch Sequence for the Maintenance Phase | 102 |
| 10.2 Recommendations | 103 |
| REFERENCES..... | 106 |

LIST OF FIGURES

CHAPTER 2

| | |
|--|----|
| <i>Fig 2.1 Luna 16 orbit trajectory [NASA, 2001]</i> | 5 |
| <i>Fig 2.2 ISS [JAXA website, 2009]</i> | 5 |
| <i>Fig 2.3 ATV-ISS rendezvous [EADS Astrium website, 2009]</i> | 6 |
| <i>Fig 2.4 Configuration for the lunar base [Zuccarelli, 2008]</i> | 9 |
| <i>Fig 2.5 Configuration for the spaceport [Zuccarelli, 2008]</i> | 9 |
| <i>Fig 2.6 Ares V assembly [Tallgeorge website, 2009]</i> | 13 |

CHAPTER 3

| | |
|--|----|
| <i>Fig 3.1 Apollo mission details [Univ. of Oregon 2008]</i> | 17 |
| <i>Fig 3.2 Type 1 transfer in Earth-Centered Inertial Coordinates [Loucks et al., 2005]</i> | 17 |
| <i>Fig 3.3 The 3D Shoot the Moon transfer (blue) plotted alongside the stable (green) and unstable (red) manifolds of the EL₂ halo staging orbit and the stable (green) manifold of the LL₂ halo staging orbit [Parker and Lo, 2006]</i> | 18 |
| <i>Fig 3.4 8 SMART-1 osculating 3D-orbit [ESA, 2006]</i> | 20 |
| <i>Fig 3.5 Vega performances for circular orbits [ESA User's Manual, 2006]</i> | 22 |

CHAPTER 4

| | |
|---|----|
| <i>Fig 4.1 n-body problem [Kumar, 2008]</i> | 24 |
| <i>Fig 4.2 Elliptic orbit around the Sun [Relativity Calculator website, 2009a]</i> | 26 |
| <i>Fig 4.3 The orbital elements of a satellite [Wakker, 2007a]</i> | 26 |
| <i>Fig 4.4 Angular momentum components [Wakker, 2007a]</i> | 27 |
| <i>Fig 4.5 Eccentric anomaly [Cornelisse, 1979]</i> | 28 |
| <i>Fig 4.6 Magnitudes of the perturbing forces as function of the distance from the Earth [Wertz, 2001]</i> | 30 |
| <i>Fig 4.7 Change of inclination [after Rocket and Space Technology website, 2009]</i> | 32 |
| <i>Fig 4.8 Hohmann transfer [Wikipedia website, 2009a]</i> | 33 |
| <i>Fig 4.9 Geometry of Lambert's problem</i> | 36 |

CHAPTER 5

| | |
|--|----|
| <i>Fig 5.1 Interplanetary module: LW mode GUI</i> | 39 |
| <i>Fig 5.2 ΔV and TOF functions of two months periods in 2015</i> | 40 |
| <i>Fig 5.3 ΔV and TOF functions of five days periods in January 2015</i> | 41 |
| <i>Fig 5.4 Moon inclination to the Ecliptic [Wikipedia, 2009b]</i> | 42 |
| <i>Fig 5.5 Interplanetary module: TARG mode GUI</i> | 43 |
| <i>Fig 5.6 Earth-Moon high-thrust trajectory screenshot 1</i> | 45 |
| <i>Fig 5.7 Earth-Moon high-thrust trajectory screenshot 2</i> | 46 |

CHAPTER 6

| | |
|--|----|
| <i>Fig 6.1 SOHO trajectory [MSU Polar Phisycs website, 2009]</i> | 48 |
| <i>Fig 6.2 Inertial and rotating reference frames [Wiesel, 1989]</i> | 50 |
| <i>Fig 6.3 First body-centred inertial r.f. (XYZ) and co-rotating r.f. (xyz)</i> | 51 |
| <i>Fig 6.4 Hill's surfaces [Wakker, 2007a]</i> | 53 |
| <i>Fig 6.5 Symmetry with the xz-plane [Russell, 2006]</i> | 59 |

| | |
|--|----|
| <i>Fig 6.6 EL₂ halo orbit and its stable manifold</i> | 61 |
| <i>Fig 6.7 EL₂ halo orbit and its unstable manifold</i> | 61 |
| <i>Fig 6.8 LL₂ halo orbit and its stable manifold</i> | 61 |
| <i>Fig 6.9 LL₂ halo orbit and its unstable manifold</i> | 61 |
| <i>Fig 6.10 The 3D Shoot the Moon transfer plotted alongside the stable and unstable manifolds of the EL2 halo staging orbit and the stable manifold of the LL2 halo staging orbit [Parker and Lo, 2006]</i> | 61 |
| <i>Fig 6.11 Earth-Moon and Sun-Earth reference frames [Howell and Kakoi, 2006]</i> | 63 |
| <i>Fig 6.12 Connection section in the Sun-Earth reference frame [Howell and Kakoi, 2006]</i> | 63 |

CHAPTER 7

| | |
|---|----|
| <i>Fig 7.1 3BM GUI for mode 1</i> | 66 |
| <i>Fig 7.2 SE Az=200,000 km Halo orbit GUI</i> | 69 |
| <i>Fig 7.3 SE Az=200,000 km Halo orbit</i> | 69 |
| <i>Fig 7.4 Relationship between a and SE Az for each EM Az [Howell and Kakoi, 2006]</i> | 70 |
| <i>Fig 7.5 Relationship between b and SE Az for each EM Az [Howell and Kakoi, 2006]</i> | 70 |
| <i>Fig 7.6 Sketch Earth-Moon transfer orbit</i> | 72 |
| <i>Fig 7.7 Leg 1 in the orbital plane</i> | 73 |
| <i>Fig 7.8 Leg 1 change of inclination around the Earth</i> | 74 |
| <i>Fig 7.9 Leg 1 entire trajectory</i> | 74 |
| <i>Fig 7.10 Leg 2-Leg 3 patching point</i> | 75 |
| <i>Fig 7.11 Leg 3 transfer orbit</i> | 76 |
| <i>Fig 7.12 Leg 4 transfer orbit</i> | 77 |
| <i>Fig 7.13 Halo orbit for Earth-Moon communication satellites</i> | 78 |
| <i>Fig 7.14 Entire trajectory for communication satellites</i> | 79 |

CHAPTER 8

| | |
|--|----|
| <i>Fig 8.1 Description of the parameters involved [Vasile et al., 2006]</i> | 83 |
| <i>Fig 8.2 Visualization of all the feasible exponential sinusoids in the classes $S_{1/2}[1, 5, \pi/2, 0]$ and $S_{1/4}[1, 5, \pi/2, 1]$ [Izzo, 2006]</i> | 85 |
| <i>Fig 8.3 SLA on SquareRigger platform [O'Neill, 2007]</i> | 87 |
| <i>Fig 8.4 SquareRigger platform deployment [O'Neill, 2007]</i> | 87 |
| <i>Fig 8.5 SLA deployment on the SquareRigger</i> | 88 |
| <i>Fig 8.6 Entech technology road-map [O'Neill, 2007]</i> | 89 |

CHAPTER 9

| | |
|--|----|
| <i>Fig 9.1 STA Low-Thrust Interplanetary module GUI</i> | 91 |
| <i>Fig 9.2 Simulation A trajectory (2015)</i> | 93 |
| <i>Fig 9.3 Simulation A trajectory (2016)</i> | 93 |
| <i>Fig 9.4 Simulation A trajectory in the geocentric r.f. (2015)</i> | 94 |

CHAPTER 10

| | |
|---|----|
| <i>Fig 10.1 Moon payload mass plot for cargo missions</i> | 94 |
|---|----|

LIST OF TABLES

CHAPTER 2

| | |
|--|----|
| <i>Table 2-A Masses definition summary</i> | 7 |
| <i>Table 2-B Mass breakdown for each module type</i> | 8 |
| <i>Table 2-C Total mass breakdown.....</i> | 10 |
| <i>Table 2-D Mass budget for the Ares V crew and cargo lander [after Donahue et al., 2008] .</i> | 11 |
| <i>Table 2-E Ares V payload</i> | 12 |
| <i>Table 2-F Mass estimation of a S/C launched by Ares V.....</i> | 12 |
| <i>Table 2-G Mass estimation of a S/C launched by other launchers.....</i> | 12 |
| <i>Table 2-H Preliminary launch sequence during building phase</i> | 14 |
| <i>Table 2-I Preliminary launch sequence during maintenance phase.....</i> | 15 |

CHAPTER 3

| | |
|---|----|
| <i>Table 3-A A comparison of three lunar transfer types from a 200-km LEO parking orbit to an orbit temporarily captured by the Moon [Parker and Lo, 2006].....</i> | 19 |
| <i>Table 3-B Summary of launchers and LEO parking orbit [Isakowitz et al., 2004]</i> | 21 |
| <i>Table 3-C Parking orbit around the Moon</i> | 23 |

CHAPTER 4

| | |
|--|----|
| <i>Table 4-A RD-0126E performances [Astronautix, 2008]</i> | 35 |
|--|----|

CHAPTER 5

| | |
|--|----|
| <i>Table 5-A Inputs/outputs and the model/optimizer adopted for each mode</i> | 38 |
| <i>Table 5-B Results LW simulations</i> | 39 |
| <i>Table 5-C Results LW simulation to further reduce the launch window</i> | 40 |
| <i>Table 5-D Optimal departure and arrival Epochs.....</i> | 41 |
| <i>Table 5-E Results TARG simulation.....</i> | 43 |
| <i>Table 5-F ΔV required to correct the initial inclination</i> | 44 |
| <i>Table 5-G Final Moon payload deliver per each launcher</i> | 44 |

CHAPTER 6

| | |
|--|----|
| <i>Table 6-A 3BM functionalities scheme.....</i> | 49 |
| <i>Table 6-B Conversion between adimensional and dimensional quantities.....</i> | 50 |
| <i>Table 6-C Position of the Libration points and bondary value of C for the Earth-Moon system</i> | 54 |

CHAPTER 7

| | |
|---|----|
| <i>Table 7-A Initial conditions and results for test case 1 around L1 point.....</i> | 67 |
| <i>Table 7-B Initial conditions and results for test case 1 around L2 point.....</i> | 67 |
| <i>Table 7-C SE Halo orbits initial conditions.....</i> | 68 |
| <i>Table 7-D EM Halo orbits initial conditions</i> | 68 |
| <i>Table 7-E Initial orbit</i> | 71 |
| <i>Table 7-F Final lunar orbit.....</i> | 72 |
| <i>Table 7-G Total ΔV and mass budget for the Earth-Moon transfer orbit.....</i> | 77 |
| <i>Table 7-H Optimization parameters for the Earth-Moon transfer orbit.....</i> | 77 |
| <i>Table 7-I Halo orbit data for Earth-Moon communication satellites</i> | 78 |

| | |
|---|-----|
| <i>Table 7-K Total ΔV and initial mass (in LEO) for the Earth-Moon communication satellites</i> | 79 |
| CHAPTER 8 | |
| <i>Table 8-A Ranges of typical performances for various types of electrical propulsion systems [Sutton and Biblarz, 2001]</i> | 86 |
| <i>Table 8-B Vx-200 performances</i> | 87 |
| <i>Table 8-C Solar and Laser SLA performances on SquareRigger platform [O'Neill et al., 2006]</i> | 88 |
| CHAPTER 9 | |
| <i>Table 9-A Simulations plan for STA Interplanetary Low-thrust module</i> | 92 |
| <i>Table 9-B Simulation A results</i> | 92 |
| <i>Table 9-C Simulation B results</i> | 94 |
| <i>Table 9-D Simulation C results</i> | 95 |
| CHAPTER 10 | |
| <i>Table 10-A Check on the mass delivered for manned mission</i> | 98 |
| <i>Table 10-B Check on the Moon payload mass delivered for cargo missions</i> | 98 |
| <i>Table 10-C Launchers and trajectories selected depending on the maximum payload</i> | 100 |
| <i>Table 10-D First launch sequence for the building phase (see Table 2-H)</i> | 100 |
| <i>Table 10-E Final launch sequence for the building phase</i> | 101 |
| <i>Table 10-F First launch sequence for the maintenance phase (see Table 2-I)</i> | 102 |
| <i>Table 10-G Final launch sequence for the maintenance phase</i> | 102 |

CHAPTER 1

1. Introduction

At this moment, a new Moon race is already started. In the last years many lunar missions have been designed and developed in U.S., Europe, China and India. Why did the Moon become so important? Mainly the Moon can be viewed as an intermediate step for the Sun system exploration, and because the U.S. want to go to Mars before 2030 [BBC website, 2009], the importance of the Moon in this scenario is quite clear. Moreover the discovery of ice on the Moon South pole [Discovery Science website, 2009] increases the chances to establish there a permanent base, that can be used not only for the Solar system exploration, but also for scientific purposes. Therefore some preliminary studies have to be conducted in order to understand the feasibility and the difficulties of such a project.

For this reason, ESA entrusted a preliminary study to TU Delft in order to evaluate the real feasibility of building a permanent base on the Moon. As requirement of this mission, the base has to be built before July 1st 2020 and then the maintenance for another ten years has to be guaranteed. For this reason the project will have two different parts: in the first part the building phase will be tackled and in the second one the maintenance. For each part the best management of each single mission will be crucial within the launch strategy designed. In the first phase a series of launches will be scheduled in order to build the base in time, while during the maintenance phase, periodic launches will guarantee the base supply.

The project is focused on orbit design aspects. Building and maintaining the base, and optimizing (in terms of fuel consumption and payload) each single mission will be the goals of this thesis work. The use of STA, software under development by ESA, for all trajectory computations is another requirement imposed by ESA [Ortega, 2008].

The entire mission has been split in three different parts, each of them assigned to a different student: ascent, transfer and landing phase. This thesis is focused on the central part of the mission, the transfer phase. Therefore searching for the best solution in order to transfer a spacecraft from the neighbourhood of the Earth into a lunar parking orbit is the main objective of this work.

In an ideal case, the entire mission should have been optimized “at once” by means of a continuous exchange of inputs and outputs between the three participants. This has not been possible, since the three works have not been carried out in parallel. This work is the first one to be completed, therefore some assumptions regarding data of the other two mission arcs

have been done to allow the transfer orbit computations. All these assumptions will be explained during this work.

In order to get the best transfer trajectory, three different options will be explored: high-thrust, invariant manifolds (within the 3BP) and low-acceleration trajectories. For each of them some theoretical aspects will be explained in order to better understand the results obtained and then the results themselves will be provided. Also the respective STA modules used will be briefly introduced. Finally the results will be compared and discussed.

Therefore, to tackle all these aspects, the following structure will be followed:

- Moon Mission: Scenario and Logistic Aspects (Chapter 2)
- Earth-Moon Transfer Orbits: Options (Chapter 3)
- High-Thrust Trajectories: Theory (Chapter 4)
- High-Thrust Trajectories: Results (Chapter 5)
- Three-Body Trajectories: Theory (Chapter 6)
- Three-Body Trajectories: Results (Chapter 7)
- Low-Acceleration Trajectories: Theory (Chapter 8)
- Low-Acceleration Trajectories: Results (Chapter 9)
- Conclusions and Recommendations (Chapter 10)

In Chapter 2, some practical aspects about the base are tackled. All requirements of the base are shown and explained along with the architecture designed. Then an estimation of the total payload mass follows. Thereafter a first preliminary launch sequence is provided. Actually this is one of the purposes of this work: providing a launch sequence specifying what kind of trajectory has to be followed by each mission.

Then in Chapter 3, an overview about the three different techniques is given and the inputs of this work are listed. Since a transfer orbit from the Earth to the Moon has to be found, Earth and lunar parking orbits as well as the launchers to use should be known. In this part those assumptions already mentioned about the other two mission arcs will be explained.

In Chapter 4, the theory about high-thrust trajectories is tackled. The 2BP will be explained, as well as all the impulsive manoeuvres used during this work. Some coordinates transformations will be addressed here. Finally a high-thrust motor will be selected.

Thereafter the results for high-thrust trajectories will be presented and discussed (Chapter 5). In this section the STA Interplanetary Module will be presented and all the main functionalities will be explained along with all the inputs and outputs for each computation.

In Chapter 6, the 3BP will be introduced and thoroughly explained. Important information will be provided about Halo orbits and manifolds trajectories, since they will be widely used in Chapters 6 and 7. Since this part was not covered by any STA module, a new STA module, called the 3-Body Module (3BM) has been developed during the internship at ESA-ESTEC. Therefore also some algorithms used in the 3BM are addressed here.

In Chapter 7, the 3BM is presented and all the main features are shown. Also the validation process for the 3BM will be briefly mentioned. Then all the results, regarding Halo orbits and transfer trajectories, obtained with the 3BM, are collected and discussed here.

Thereafter the theory behind the low-acceleration trajectories will be briefly explained. Mainly the exposins theory will be tackled. Furthermore some technical information will be given about the low-acceleration engine used for computations and its power supply.

In Chapter 9, all the results regarding the low-acceleration trajectories are given. The STA Interplanetary Low-Thrust Module will be briefly introduced and then used to get the results for this kind of trajectory.

In the final chapter, all results will be summarized and then discussed to design a launch sequence to build the Moon base. Then another launch sequence will be designed for the maintenance phase of the base. For each mission of the two phases, the best transfer trajectory will be selected.

Finally some recommendations for further studies will be given, in order to help those who want to continue this work, trying to improve the results already obtained.

CHAPTER 2

2. Moon Mission: Scenario and Logistic Aspects

In this chapter, many practical problems of the Moon base will be discussed:

- Mission requirements
- Mission scenario
- Masses definition
- Base and spaceport architectures
- Preliminary launches schedule

This chapter is written by the three authors that are designing this lunar mission for ESA. Some decisions were already made during the literature study and can be found in [Zuccarelli, 2008].

2.1 Mission Requirements

In this first paragraph, all requirements imposed by ESA [Ortega, 2008], that have to be matched in this project, are listed:

- The exercise shall focus on trajectories and trajectory optimization with the aim of designing, building, and operating a permanent base on the South Pole of the Moon.
- The mission base shall be in place and commissioned before 1 July 2020.
- The entire mission shall be divided in two phases:
 - Building the base
 - Operating and maintaining the base (for 10 years)
- Permanent telescope of 1m diameter Newton type.
- Communications equipment to reach 3 Earth ground stations separated 120 deg each.
- Human base shelter for a minimum of 3 astronauts.
- Mobility means to displace a crew of 2 for 15 km around the base.
- Spaceport for landing and launchers.

2.2 Mission Scenario

There are several possible trajectories that can be used to travel from the Earth to the Moon. Many of these so-called mission scenarios were listed in [Zuccarelli, 2008] and only four of them were selected as feasible. These mission scenarios will all have to be considered in the design of a mission to build a base on the South Pole of the Moon. In this section, a brief overview of these mission scenarios will be given. The final choice will be based on the results given by simulations performed in this particular thesis project.

The following mission scenarios are considered:

- Direct transfer;
- Use of International Space Station (ISS);
- Earth orbit rendezvous;
- Lunar orbit rendezvous.

The fastest way to reach the Moon is by direct transfer. In contrast to the Apollo missions, there is no rendezvous with other S/C. Several lunar missions have used this mission scenario, e.g. Luna and Surveyor missions [Lunar and Planetary Institute, 2008].

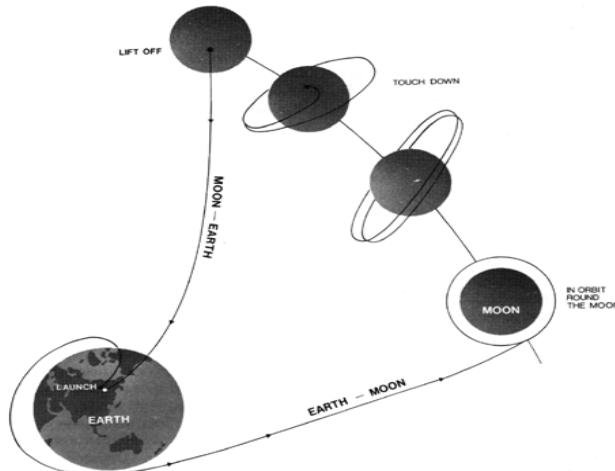


Fig 2.1 Luna 16 orbit trajectory [NASA, 2001]

Within the scenarios regarding the use of the ISS, many different options are available. It is possible to send cargoes to the station and then assemble them, or it is possible to send astronauts to the ISS in order to guarantee a continuous link between the lunar base and the station. Moreover, it is possible to use a S/C to travel just between the station and the Moon (orbiting around it and dropping off the payload or landing on the Moon) and another (or many other) S/C that delivers payload from the Earth to the station and the other way around.

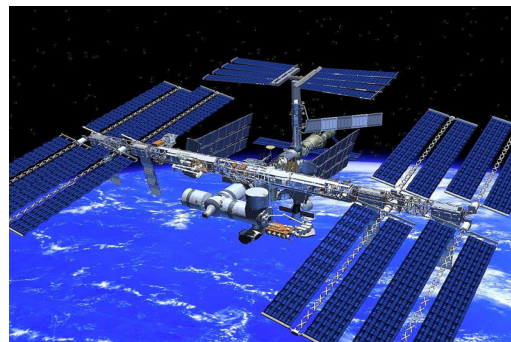


Fig 2.2 ISS [JAXA website, 2009]

If multiple launchers are needed the S/C can rendezvous in space. Earth orbit rendezvous



allows the assembly of cargo in an Earth orbit. In addition, a transport S/C can pick up cargo in an Earth orbit and release it in an orbit around the Moon. Rendezvous in LEO has already been accomplished successfully.

The lunar orbit rendezvous is similar to the previous one, but rendezvous is accomplished in a lunar orbit.

Fig 2.3 ATV-ISS rendezvous [EADS Astrium website, 2009]

Of these four mission scenarios, the ISS scenario seems to be the worst candidate for this mission, for many different reasons. First of all, the availability of the ISS can't be guaranteed. The international regulations are quite strict and permission may be denied. Moreover, many missions visit the ISS causing the ISS to be unavailable at certain times [Russianspaceweb website, 2009].

Besides these practical aspects, it also does not seem so attractive from an orbital point of view. Launchers deliver S/C and cargo into a low Earth orbit. In order to reach the ISS, a high inclination and a raise of the altitude are needed. This is quite expensive. At the ISS they will be assembled and finally sent to the Moon. This entire scenario is much more expensive than, for instance, the Earth orbit rendezvous, because no changes of inclination and altitude are required. Although the ISS offers infrastructure (like mechanical arms, etc.) that can simplify the assembling phase, it does not seem to outweigh the disadvantages. Therefore, the ISS mission scenario will be discarded.

As mentioned before, three students are designing the lunar base mission for ESA. Unfortunately, the work is not carried out at the same time. It has therefore been decided to split the final choice of the mission scenario over different studies. In the work of Antonio Pagano, responsible for the ascent phase, a trade-off between the direct transfer and the Earth orbit rendezvous will be given, comparing the amount of payload that can be brought into a LEO orbit. The optimization of the ascent phase could vary depending on the payload mass and indeed the size of the launcher. Therefore Pagano can evaluate if a rendezvous scenario is more convenient than a more massive single launch. The best of both scenarios will be compared with the lunar orbit rendezvous in the thesis work of Mirjam Boere, which is to describe the lunar phase of the mission. There, the fuel consumption of both mission scenarios will be compared and the final mission scenario will be selected.

2.3 Masses Naming Convention

Before showing the base elements and starting the discussion about payloads and masses, some definitions are given here and they will be adopted through the entire thesis in order to clarify the nomenclature and simplify the life of the reader. The following scheme summarizes the definitions adopted.

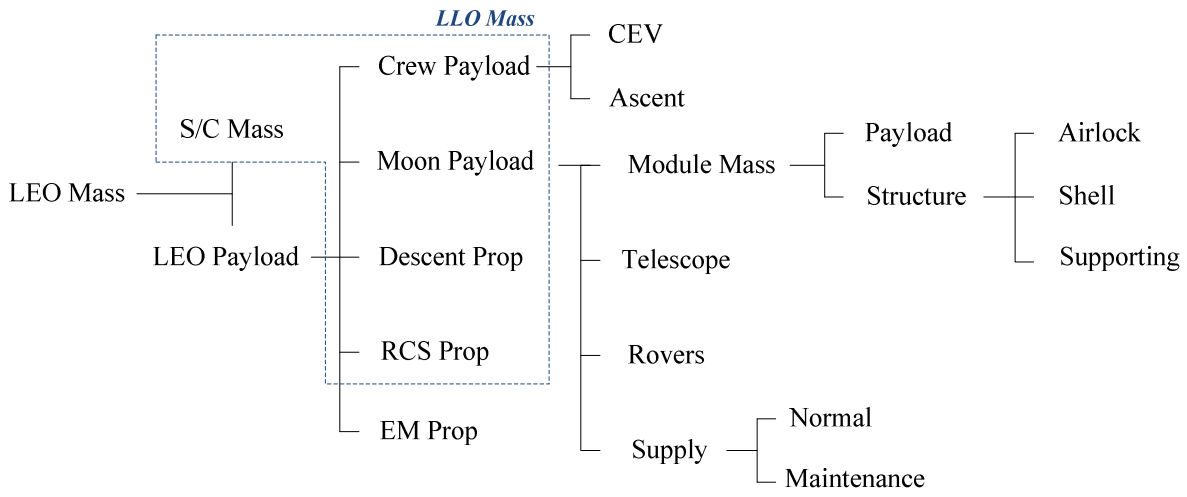


Table 2-A Masses definition summary

LEO Mass: mass delivered by a launcher into a LEO orbit.

S/C Mass: dry mass of the S/C used for the transfer orbit.

LEO Payload: all LEO Mass except for the S/C Mass.

Crew Payload: masses of the *CEV* (including the astronauts) and for the *Ascent* phase. It doesn't include any mass for the construction or the maintenance of the lunar base. The LEO Payload includes this mass **only** during manned missions.

Moon Payload: all mass brought on the lunar surface to build the base (so called "cargo missions" or unmanned). It doesn't include any mass for the manned mission. Manned missions **might have also** a Moon Payload.

Descent Prop: propellant for the lunar descent phase.

RCS Prop: propellant for the RCS.

EM Prop: propellant consumed for the Earth-Moon transfer orbit.

LLO Mass: mass brought into a lunar parking orbit. It is given by: S/C Mass + Crew Payload + Moon Payload + Descent Prop.

Module Mass: all mass of a module of the lunar base. It will be further discussed in the next section. It consists of the Structure mass and the Payload mass (including all the equipments, instrumentation, scientific experiments, etc.).

Telescope: mass of the observatory (see 2.4).

Rovers: mass of the rovers (see 2.4).

Supply: mass for food, water, oxygen, etc. (Normal) and for the Maintenance of the base.

Another useful mass is the *TLI Mass*, actually it is the LEO Mass except for the EM Propellant mass used to escape from the LEO orbit (only the first manoeuvre, TLI).

2.4 Base and Spaceport Architecture

The lunar base and spaceport architecture was presented in [Zuccarelli, 2008]. A short summary will be given in this section. The requirements for the lunar base were set by ESA. For more details and design decisions the reader is encouraged to read [Zuccarelli, 2008].

The lunar base consists of four modules, i.e., two habitation modules, one science module and one control module. These modules are connected with airlocks, providing access between the modules and the lunar environment. The modules are fixed, inflatable and made of Earth materials. The mass of one lunar base, emergency and spaceport module (Module Mass) consists of 0.7 tons inflatable shell, 3 tons supporting structure, 5 tons airlock and payload mass 8 tons for the base modules and 6.5 tons for the others (see Table 2-B). The payload mass can be divided in different parts, while shells, supporting structures and airlock for each module can't be split in small pieces. The configuration of the lunar base can be found in Fig 2.4. This base is able to host a minimum of three astronauts, as required by ESA.

| Module Type | Shell (tons) | Supporting (tons) | Airlock (tons) | Payload (tons) | Module Mass (tons) |
|-------------|-----------------|----------------------|-------------------|-------------------|-----------------------|
| Base | 0.7 | 3 | 5 | 8 | 16.7 |
| Emergency | 0.7 | 3 | 5 | 6.5 | 15.2 |
| Spaceport | 0.7 | 3 | 5 | 6.5 | 15.2 |

Table 2-B Mass breakdown for each module type

Finally, a 1 m diameter Newton type permanent telescope will be placed near the lunar base (another requirement from ESA). This lunar telescope is not obstructed by atmospheric pollution and will have a clear view when placed into a permanent shadowed crater.

In addition to the lunar base described above, one module with one airlock will serve as an emergency module of the lunar base. In case of an emergency in the lunar base the astronauts can go to this emergency base and communicate with the Earth. Only equipment will be installed that is absolutely necessary in the case of an emergency, like the communication system, food and water for a couple of days, a thermal system, etc. If the base can't be repaired, a spacecraft will be sent from Earth and the astronauts will leave the emergency base and go to the spaceport for their return to Earth.

The spaceport consists of two modules, i.e. the control module and the maintenance module. Its configuration can be found in Fig 2.5.

For the emergency module and for the modules of the spaceport less payload (6.5 tons) than for the lunar base is needed [Zuccarelli, 2008].

Both the lunar base and the spaceport have the ability to attach containers for supplies, e.g. water, air and food.

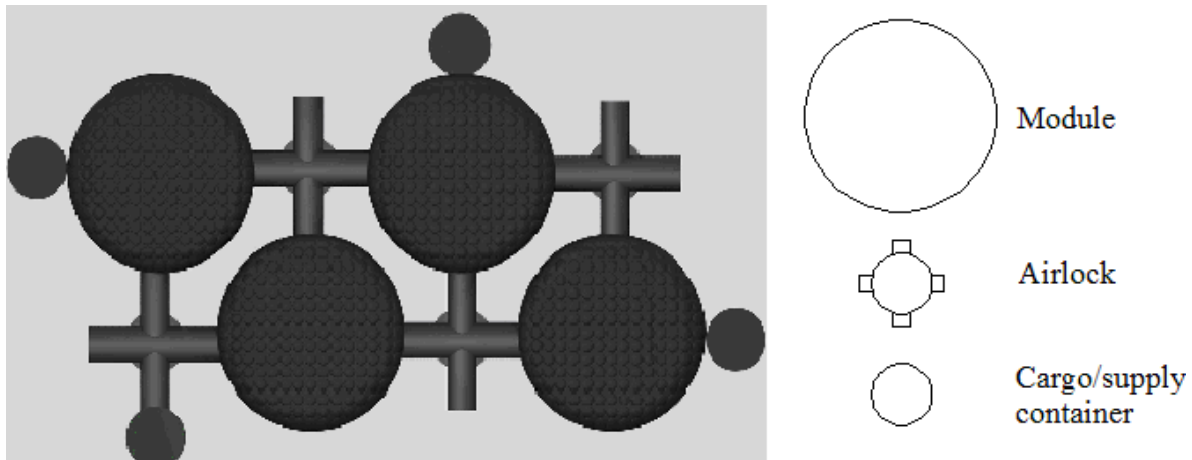


Fig 2.4 Configuration for the lunar base. The base consists of four modules and four airlocks. Containers are used to store fuel, food, water, etc. [Zuccarelli, 2008]

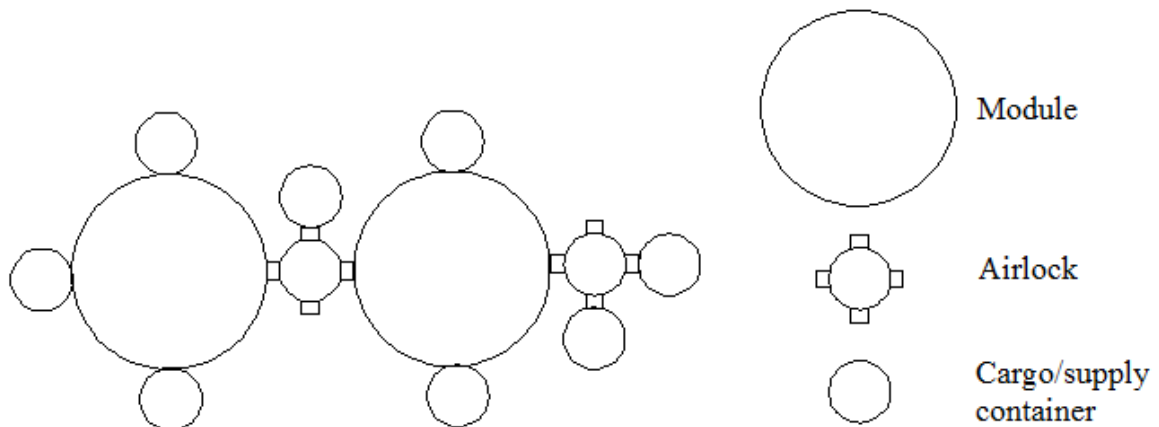


Fig 2.5 Configuration for the spaceport. The spaceport consists of two modules; one for communication (right module) and one for maintenance (left module). Containers are used to store fuel, water, etc. [Zuccarelli, 2008]

A link between the lunar base, the emergency base and the spaceport sites should be guaranteed by using different rovers. In addition, mobility to displace a crew of two for 15 km around the base should be guaranteed (ESA requirement). The following rovers will be brought to the lunar surface:

- Unpressurized manned rover, for short excursions;
- Pressurized manned rover, for long excursions (for example in the lunar craters);
- Cargo rover, to transport equipment and supplies.

Finally a communication system has to be guaranteed between the Earth and the Moon. For this reason two satellites will be put into a halo orbit around the Lagrangian point L2 with a 7.5-days period, in order to continuously cover the entire South Pole. They will be able to guarantee communications with three Earth ground stations separated 120 deg each [Zuccarelli, 2008].

Determining the total mass that has to be brought to the lunar surface is the most important aspect of this phase. A mass breakdown is shown in table Table 2-C. The masses of the different parts were already determined in section 2.3 from [Zuccarelli, 2008]. From the mass breakdown it becomes apparent which parts can be launched together and whether some parts exceed the capability of the launcher.

| Lunar base | | |
|----------------------------|---------------|--|
| Module mass Structure (4x) | 8.7 tons (4x) | [Roberts, 1988] and [Zuccarelli, 2008] |
| Module mass Payload (4x) | 8 tons (4x) | [Roberts, 1988] and [Zuccarelli, 2008] |
| Emergency module | | |
| Module mass Structure | 8.7 tons | [Roberts, 1988] and [Zuccarelli, 2008] |
| Module mass Payload | 6.5 tons | [Roberts, 1988] and [Zuccarelli, 2008] |
| Spaceport | | |
| Module mass Structure (2x) | 8.7 tons (2x) | [Roberts, 1988] and [Zuccarelli, 2008] |
| Module mass Payload (2x) | 6.5 tons (2x) | [Roberts, 1988] and [Zuccarelli, 2008] |
| Observatory | | |
| Telescope mass | 1.2 tons | [Sutherland et al., 2007] |
| Rover | | |
| Unpressurized rover mass | 0.2 tons | [Woytach et al., 2005]: |
| Pressurized rover mass | 6 tons | [Woytach et al., 2005]: |
| Cargo rover mass | 0.5 tons | [JPL Robotics, 2008] |
| Communication | | |
| Satellite mass (2x) | 0.4 tons (2x) | [Hamera et al., 2008] |

Table 2-C Total mass breakdown

2.5 Launch Capability

At the moment of writing, the minimum Moon payload mass for a single mission is not known yet, because this will result from simulations and shown in the next chapters.

At this moment, a minimum Moon payload mass of 5 tons will be assumed. A smaller payload mass would not allow to build up this base, because it is not possible to split the biggest part of a module (the airlock, weighing 5 tons) into smaller pieces. Therefore for all the most powerful launchers available on the market, this will be the minimum payload. Actually a bigger payload mass would allow to deliver the entire payload mass but with less launches. Therefore that value turns out to be “conservative”. Once the real value will be known this analysis will be reviewed.

For the manned flights, required to build and maintain the base, only one launcher is available, namely Ares V, which is currently under development by NASA. The TLI mass is about 65 tons (against the 45 tons for Saturn V). It allows to bring at least 20 tons of mass more than in the Apollo missions, which actually did not carry Moon payload next to the astronauts and their module. Ares V will be used for the transport of astronauts as well as cargo.

| Mass type | Element | Crew mission (ref.) (tons) | Cargo common descent stage (tons) |
|----------------|----------------|-------------------------------|---|
| TLI | Total | 65 | 45 |
| - EM Prop | LOI Prop | 12.004 | 8.302 |
| - LLO | Total | 52.996 | 36.650 |
| | - Subtotal 1 | 23.777 | 36.650 |
| | · Descent Prop | 11.855 | 13.196 |
| | · RCS Prop | 0.385 | 0.348 |
| | · S/C | 6.756 | 6.756 |
| | · Moon Payload | 4.781 | 16.350 |
| (Crew Payload) | - Subtotal 2 | 29.219 | - |
| | · CEV | 20 | - |
| | · Ascent | 9.219 | - |

Table 2-D Mass budget for the Ares V crew and cargo lander [after Donahue et al., 2008]

In [Donahue et al., 2008] a model was used to assess the performance of the lunar lander. The lander has a separate descent and ascent stage. The lander has a single O2/H2 RL10-A4 engine for the Lunar Orbit Injection (LOI)/descent stage and a single pressure-fed N2O4/MMH engine for the ascent stage. The ascent stage is used to return humans back to Earth. The total mass of the lander is equal to 45 tons, namely the total mass that the Ares-V Earth Departure Stage (EDS) can boost into TransLunar Injection (TLI), except for the CEV mass.

Two options are considered, the manned and the cargo mission. The manned mission will return to a 100 km lunar orbit after its visit on the Moon while the cargo mission stays on the lunar surface. The mass budget of these two missions can be found in Table 2-D. The manned mission can carry a Moon payload of 4.781 tons, while the cargo mission 16.35 tons. Both missions use the same NASA Exploration Systems Architecture Study (ESAS) descent stage. However, in [Donahue et al., 2008] it is mentioned that the manned mission can be optimized further by using another type of staging (so-called descent staging) and another ascent propellant, namely LO2/LCH4 instead of H2O4/MMH, increasing the Moon payload to 6.05 tons (here assumed for the computations).

In addition, also the cargo mission can be optimized further. In the computations by [Donahue et al., 2008] the CEV was taken into account. However, the CEV is not needed for the cargo mission and the capability of the Ares-V to TLI can increase. This would result in a Moon payload of 19.84 tons and a redesign of the descent stage to account for increase in thrust, i.e., larger descent tanks, more propellant and heavier frame than the reference manned mission descent stage. For simplicity, a Moon payload mass of 16.7 tons (as the highest Module mass, see Table 2-B) is assumed without changing the other parameters, because it allows simple computations for the first preliminary launch sequence. Anyway this value has to be recomputed during this work. Besides, this improved value can be reached just using some of the previous more advanced propellant also for the descent phase [Donahue et al., 2008].

Considering Table 2-D the following maximum payloads are assumed in case of manned mission (M) or completely unmanned (U) for Ares V:

| Mission | Moon Payload (tons) |
|---------|---------------------|
| M | 6 |
| U | 16.7 |

Table 2-E Ares V payload

The values of the last table are actually given by NASA, depending on the transfer orbit they use. To compute in this work the Moon payload mass delivered, the S/C mass has to be known. The launcher is able to put a certain payload mass in a LEO orbit (LEO mass), then it will be transferred to the Moon, by using a certain S/C built on purpose. Then the S/C should brake to enter into a lunar parking orbit and then land on the Moon.

The structural mass of this S/C should be subtracted from the LLO mass as well as the propellant required for the descent phase and for the RCS, in order to evaluate the real payload mass that can be transferred on the Moon (Moon payload, see Table 2-A). The EM propellant will be computed by means of the ΔV required for the transfer orbit (computed in this work). In this way subtracting the EM propellant mass from the LEO mass, the LLO mass will be computed. Then the Descent, RCS and S/C masses have to be subtracted in order to compute the Moon payload. Therefore here an estimate of this mass (LLO mass – Moon payload = S/C + Descent propellant + RCS propellant masses) will be given by using Table 2-D for the Ares V missions.

Since in that table, the TLI mass is given (instead of the LEO mass), only the LOI propellant has to be subtracted in order to compute the LLO mass.

Therefore, in case of manned and cargo missions the estimated masses are:

| Mission type | TLI (tons) | LOI prop (tons) | Moon Payload (tons) | LLO mass – Moon payload (tons) |
|--------------|------------|-----------------|---------------------|--------------------------------|
| Manned | 65 | 12 | 6 | 47 |
| Cargo | 45 | 8.3 | 16.7 | 20 |

Table 2-F Mass estimation of a S/C launched by Ares V

The Moon payload mass has been subtracted since it has to be computed through this work.

The same computation is required for the other launchers. They can bring less mass in a LEO orbit than the Ares V, therefore the lander mass, as well as all other masses (LOI prop and Moon payload) should be smaller. However no other lunar lander is now available or under development, since the only real project to go back to the Moon is followed by NASA by means of Ares V. Therefore as a rough estimation, the Ares V lander can be resized considering the Moon payload (Table 2-D). Since the minimum Moon payload required from the other launchers is 5 tons, and the Moon payload delivered by Ares V is 16.7 tons, a scaling factor of 3.35 for all the masses will be considered:

| Mission type | TLI (tons) | LOI prop (tons) | Moon Payload (tons) | LLO mass – Moon payload (tons) |
|--------------|------------|-----------------|---------------------|--------------------------------|
| Cargo | 13.4 | 2.5 | 5 | 5.9 |

Table 2-G Mass estimation of a S/C launched by other launchers

The last computations state that at the end of the transfer orbit the total mass delivered (LLO mass) should be 47 tons for the manned mission (considering zero the Moon payload); 20

tons + Moon payload for Ares V cargo missions and 5.9 tons + Moon payload for other cargo missions. In order to build the base the Moon payload should be at least 5 tons.

Furthermore, at this moment of writing, the real availability (date of the first launch, how many launches per year, etc.) and capabilities (cargo missions, Moon payload mass, etc.) of the Ares V launcher are not known yet. When the literature study was started, Ares V was considered available for this mission. Therefore in this paragraph, it is assumed that Ares V will be available on time, without any limitations on the number of launches, and that it is the only launcher able to send astronauts on the Moon.

It is also assumed that no other launcher can launch a payload of more than 5 tons. Actually, the last assumption has to be verified during this study, because at this moment there is no data about TLI masses for other launchers.

For this reason, only Ares V will be used to build the base, (except for a small launcher that will carry the communication satellites). Since it is the most powerful launcher, it would allow to reduce the required number of launches.

Actually, the possibility to use a launcher able to deliver at least 5 tons of Moon payload has to be confirmed by computations (like Atlas V, Ariane V, etc.). The use of such a launcher could allow to split some Ares V missions in two different ones, in order to decrease the risks of launching two modules at once, since Ares V would take them to orbit with just one launch.

Moreover in case a mission will require only 5 tons of payload, a smaller launcher will be preferred to Ares V. Anyway it is important to verify the real capabilities of other launchers, because in case of a temporary unavailability of Ares V (for instance a failure), it should be possible to continue building and/or servicing the base.

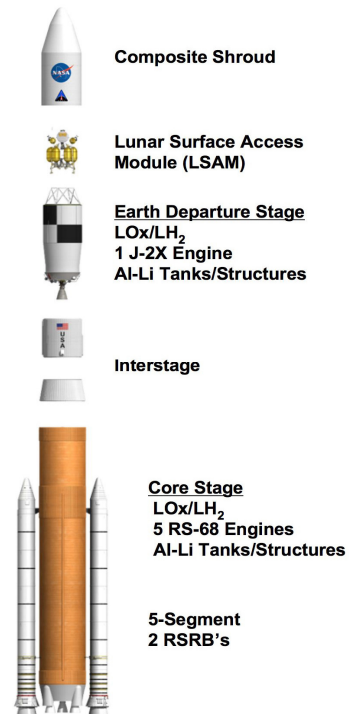


Fig 2.6 Ares V assembly [Tallgeorge website, 2009]

2.6 Preliminary Launches Sequence

The launch sequence can be found in Table 2-H, and a description of it will follow hereafter. The first goal is to guarantee communication cover on the Moon, for this reason the first launch will be used to put two satellites into an L2 orbit. For this first launch the total payload mass is 0.8 tons, therefore a small launcher will be used.

Then, the lunar base will be built. The modules will be brought directly to the base site, so that these massive structures do not have to be transported over large distances. However, no crew will be present when the lunar base parts are delivered due to safety considerations. Launches 2-5 will deliver the four lunar base modules, including their payload (i.e., thermal, electric and communication systems, kitchen, gym equipment etc.). Launch 6 will carry the emergency module and also a cargo rover, so the astronauts will be able to move the modules. It is assumed that these five launches are sent toward the Moon in one year.

Then astronauts will be delivered to assemble the lunar base and the emergency base. In each mission four astronauts will land on the lunar surface, near the base site. Four missions (7-10),

lasting about a week, are necessary to build up the four modules, followed by four missions (11-14) to integrate the payload inside the modules. Finally, two missions (15-16) are necessary to build the emergency module and integrate the payload.

After the lunar base is built, the spaceport can be built and the telescope can be placed. Two missions (17-18) are needed to bring the two modules, including the payload. This is followed by two astronauts missions (19-20) to build up the spaceport, two (21-22) to integrate the payload and place the telescope.

When both the lunar base and the spaceport are built, the construction phase is ended and the operative phase is started. Astronauts will be sent for permanent residence. They will land on the spaceport and travel to the lunar base with the unpressurized rover, over a distance of about 10 km. After some years it may be necessary to have a pressurized rover. However, it is uncertain if this 6 tons rover (Table 2-C) will be brought to the lunar base. Currently, it has not been designed yet. It is assumed that the lander is capable of staying 210 days on the lunar surface [NASA Study, 2005], meaning that the astronauts will replace each other after this period. Moreover, a cargo supply per year of circa 8 tons is required [NASA International Space Station, 2008], [Baker and Eichstadt, 2005]. It consists of water, oxygen, food, nitrogen, etc. That value does not take into account the mass of equipment that is needed when something on the base needs to be repaired or replaced due to a failure. This mass depends on the particular situation of the failure and will therefore not be taken into account for the normal supply mass. For this reason another cargo supply of circa 4 tons per year can be assumed to cover these kinds of problems.

Table 2-H and Table 2-I don't take into account the real payload mass on the Moon, which can be estimated only at the end of this work. Therefore this analysis is quite qualitative, but it is a reasonable basis to start from. Those tables summarize the launch sequence respectively for the building and the maintenance phase.

| Year | Number of launch | Payload type | Moon Payload (tons) | Manned/ Unmanned |
|------|------------------|--|---------------------|---------------------|
| 1 | 1 | Two comm. satellites | 0.8 | U |
| 1 | 2 | Base module 1+payload | 16.7 | U |
| 1 | 3 | Base module 2+payload | 16.7 | U |
| 1 | 4 | Base module 3+payload | 16.7 | U |
| 1 | 5 | Base module 4+payload | 16.7 | U |
| 1 | 6 | Emergency base+payload + cargo rover | 15.7 | U |
| 2,3 | 7-16 | Astronauts | - | M |
| 4 | 17 | Spaceport module 1 + payload + unpressurized rover + telescope | 16.6 | U |
| 4 | 18 | Spaceport module 2 + payload | 15.2 | U |
| 4 | 19-22 | Astronauts | - | M |

Table 2-H Preliminary launch sequence during building phase

| Number of launch per year | Payload type | Moon Payload (tons) | Manned/ Unmanned |
|---------------------------|---------------------------------------|---------------------|---------------------|
| 1 | Astronauts/Cargo supply (maintenance) | 4 | M |
| 2 | Cargo supply | 8 | U |
| 3 | Astronauts | - | M |

Table 2-I Preliminary launch sequence during maintenance phase

CHAPTER 3

3. Earth-Moon Transfer Orbits: Options

In this chapter, the first aspects of the mission will be tackled. So far only those aspects, regarding the Moon base and the framework, where this work was assessed, have been considered. Now some information will be given about what kinds of orbits from the Earth to the Moon are available and how they are going to be analyzed and compared during this work. Finally the launchers, and the initial and final parking orbits, respectively around the Earth and the Moon, will be addressed here.

3.1 Transfer Orbits

All the different options to send a S/C from the Earth to the Moon can be grouped in three different classes, that will be discussed in detail in the next chapters:

- High-Thrust trajectories
- 3-Body trajectories
- Low-acceleration trajectories

The high-thrust orbits represent the canonical way to leave the Earth and to get into an interplanetary trajectory. Actually it is the only successful way already used to send astronauts to the Moon, for this reason this kind of trajectories is the benchmark.

On the other hand, there are 3-body and low-accelerations trajectories, that represent alternative ways to get to the Moon. Recently particular emphasis has been given to them in order to reduce the total propellant consumption, and indeed to maximize the final payload. The idea is to verify if they are suitable for this kind of mission, or if the high-thrust orbits represent still the best way to perform this mission.

In the next paragraphs a brief overview will be given for each of them.

3.1.1 High-Thrust Orbits

So far, the only successful way to bring men on the Moon is represented by high-thrust orbits, and actually by the Apollo missions design. Those missions made use only of impulsive manoeuvres in order to directly reach the target. The mathematical model used to describe

these orbits is the 2BP problem, where a main body generates the gravitational field. If the S/C reaches the border of that area, where the gravity field of another body becomes predominant (sphere of influence, treated in section 4.4), then the initial attracting body is replaced by another one. For Earth-Moon missions, this is not considered an issue, since the entire trajectory stays in the Earth sphere of influence, as explained in the next Chapter.

The main advantage are the short TOF required, the reliability and the solid know-how; of course the drawback is that they can be more expensive than other solutions.

Apollo missions made use of phasing loops transfer trajectories. Before entering in the transfer orbit the S/C made some loops around the Earth in order to control the injection parameters and to check all subsystems. After this phase, by using an impulsive shot, the S/C entered into a transfer trajectory following a regular fast Hohmann transfer to reach the Moon. Then, after a number of days, the S/C reached the sphere of influence of the Moon, and, by using a new impulsive shot to brake, it entered in a parking orbit around the Moon (as shown in Fig 3.1). For the Apollo 11 mission the entire transfer cost 3.943 km/s in terms of total ΔV [NASA, 2004].

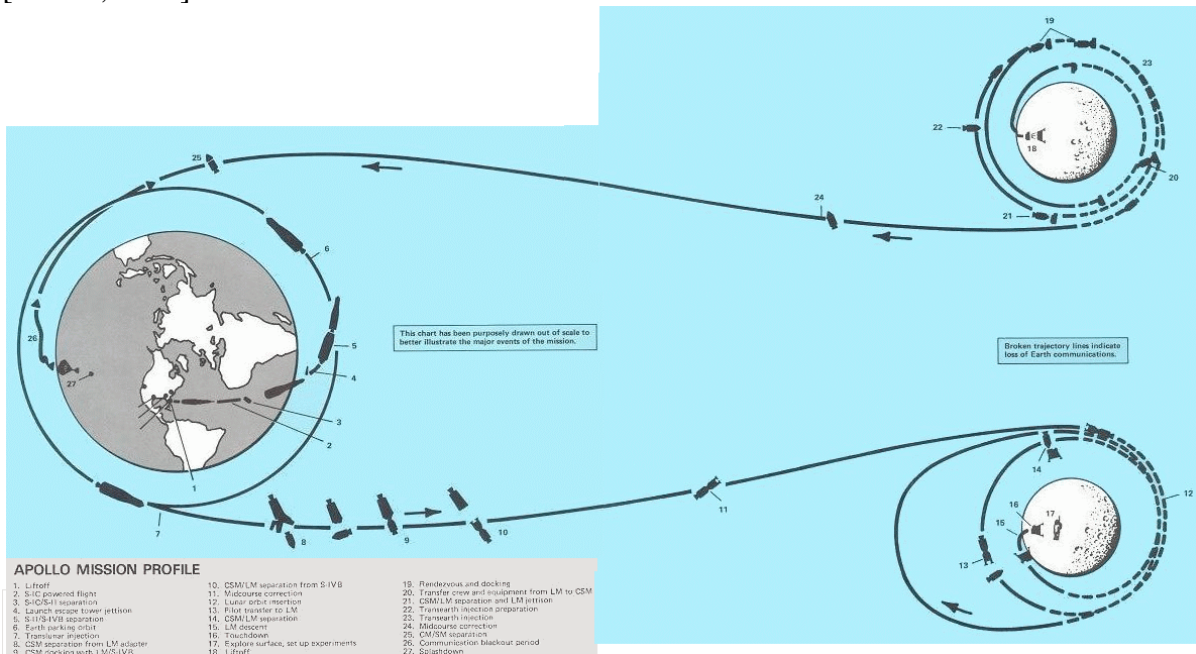
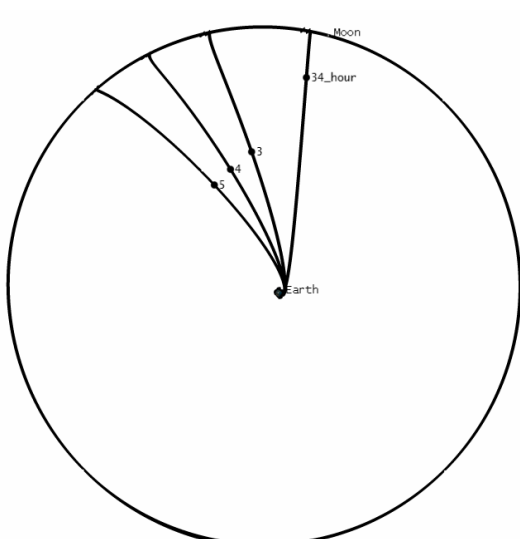


Fig 3.1 Apollo mission details [Univ. of Oregon 2008]



A Hohmann transfer is the cheapest way to change the apoapsis of a trajectory. Once the apoapsis has been increased such that the S/C is close to the Moon, then it is possible to inject it into a lunar orbit. Since the Hohmann transfer is also the slowest way to do that, within the high-thrust orbits, it is possible to slightly modify it, in order to make the transfer faster with a small additional propellant consumption. For this reason, these trajectories are called fast Type 1 transfer trajectories, and examples are shown in Fig 3.2.

Fig 3.2 Type 1 transfer in Earth-Centered Inertial Coordinates [Loucks et al., 2005]

Since these trajectories are the only ones tested for manned Earth-Moon transfers, they will be the reference trajectories.

3.1.2 3-Body Orbits

The 3-body orbits are obtained within the 3-body problem formulation (3BP). In this model two main masses (the Earth and the Sun or the Moon) are generating a complex gravity field, in which the S/C is moving, without influencing it. This model became very interesting in the last years, due to some special “features” specific for this problem, as Halo orbits, manifolds, etc. Studies (eg. [Parker, 2006], [Miller, 1992]) have demonstrated that, by using and combining them, the Moon can be reached saving propellant mass w.r.t. the usual trajectories based on impulsive manoeuvres.

Moreover also some real missions made use already of this kind of orbits, as for instance the S/C Hiten (Muses-A), launched on January 24, 1990 ([Uesugi, 1996] and [NASA/GSFC, 2008]). That mission used the weak stability boundary, a theory based on the 3BP, but not treated in this work.

Besides other missions took advantages of Halo orbits and manifold trajectories, even if they didn't have the Moon as final target. For instance the SOHO mission [Roberts, 2002], that was able to successfully send a satellite to the L1 point of the Sun-Earth system (1996).

The most attractive case for this lunar base mission is thoroughly discussed in [Parker and Lo, 2006]. The basic idea is to use two different three-body systems: Sun-Earth and Earth-Moon. By combining and patching the manifold trajectories of these systems (as shown in Fig 3.3), the S/C would be able to fly from the Earth to the Moon in a “attractive way” (Table 3-A), in terms of total ΔV .

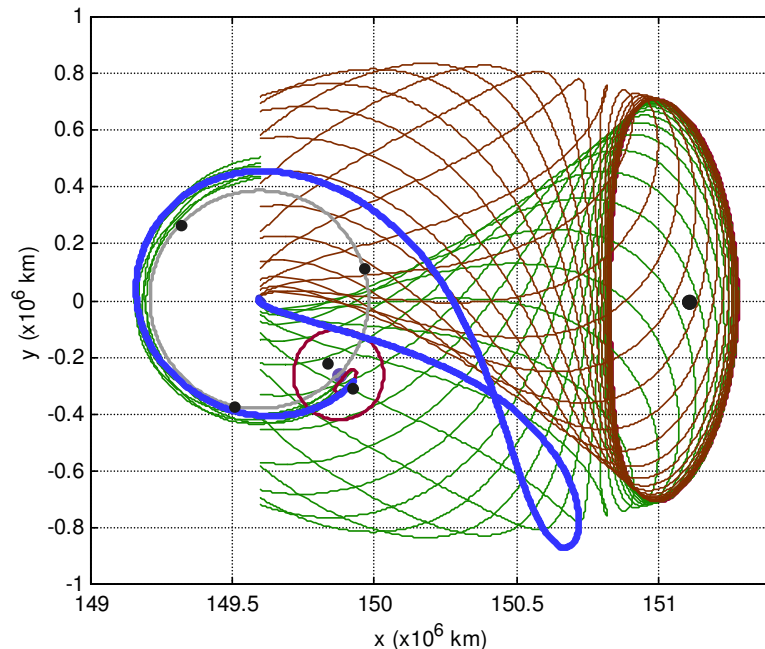


Fig 3.3 The 3D Shoot the Moon transfer (blue) plotted alongside the stable (green) and unstable (red) manifolds of the EL₂ halo staging orbit and the stable (green) manifold of the LL₂ halo staging orbit [Parker and Lo, 2006]

| Transfer Type | Hohmann | 3D Shoot the Moon |
|---|----------------|--------------------------|
| ΔV [km/s] | 3.73 – 3.95 | 3.26 |
| Inclination range of LEO parking orbit [$^{\circ}$] | 0 | Any |
| Inclination range of final lunar orbit [$^{\circ}$] | 0 | Any |
| Transfer duration [days] | 3.9 – 5.2 | 105 |

Table 3-A A comparison of three lunar transfer types from a 200-km LEO parking orbit to an orbit temporarily captured by the Moon [Parker and Lo, 2006]

From Table 3-A, the reason for all the interest in this kind of orbits is clear: saving 0.5-0.7 km/s of total ΔV would mean a large increase of the total payload (even if just a temporarily captured lunar orbit has been considered). For any space mission this represents one of the main goals to achieve, particularly in this mission, since a base on the Moon has to be delivered and built. Therefore in this work it has been decided to seriously consider such trajectories.

They will be obtained and then compared with the high-thrust ones in the next chapters, where also the theory and the techniques required to get such a orbit will be explained and discussed.

This kind of trajectory will be used to send two communication satellites into a Halo orbit around LL2. The high-thrust and low-acceleration trajectories will be considered unsuitable for this mission, since it perfectly fits within the 3BP. Actually it would be very difficult to design a trajectory toward such a Halo orbit, defined already within the 3BP, with any other technique. For this reason no trade-off will take place.

3.1.3 Low-Acceleration Orbits

In the last years many S/C's carried low-thrust propulsion systems on board. This kind of engines is very fuel-efficient and can allow to save huge amounts of propellant. While the impulsive manoeuvres require thrust for just a few seconds or minutes, these engines usually are used continuously even for months, due to the small thrust they can deliver. Also in this case the mathematical model would be the 2BP, the only difference is about the manoeuvres, because in this case a continuous acceleration is given by the thruster.

In order to integrate the trajectory, the direction of the thrust should be known. Therefore the analytical simplified model, called “Exposins”, will be used in this work to model the thrust profile.

Usually low-thrust engines have been used just on board of small satellites, that is because the thrust delivered so far was too small (in the order of mN) to transport any big payloads. For instance, the well-known SMART-1 ESA mission, launched on 27 September 2003, can be briefly mentioned here.

It combined the WSB theory, low-force thrusters and the resonance of the Moon in order to reduce the total ΔV needed to accomplish the mission, and indeed to reach the Moon [Camino

et al., 2007]. From a GTO orbit, it used its Solar Electric Primary Propulsion to gradually spiral out during thirteen months. The solar arrays powered the thruster, giving a nominal thrust of 68 mN, hence an acceleration of 0.2 mm/s^2 or a ΔV of 0.7 m/s per hour. As for all low-thrust powered craft, orbital maneuvers were not carried out in short bursts but very gradually. The particular trajectory taken by SMART-1 (Fig 3.4) to the Moon required thrusting for about one third to one half of every orbit.

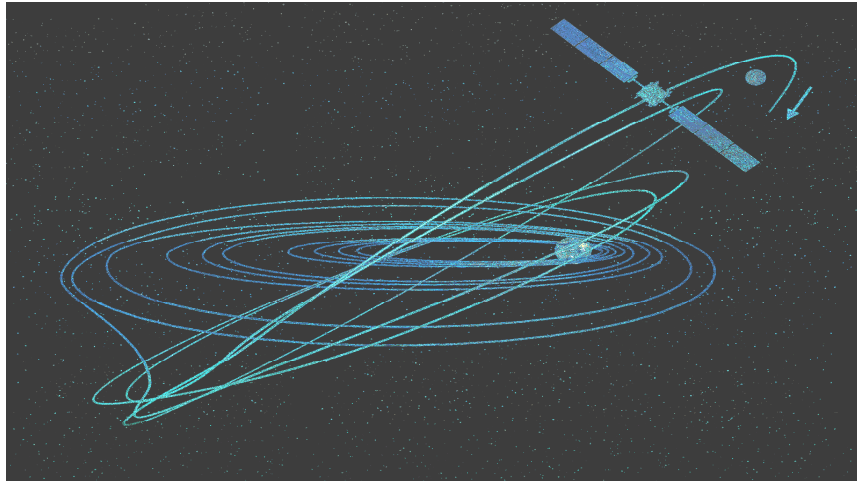


Fig 3.4 8 SMART-1 osculating 3D-orbit [ESA, 2006]

Since this technique has been very successful for many “small” missions, applying it to bigger S/C would be very interesting. Therefore, recently, many studies have been focused on designing low-thrust engines able to deliver a thrust in the order of some N ([Manzella et al., 2002] and [Bering III et al, 2008]), instead of mN. They would not anymore be low-thrust engines, but low-acceleration engines, because the thrust would not anymore be “low”, but the acceleration given to big S/C’s would still be “low”. Anyway they could allow propellant saving, thanks to their high efficiency.

For this reason, in this work, also this option will be explored, because the lunar base should be delivered in ten years and in the mean time this kind of engines should already be available. The problem with this technique is that there are no reference data for this kind of massive missions that will be considered here. Therefore benchmarking it would be difficult.

3.2 Parking Orbits

In this section the starting parking orbits around the Earth and the target parking orbit around the Moon will be defined.

3.2.1 Initial Parking Orbits

The initial parking orbit depends on the launcher selected. For instance, usually, the minimal inclination is given by the latitude of the launch site. Anyway a big range of values could be selected still. For instance, considering the Ariane V launcher, its launch site is Kourou at a

latitude of 5° . Then still a big range of inclinations is available. Also the altitude of the parking orbit can be considered as a free parameter.

As already explained in section 2.1, this group work is not carried out at the same time with the other colleagues. It means that it is not possible to optimize the entire transfer trajectory now, including the selection of the parking orbit for each launcher. For this reason some assumptions are required.

In this work, only the nominal LEO parking orbit will be used for the computations of each launcher. The altitude and the inclination of this orbit influence LEO mass. Of course, increasing the inclination and the altitude means a smaller LEO mass. Since the S/C will execute some manoeuvres in order to arrive at the proper altitude and inclination to inject into the transfer orbit, the best solution is to assume the initial parking orbit at the minimum altitude and inclination, where the LEO mass is maximum. If manoeuvres are required to change this orbit and to reach the transfer orbit, they will be executed and the propellant consumption will be then considered.

A list of inclinations and altitudes, depending on the launcher, is given in Table 3-B. The parking orbit is assumed circular. Moreover the RAAN is left free, because it depends on the launch epoch (which is not optimized here). The following launchers have been selected since they are the most powerful ones, and in this mission the highest possible payload has to be achieved.

| Launcher | Launch site | Inclination ($^\circ$) | Altitude (km) | LEO mass (tons) |
|----------|----------------|--------------------------|---------------|-----------------|
| Ariane V | Kourou | 5 | 185 | 22.6 |
| Proton | Baikonur | 51.6 | 185 | 21 |
| Ares V | Cape Canaveral | 28.5 | 185 | 130 |
| Ares I | Cape Canaveral | 28.5 | 185 | 25 |
| Atlas V | Cape Canaveral | 28.5 | 185 | 20.25 |

Table 3-B Summary of launchers and LEO parking orbit [Isakowitz et al., 2004]

The latitude of Baikonur is 45.6° , but the minimum inclination that can be reached from that site is 49° . In the last table an inclination of 51.6° has been considered, because the data for the Proton launcher have been found only at that inclination.

It is already known that Ares V will be the best choice to perform this mission (highest payload), but in case of a failure, a back-up launcher has to be available. For manned missions no back-up launchers can be identified, because only Ares V will have the capability to carry astronauts.

On the other hand back-up launchers can be found for cargo missions. For this reason all other launchers listed in Table 3-B will be investigated. As already explained in section 2.6, they should be able to deliver at least 5 tons of Moon payload (considering also the S/C and the propellant, the LLO mass is about 10.9 tons), enough for a single module of the lunar base. Anyway this value has to be confirmed by computing the real Moon payload mass.

Actually, most likely, it would be not possible to use Ares I as backup launcher of Ares V for cargo missions, because in case of failure of Ares V, it seems reasonable to stop also Ares I launches (they have a similar design). Therefore it will be considered only if a smaller launcher (than Ares V) will be required to deliver a smaller payload on the Moon. As back-up launchers only Ariane V, Atlas V and Proton will be considered suitable.

Furthermore it is assumed that the payload will be compatible with all of these launchers (no problems with vibrations, acoustic noise, etc.). Moreover it is assumed that the payload can be sent from all the launch sites indicated.

The mission to send communication satellites into an LL2 orbit will be the only one not using one of the launchers listed in Table 3-B. That is because the mass of the satellites is very small (400 kg each), therefore the use of a massive launcher would be meaningless. For this reason a very small one has been selected. Actually, for this mission, the estimated payload to deliver in a LEO orbit (LEO mass) is around 2 tons, and just few launchers are suitable.

The most attractive one is the ESA Vega launcher, that should be launched for the first time at the end of 2009 or at the beginning of 2010. The launch site is Kourou, but this launcher is suitable for many different mission orbits.

The performances of Vega (LEO mass, as the payload mass of the next figure has been called here), depending on the altitude of the LEO orbit and the inclination required, are here shown:

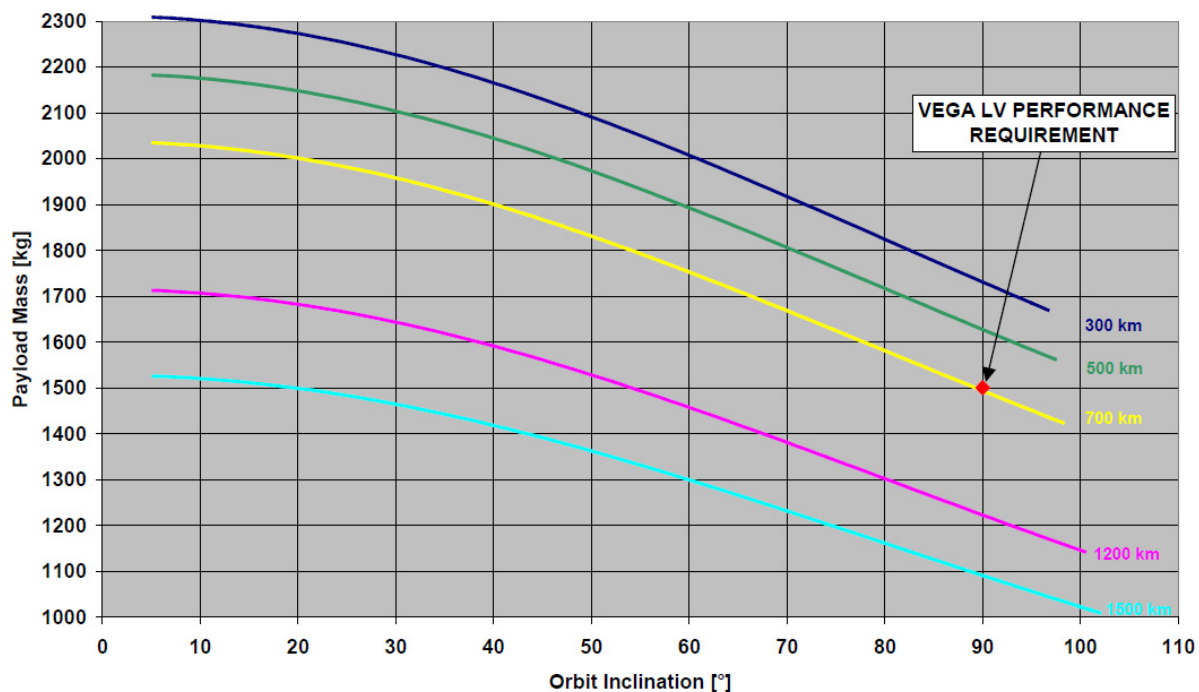


Fig 3.5 Vega performances for circular orbits [ESA User's Manual, 2006]

This plot will be used in order to check if this launcher is really suitable for this mission, once the inclination and the payload mass required will be known.

3.2.2 Lunar Parking Orbit

As for the parking orbit around the Earth, also in this case it is not possible to design the lunar orbit optimizing also the landing phase. For this reason, a target final orbit will be defined without taking into account the optimization of the landing segment of the mission.

Since the goal of this mission is to build a base on the South pole, the final parking orbit around the Moon should be almost polar. Together with the colleague responsible for the landing, the following final orbit has been selected:

| Altitude (km) | Inclination ($^{\circ}$) |
|---------------|----------------------------|
| 100 | 89 |

Table 3-C Parking orbit around the Moon

Therefore the goal of this thesis work will be to optimize the transfer orbit from the initial parking orbits (defined in Table 3-B) to the final lunar orbit (defined in Table 3-C). The optimization of the ascent phase and of the landing phase will be tackled by the other two students and it will be not treated in this work.

CHAPTER 4

4. High-Thrust Trajectories: Theory

This chapter is focused on the 2-body problem (2BP) and on the trajectories that can be obtained within it. Therefore first an introduction to this model will be given.

As all other orbits, also these high-thrust trajectories will be computed by using an STA tool: the Interplanetary Module. To understand how it works, the most important theoretical topic, tackled within this module, will be briefly explained: the Lambert's problem.

Thereafter, some interesting impulsive manoeuvres that might be applied through this work will be addressed here.

4.1 N-Body Problem

The 2BP is a particular case of the most general case: the n-body problem.

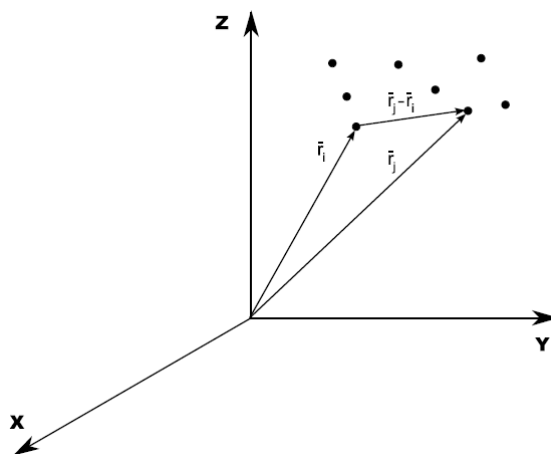


Fig 4.1 n-body problem [Kumar, 2008]

The n-body problem (shown in the previous figure), that studies the motion of a body within the gravitational field generated by another n-1 massive bodies, is defined in the inertial reference frame by the following equation [Wakker, 2007a]:

$$\frac{d^2 \vec{r}_i}{dt^2} = G \cdot \sum_{j=1(j \neq i)}^n \frac{m_j}{|r_i - r_j|^3} \cdot (\vec{r}_j - \vec{r}_i) \quad (4.1)$$

where “r” represent the respective radius vectors starting from the center-of-mass of the system and “m” the individual masses. G is the gravitational constant ($6.67300 \times 10^{-11} \text{ m}^3 \text{ kg}^{-1} \text{ s}^{-2}$). Only gravitational forces have been considered.

4.2 2-Body Problem

The 2BP is a particular case of the n-body problem. Only two bodies are considered, and one of them (usually the S/C) has a negligible mass m_2 (it can't influence the gravitational field generated by the other one). That model can be expressed, in the inertial reference frame, in the following way:

$$\ddot{\bar{r}} + \mu \frac{\bar{r}}{r^3} = \bar{a}_d \quad (4.2)$$

where $\mu = Gm_1$ is the gravitational parameter of the main body (m_1 is the mass of the main body), \bar{r} is the radius vector (directed from m_1 toward the S/C), and \bar{a}_d is the perturbing acceleration.

In the “pure” 2-body problem, this last term is zero. Perturbing forces will be tackled in one of the next paragraphs.

In the 2-body problem two conservation laws can be derived, namely the conservation of energy and the conservation of angular momentum [Wakker, 2007a]:

$$\frac{1}{2}V^2 - \frac{\mu}{r} = const = E \quad (4.3)$$

$$\bar{r} \times \bar{V} = \bar{H} \quad (4.4)$$

where \bar{r} is again the radius vector, \bar{V} is the velocity vector and \bar{H} is the angular momentum. The first and the second term of equation 4.3 indicate respectively the kinetic energy and the potential energy of m_2 (all per unit of mass).

Reworking the last two equations, it's possible to demonstrate that solutions of equation 4.2 are given by conic sections (in this case called Kepler orbits), described by the following relation [Wakker, 2007a]:

$$r = \frac{p}{1 + e \cos \theta} \quad (4.5)$$

where $p = a(1 - e^2)$

p is the semilatus rectum, a the semimajor axis, e the eccentricity and θ the true anomaly (starting from the pericenter). These parameters are shown and defined in Fig 2.1.

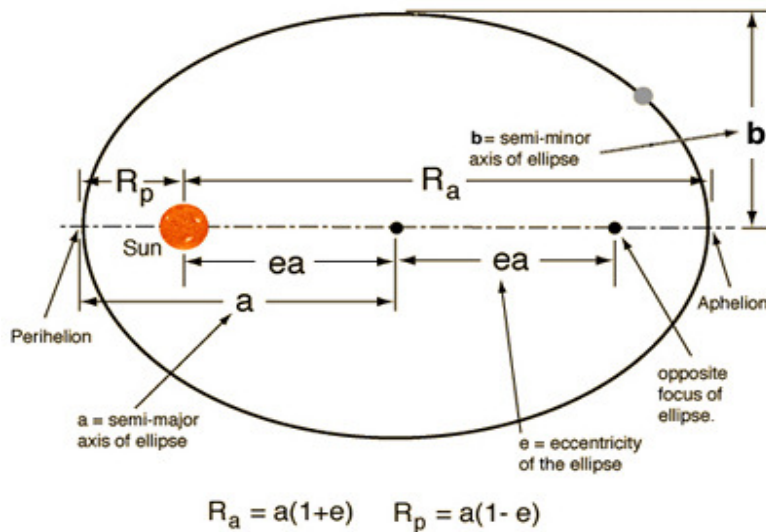


Fig 4.2 Elliptic orbit around the Sun [Relativity Calculator website, 2009a]

Depending on the eccentricity, the orbit can be elliptic ($e < 1$), circular ($e = 0$), parabolic ($e = 1$) or hyperbolic ($e > 1$).

4.3 Orbital Coordinates

The most used r.f.'s for the 2-body problem are centred in the center-of-mass of the main body. The origin is the center of the planet, the Z-axis points to the north pole and the equatorial plane forms the X-Y reference plane. The X-axis could be aligned with the vernal equinox (γ), which describes the direction of the Sun as seen from the body at the beginning of spring time (or equivalently the intersection of the equatorial plane with the planet's orbital plane), in case of inertial reference frame, or with a reference meridian (as the Greenwich meridian for the Earth), in case of rotating reference frame.

The position of a point in the equatorial coordinate system may be specified by either the Cartesian coordinates or the spherical coordinates, but a third set of parameters is the orbital ones (shown in the next figure): $a, e, i, \Omega, \omega, \tau$.

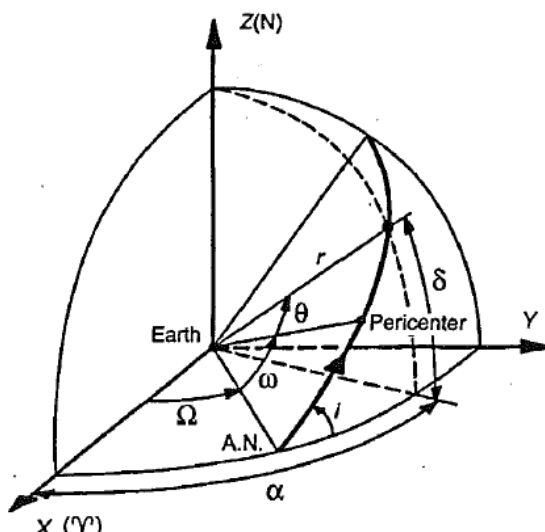


Fig 4.3 The orbital elements of a satellite [Wakker, 2007a]

This system holds within the two-body problem, because it describes the orbit of the spacecraft by using a Keplerian orbit. The semi-major axis a and the eccentricity e determine the shape and the size of the orbit; the orientation of the conic section in the orbital plane is determined by the angle ω between a fixed reference direction in the orbital plane and the radius vector from the origin to the pericenter. That angle is called argument of perigee and it is measured from the ascending node in the direction of the motion of the body in its orbital plane (from 0° to 360°). The integration constant τ , the time of pericenter passage, is needed to link time and position in the orbit.

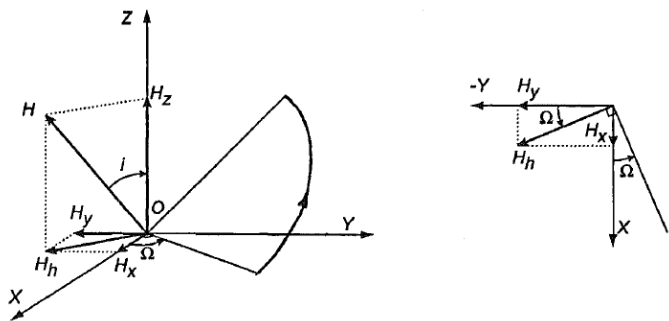
Moreover the orientation of the orbital plane relative to the r.f. can be determined by two angles. First the line of intersection of the orbital plane with the reference plane of the r.f. is considered. The point where this line passes these nodes from South-to-North is referred to as the ascending node. The first angle is the angle from the reference direction towards the point γ to the ascending node and it is indicated by Ω . It is called longitude of the ascending node or right ascension of the ascending node (RAAN), measured eastward from 0° to 360° . The second angle is that between the orbital plane and the r. f.: the inclination i . The convention is that when one looks from the ascending node to the origin of the reference frame, the angle is measured counter-clockwise from the r. f.. It can vary from 0° to 180° . If $i < 90^\circ$ the satellite moves in the same direction as the Earth rotates about its axis, direct motion, while if $i > 90^\circ$ the motion is retrograde.

Therefore in this subsection the following parameters are considered:

- rectangular (or Cartesian) coordinates: $X, Y, Z, \dot{X}, \dot{Y}, \dot{Z}$
- orbital elements: $a, e, i, \Omega, \omega, \tau$

In order to go from the Cartesian to these new set of parameters, the angular momentum has to be computed [Montenbruck and Gill, 2005]:

$$\bar{H} = \bar{r} \times \bar{V} = \begin{pmatrix} y\dot{z} - z\dot{y} \\ z\dot{x} - x\dot{z} \\ x\dot{y} - y\dot{x} \end{pmatrix} \quad (4.6)$$



where $r = \sqrt{x^2 + y^2 + z^2}$
 $V = \sqrt{\dot{x}^2 + \dot{y}^2 + \dot{z}^2}$

Fig 4.4 Angular momentum components [Wakker, 2007a]

Also the flight path angle γ can be obtained [Wakker, 2007a]:

$$\bar{r} \cdot \bar{V} = rV \sin \gamma \Rightarrow \sin \gamma = \frac{x\dot{x} + y\dot{y} + z\dot{z}}{rV} \quad (4.7)$$

The semi-major axis and the eccentricity are derived:

$$a = \frac{r}{2 - \frac{rV^2}{\mu}} \quad (4.8)$$

$$e^2 = 1 - \frac{rV^2}{\mu} \left(2 - \frac{rV^2}{\mu} \right) (1 - \sin^2 \gamma) \quad (4.9)$$

By using the previous equation, it is possible to find out the following relations, describing unambiguously the parameter E, called eccentric anomaly (shown in the figure below):

$$e \sin E = \sqrt{\frac{1}{\mu a}} (x\dot{x} + y\dot{y} + z\dot{z}) \quad (4.10)$$

$$e \cos E = 1 - \frac{r}{a} \quad (4.11)$$

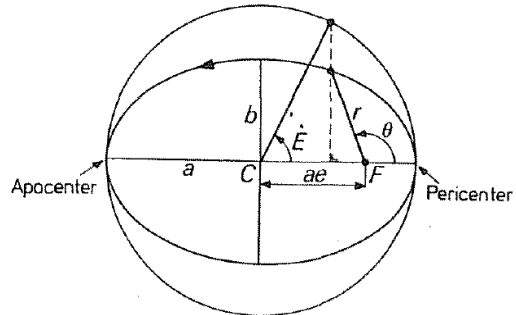


Fig 4.5 Eccentric anomaly [Cornelisse, 1979]

Now it is possible to compute the true anomaly θ and the time of perigee passage τ :

$$\tan \frac{\theta}{2} = \sqrt{\frac{1+e}{1-e}} \tan \frac{E}{2} \quad (4.12)$$

$$\tau = t - \sqrt{\frac{a^3}{\mu}} (E - e \sin E) \quad (4.13)$$

where $\theta/2$ and $E/2$ are located in the same quadrant and t is the moment of time for which the transformation is executed.

So far all in-plane parameters have been computed. Hereafter it is necessary to compute those describing the orbital plane orientation [Wakker, 2007a]. The inclination is given by:

$$i = \arccos \left(\frac{x\dot{y} - y\dot{x}}{H} \right) \quad (4.14)$$

which gives an unambiguous solution for i , since $0 \leq i < 180^\circ$. Subsequently, the following two relations for the RAAN are used:

$$\sin \Omega = \frac{y\dot{z} - z\dot{y}}{H \sin i} \quad (4.15)$$

$$\cos \Omega = \frac{x\dot{z} - z\dot{x}}{H \sin i} \quad (4.16)$$

Two other relations are required to obtain the argument of perigee:

$$\sin(\omega + \theta) = \frac{z}{r \sin i} \quad (4.17)$$

$$\cos(\omega + \theta) = \frac{x}{r} \cos \Omega + \frac{y}{r} \sin \Omega \quad (4.18)$$

For the inverse transformation, from the spherical to the Cartesian coordinates, the procedure is well explained in [Wakker, 2007a], and it will not be reported here, since the goal of this analysis was just to introduce some parameters (RAAN, inclination, etc.) that will be widely used in this work.

4.4 Sphere of Influence

During an interplanetary trajectory, the gravitational forces acting on the spacecraft are generated by all celestial bodies. However, for a first-order analysis one can often build the trajectory such that it is composed of successive central-body (or 2-body) trajectories. The key parameter for this is the so-called sphere of influence of the planets or moons. For the planets, it is the region where the gravitational attraction of the planet is greater than the Sun's attraction. This is similar for the moon's sphere of influence, where the gravitational attraction is greater than that of the corresponding planet. Therefore, the sphere of influence of a celestial body is always considered w.r.t. the body that causes the greatest disturbance acceleration in its vicinity.

The radius of the Earth's sphere of influence is almost three times the mean Earth-Moon distance (920,000 km vs. 384,400 km [Wikipedia website, 2009d]). Therefore, initially, the idea was to consider the S/C as being under the influence of Earth's gravitational field only since the moment of the launch in a transfer path, called geocentric conic, until the instant it reaches the Moon's sphere of influence (first part). There the probe should have been considered under the influence of the Moon's gravitational field (second part). Due to technical problems of the STA Interplanetary Module, as explained in the next chapter, the entire path will be considered in the Earth's sphere of influence, without taking into account the Moon.

Furthermore, in this way perturbations of the other bodies are not taken into account. For this reason when the orbit will be integrated numerically, the perturbation of the Sun will be considered (perturbations due to third body effects will be explained in the next paragraph). The third body effect of the Moon has not been included, because the STA Interplanetary Module (and Interplanetary Low-Thrust Module) didn't allow it.

By using the classical Laplace's definition, an expression for the radius of the sphere of influence of the Moon yields [Wakker, 1997]:

$$R_{s.i.Moon} \approx r_M \left(\frac{M_M}{M_E} \right)^{\frac{2}{5}} \approx 66,300 \text{ km} \quad (4.19)$$

where r_M is the mean distance between the Earth and the Moon (circa 384,400 km) and M_E and M_M are the respective masses.

Even though, the gravitational field generated by the Moon is not taken into account at all, the trajectory obtained will be still reasonably accurate, considered as a first approximation of the real trajectory. That is because the S/C will be flying through the Moon's sphere of influence only for the last small part of the entire trajectory (66,300 km over 384,400 km).

4.5 Perturbations

As explained in section 4.2, the 2BP (as well as the 3BP) doesn't take into account any perturbation. Since some of them can become important for this interplanetary mission, a brief overview on the problem will be given here.

In the previous subsection, the effect due to other celestial bodies has been mentioned already. Within each sphere of influence, only the effect of the main body is considered, but sometimes the perturbation of another body might not be ignored.

Sometimes also other types of perturbations become important. For instance the effect of the solar radiation pressure could be also considered.

Moreover even the effect of the Earth's gravity field asymmetry (for instance J_2) could be taken into account. These choices depend on the magnitudes of the perturbing accelerations. For this reason Fig 4.6 will be used to compare these magnitudes.

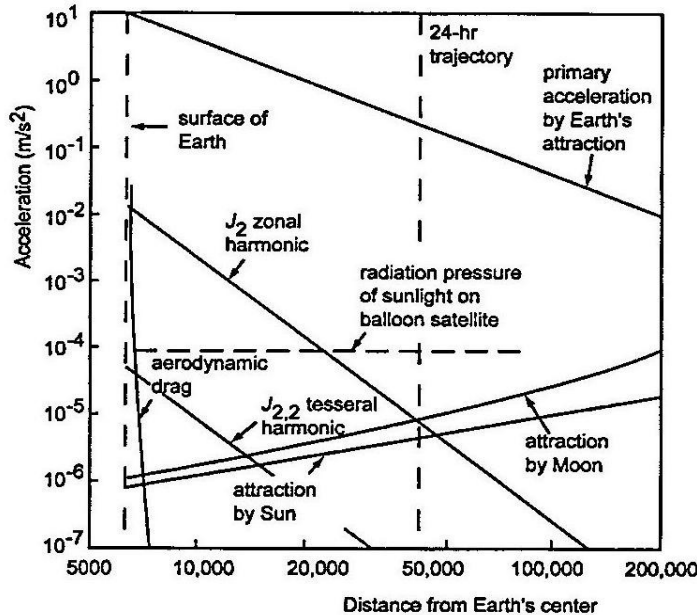


Fig 4.6 Magnitudes of the perturbing forces as function of the distance from the Earth [Wertz, 2001]

From the last figure, it's clear the only effect worth being considered is the third-body effect. Usually the solar radiation pressure contribution is very small, in particular for massive S/C as those used here. That perturbation becomes important for light-weight satellites with a big cross-sectional area.

The effect of the gravity field asymmetry is quite important, but only in a region close to the Earth. The same holds for atmospheric drag. Since these orbits will remain in the neighbourhoods of the Earth for a very short period, those effects will be neglected.

Therefore the only effect considered in this work is the third-body effect. For this reason the components of this acceleration are given here [Wakker, 2007b]:

$$\begin{aligned}
f_x &= \mu_d \left[\frac{x_d - x_s}{\{(x_d - x_s)^2 + (y_d - y_s)^2 + (z_d - z_s)^2\}^{\frac{3}{2}}} - \frac{x_d}{r_d^3} \right] \\
f_y &= \mu_d \left[\frac{y_d - y_s}{\{(x_d - x_s)^2 + (y_d - y_s)^2 + (z_d - z_s)^2\}^{\frac{3}{2}}} - \frac{y_d}{r_d^3} \right] \\
f_z &= \mu_d \left[\frac{z_d - z_s}{\{(x_d - x_s)^2 + (y_d - y_s)^2 + (z_d - z_s)^2\}^{\frac{3}{2}}} - \frac{z_d}{r_d^3} \right]
\end{aligned} \tag{4.20}$$

where the subscript d is used for the disturbing body, the subscript m for the main body and the subscript s for the spacecraft. The two distances are considered from the main body.

The third-body effect will be used only for high-thrust trajectories. In the 3-body formulation, already the effect of a third-body is somehow considered (since two bodies are generating the gravity field). In principle also a second third-body effect could be taken into account (the Sun in the Earth-Moon system and the Moon in the Sun-Earth system), but the complexity of the implementation and integration of such a effect didn't allow its use. The differences expected are quite small and actually the use of a real ephemerides model (that takes into account the gravity field of all celestial bodies) can reduce the total ΔV even, as shown in [Canalias and Masdemont, 2008].

The same holds for low-thrust trajectories. Also in this case the three-body effects don't really affect the final computations, as shown in [Herman and Conway, 1998]. Therefore perturbations will be not used in these kinds of trajectories.

Moreover this is a preliminary design study, therefore a first approximation of the real trajectory is the goal of this work. The use of perturbations is left to future refinements.

4.6 Manoeuvres

In this paragraph, an overview of the different kinds of manoeuvres will be given. They will be used in order to inject the S/C from the parking orbit around the Earth into the transfer orbit and then into the final lunar orbit. Moreover they will be used also in the 3-body trajectories to let the S/C switch legs of the entire transfer orbit (see section 7.3) and in the low-thrust trajectories too.

Three different types of manoeuvres will be discussed:

- change of inclination
- change of altitude
- combined change of altitude and inclination
- “given” manoeuvre

Finally the Tsiolkovsky law will be addressed.

4.6.1 Change of Inclination

Only a one-shot manoeuvre has been considered:

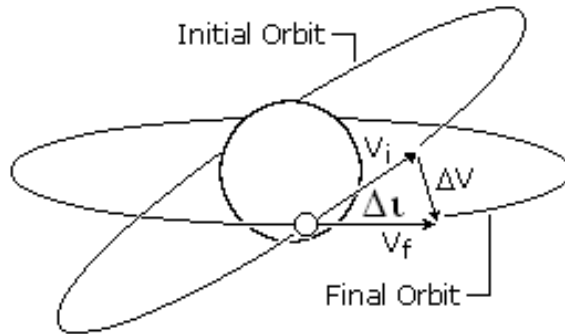


Fig 4.7 Change of inclination [after Rocket and Space Technology website, 2009]

$$\Delta V = 2V \sin \frac{\Delta i}{2} \quad (4.21)$$

where V is the local circular velocity and Δi the change of inclination required.

It allows to compute the ΔV required for a manoeuvre with just a change in inclination, without changing other orbital parameters. This is not the optimal way to perform a change of inclination, because a higher orbit can be used (at least ten times the initial altitude), with a propellant save. Anyway it would be very small [Wakker, 2007b]. In alternative a combined manoeuvre can be considered to change altitude and inclination at the same time (treated in section 4.6.3).

4.6.2 Change of Altitude

The classical transfer orbit for which the propellant consumption is minimal is an elliptical orbit that touches the initial orbit at the pericenter and the final orbit at the apocenter: the Hohmann transfer.

The well-known drawback of this manoeuvre is the TOF, usually very long, but in this case the Hohmann transfer will be used only to increase the altitude of a parking orbit, and not for the transfer orbit. For this reason the TOF will be reasonably short.

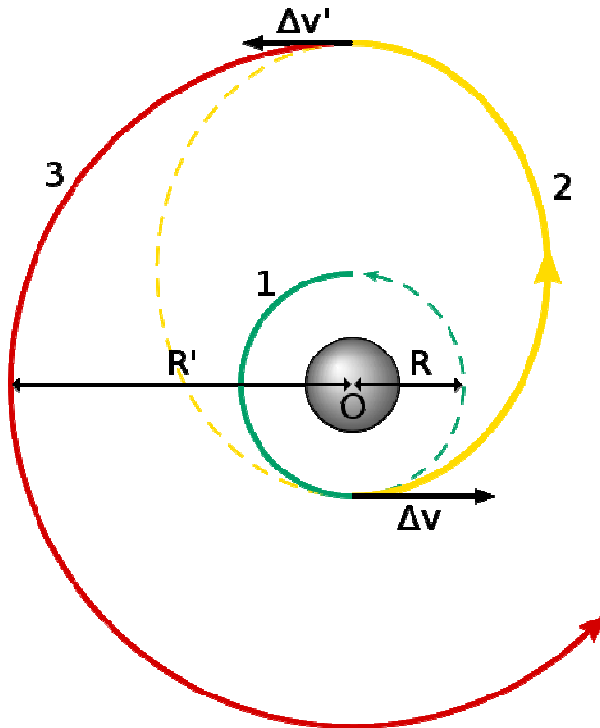


Fig 4.8 Hohmann transfer [Wikipedia website, 2009a]

Now the equations to compute the two ΔV 's and the TOF are given [Wakker, 2007b]:

$$\begin{aligned} \Delta V &= \sqrt{\frac{\mu}{R_1}} \left(\sqrt{\frac{2R_3}{R_1 + R_3}} - 1 \right) \\ \Delta V' &= \sqrt{\frac{\mu}{R_3}} \left(1 - \sqrt{\frac{2R_1}{R_1 + R_3}} \right) \\ TOF &= \pi \sqrt{\frac{(R_1 + R_3)^3}{8\mu}} \end{aligned} \quad (4.22)$$

where R_1 and R_3 are the altitudes of the initial and final orbits respectively.

4.6.3 Combined Change of Inclination and Altitude

It is executed combining a Hohmann transfer and two changes of inclination. The total change of inclination is split in two manoeuvres, the first one is executed at the same time with the first shot of the Hohmann transfer and the second one with the second shot of the Hohmann transfer:

$$\Delta i = \Delta i_1 + \Delta i_2 = s\Delta i + (1-s)\Delta i \quad (4.23)$$

where the coefficient s represents a percentage of the total inclination change.

The magnitudes of the manoeuvres are given [Vallado and McClain., 2001]:

$$\Delta V_1 = V_{C_1} \sqrt{1 + R_A^2 - 2R_A \cos \Delta i_1} \quad (4.24)$$

$$\Delta V_2 = V_{C_2} \sqrt{1 + R_B^2 - 2R_B \cos \Delta i_2} \quad (4.25)$$

where $R_A = \sqrt{2 \frac{R_3}{R_1 + R_3}}$ and V_{C_1}, V_{C_2} are the local circular velocity at R_1 and R_3 respectively.

$$R_B = \sqrt{2 \frac{R_1}{R_1 + R_3}}$$

The previous equations can be used to combine a change of inclination with any other out-plane manoeuvres, since it came from the more general formula [Vallado and McClain., 2001]:

$$\Delta V = \sqrt{V_i^2 + V_f^2 - 2V_i V_f \cos \Delta i} \quad (4.26)$$

where V_i and V_f are the velocities before and after the manoeuvre respectively.

The optimal distribution of the total inclination change Δi is given by the parameter s . An estimated (accurate to about 0.5°) value can be computed in the following way [Vallado and McClain., 2001]:

$$s \approx \frac{1}{\Delta i} \tan^{-1} \left(\frac{\sin \Delta i}{\frac{V_{C_1}^2 R_A}{V_{C_2}^2 R_B} + \cos \Delta i} \right) \quad (4.27)$$

Knowing s , Δi_1 and Δi_2 can be determined by using equation 4.23. Finally, the scalar magnitudes of the two velocity impulses can be derived from equations 4.24 and 4.25.

4.6.4 “Given” Manoeuvre

Finally a generic manoeuvre is considered. When two different legs (indicated with subscripts 1 and 2) of a trajectory have to be patched and the conditions at the border are known, then the manoeuvre required is “given”. In all those cases, the ΔV can be easily computed in the following way:

$$\Delta V = \sqrt{(V_{x1} - V_{x2})^2 + (V_{y1} - V_{y2})^2 + (V_{z1} - V_{z2})^2} \quad (4.28)$$

4.6.5 Tsiolkovsky Law

In this subsection a formula to compute the propellant consumption will be given. It is the well-known Tsiolkovsky rocket equation or ideal rocket equation. It gives an excellent approximation of the propellant consumption for continuous short manoeuvres (it is exact for impulsive ones). It doesn't take into account the gravity losses in case the manoeuvre is not executed at pericenter or apocenter of the trajectory, because the manoeuvre is considered instantaneous.

The law states [Wertz, 2001]:

$$m_1 = m_0 e^{\left(-\frac{\Delta v}{I_{sp} g_0} \right)} \quad (4.29)$$

where g_0 is the gravity acceleration at the Earth's surface equal to 9.80665 m/s^2 [Wertz, 2001], m_0 and m_1 respectively are the initial and final mass of the S/C, I_{sp} is the specific impulse of the motor and ΔV represents the magnitude of the manoeuvre.

The choice of the motor is fundamental in order to evaluate the propellant consumption, for this reason in the next subsection a high-thrust motor will be selected. It will be used for all the manoeuvres computed in this work.

4.6.6 High-Thrust Motor

In order to evaluate the propellant consumption after every manoeuvre, the specific impulse of the motor should be known. For this reason, during the literature study [Zuccarelli, 2008], many high-thrust motors have been analyzed in order to choose the best one for this mission. Actually it is assumed the launcher will deliver a S/C into a LEO orbit. Thereafter all the impulsive manoeuvres (for every payload and every kind of trajectory) will be executed by using motors on board. The high-thrust engine is defined here, while the low-acceleration engine will be described in section 8.3.

The motor selected is the RD-0126E [Astronautix, 2008]. This is a Russian concept for a cryogenic engine for upper stages. This is a design concept, but it is expected to fly before 2010. It should be included in the improved version of the Soyuz launcher, called Onega, that will be able to double the actual payload.

| Propellant | O/F mass ratio | Thrust (kN) | I_{sp} (s) | Burn time (s) | Mass Engine (kg) |
|---------------------|----------------|-------------|--------------|---------------|------------------|
| LOX/LH ₂ | ≈ 6 | 39.2 | 472 s | n/a. | 234 |

Table 4-A RD-0126E performances [Astronautix, 2008]

4.7 Lambert's Problem

The two-point boundary value problem for Keplerian motion, also known as Lambert's problem, is a classical one in astrodynamics. It's treated and tackled here, because the STA Interplanetary Module is based on it. For this reason it's presented briefly.

The goal is to find an unperturbed orbit about a given inverse-square-law centre of force C connecting the given points P₁ and P₂ with a specified flight time Δt [Gooding, 1990].

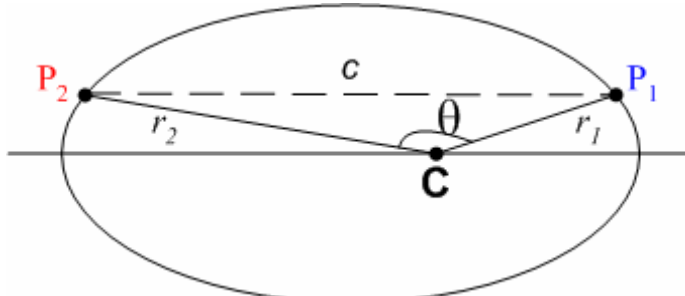


Fig 4.9 Geometry of Lambert's problem

During time, different forms of algorithms have been suggested by several mathematicians searching for computing procedures leading to more efficiency, generality and accuracy in order to solve Lambert's problem.

The approach of [Battin, 1987] will be treated here, because this method was initially also used by [Schouten, 2006] for the development of the interplanetary module in the STA-software.

A representation of the geometry of the problem is given in Fig 4.9. Here, P₁ is the geometrical position of the departure planet at time t₁ and P₂ is the geometrical position of the target planet at time t₂.

The input data for the Lambert-problem solution are the gravitational parameter μ of central force field, the position vectors \bar{r}_1 and \bar{r}_2 and the corresponding transfer time Δt . The desired output data consists of the initial and final velocity vectors \bar{V}_i and \bar{V}_f of the conic section, used to compute the magnitudes of the manoeuvres to follow this trajectory.

The starting equation required to solve the problem is the transfer-time equation which is derived from Kepler's equation:

$$\Delta t = \sqrt{\frac{a^3}{\mu}} (E_2 - E_1 - e(\sin E_2 - \sin E_1)) \quad (4.30)$$

It relates the required transfer time Δt with the semi-major axis a , the gravitational parameter μ , the transfer orbit eccentricity e and the eccentric anomaly (E_1 and E_2) at the departure and arrival object. Here, a , E_1 , E_2 and e are unknowns and can be derived by iteration and by introducing several new parameters.

In a number of steps given in [Battin, 1987], the last equation can be transformed into two expressions, which are used to calculate the semi-major axis and the initial and final velocity vectors of the conic section. Full details of the procedure will be not explained here, because it has been implemented already in the STA Interplanetary Module.

CHAPTER 5

5. High-Thrust Trajectories: Results

In this chapter, the results obtained by using the STA Interplanetary Module will be addressed. This module, already developed by Bert Naessens, has been integrated in STA by the author of this work, in order to use it and plot the final trajectory.

For this reason, a brief introduction to this tool will be given, in order to explain how the high-thrust transfer orbit has been computed. Then all the results will be collected and discussed.

5.1 STA Interplanetary Module

Three different modes that are part of the STA Interplanetary Module are interesting for this work and are described below:

- **Launch Window mode (LW):** The launch window mode is able to search for the optimal launch window of the interplanetary arc. It means that this mode will search for the optimal departure and arrival dates of the respective departure and arrival planets. The output of this mode can generate pork-chop plots and the hyperbolic excess velocities with respect to the departure and arrival planet given.
- **Numerical targeting mode (TARG):** The targeting mode searches for the departure conditions of the spacecraft in its departure orbit in order to reach the target orbit. The primary objective is to arrive at the specified pericenter-radius of the target orbit. Additionally, the target is also specified by its inclination and/or RAAN. However, the target orbit that satisfies both inclination and RAAN is not always possible. Therefore, extra manoeuvres will be required to get into the final orbit once the arrival orbit is reached.
- **Numerical simulation mode (SIM):** The numerical simulation mode is able to generate a trajectory in our solar system by using a numerical propagation method. The user has to give the initial state conditions, time, central body and ΔV manoeuvres. During interplanetary flight, each planet can be selected to be taken into account as a third body. Once the spacecraft is within the sphere of influence of a planet, the Sun can be selected as a third body. The output file contains state-vectors of the trajectory within a specific reference frame such that the trajectory can be visualized.

Inputs/outputs and the model/optimizer adopted for each mode are summarized in the following table:

| Mode | Inputs | Outputs | Model/Optimizer |
|------|--|---|---|
| LW | - Initial-final altitudes - Launch window | - Departure-Arrival Epochs - Pork-chop plots | - Lambert's problem - GA |
| TARG | - Departure-Arrival Epochs - Initial/final altitudes - Final inclination or RAAN | - Initial conditions - Manoeuvres | - 2BP + 3 rd body effect - GA |
| SIM | - Initial conditions | - Transfer orbit | - 2BP+ 3 rd body effect - GA |

Table 5-A Inputs/outputs and the model/optimizer adopted for each mode

The idea is to use these 3 modes in series. The LW mode should be used to reduce the launch window, then by using the TARG mode on the reduced launch window the selection of the final orbit (almost polar for this mission) will be possible in order to find the proper initial conditions. Finally, by applying the SIM mode to the initial conditions obtained, the complete orbit integration will be executed.

In the next paragraphs each mode will be briefly discussed along with its respective results.

It is worth emphasizing that this module makes widely use of an optimizer based on a Genetic Algorithm (GA) developed by the Massachusetts Institute of Technology. As for all GA optimizers, also here the optimization process has to be run several times in order to find the best solution. Therefore all simulations involving GA optimizers in each STA module used have been repeated many times (3-5 times depending on the discrepancy of the results) and only the best result has been considered

5.2 Launch Window Mode

To design optimal interplanetary trajectories, it is essential to analyze the launch window of an interplanetary transfer arc, because the position of the planets w.r.t. the time limits the opportunities for interplanetary transfers with minimum required energy. The launch window analysis mode is able to determine the optimal departure date and travel time for a specified transfer between two planets. This is done using JPL ephemerides of the planets (the same used in all other STA modules and implemented by the author of this work), a Lambert solver and a genetic algorithm.

An example of the GUI launch window mode is given in Fig 5.1. The user has to select departure and arrival planets. Then the user has to select a lower and upper limit for the transfer time. Moreover the user can require a pork-chop plot. If so, the number of steps within the given time ranges has to be given. Finally, settings for the GA are required. In this case default values have been selected.

All the inputs used for this mission are contained in the following figure.

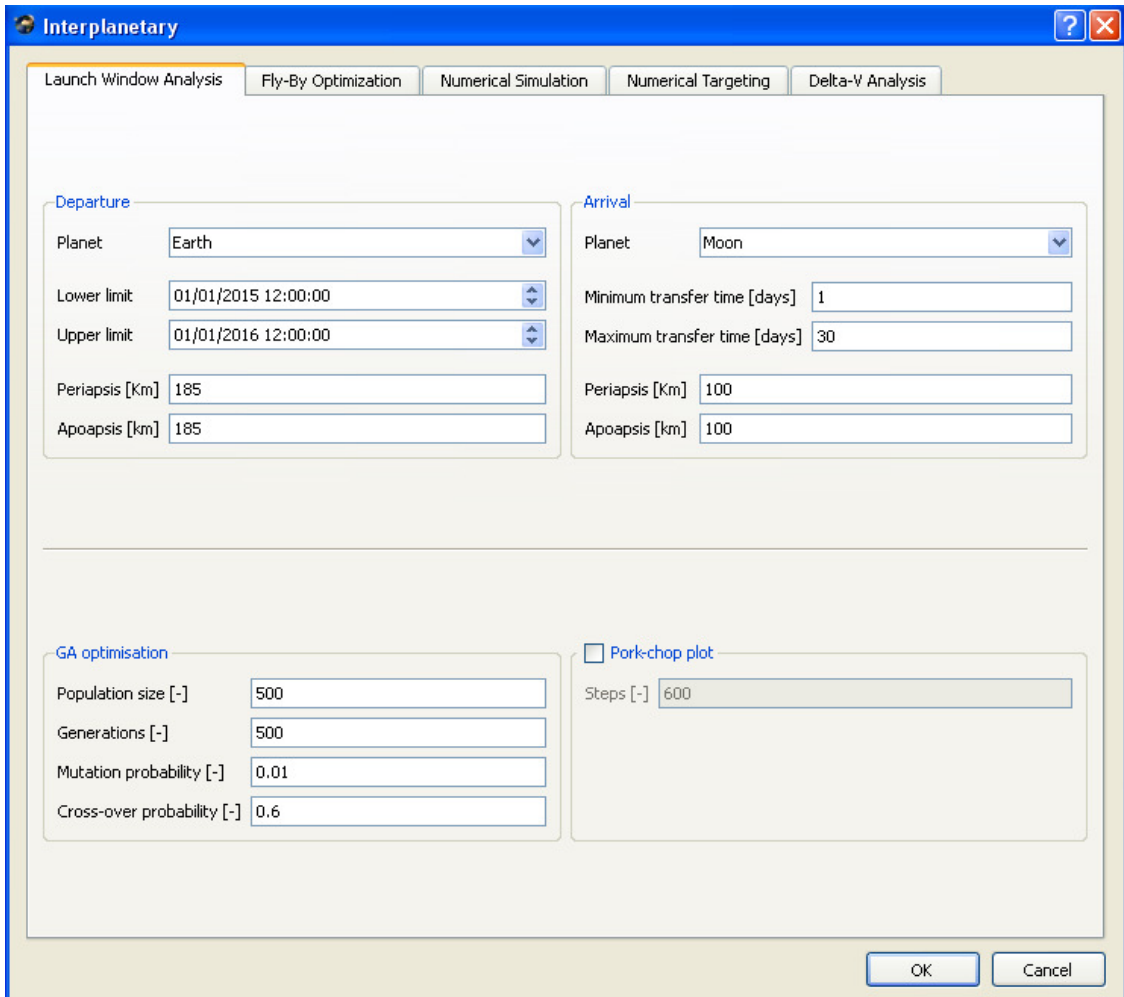


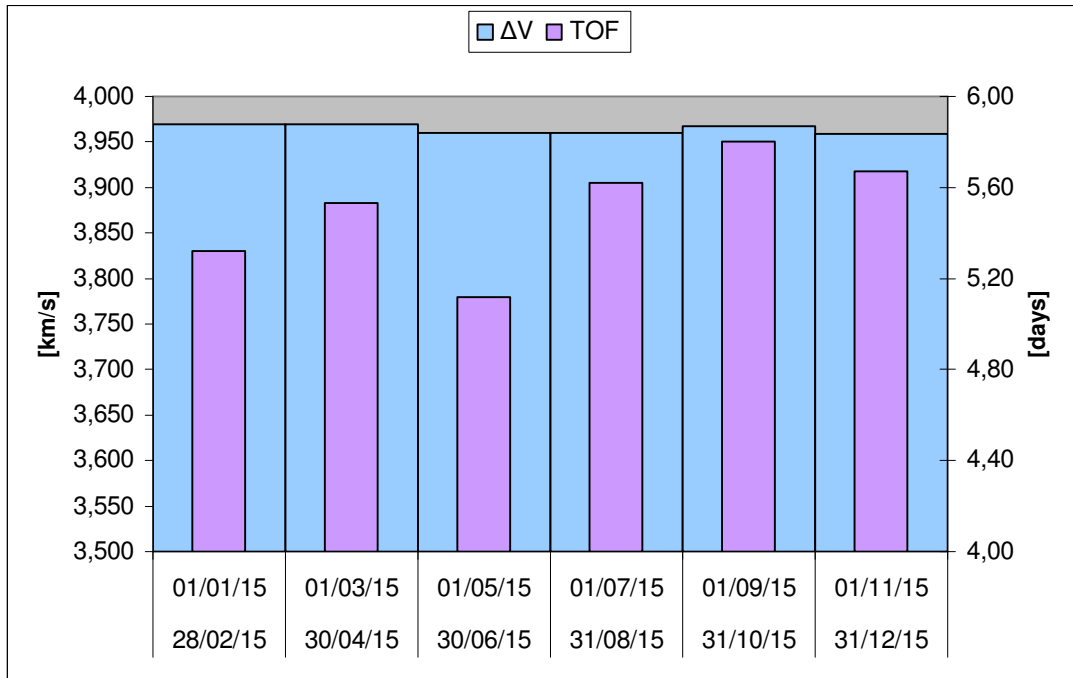
Fig 5.1 Interplanetary module: LW mode GUI

In this case a pork-chop plot is not required. This is a useful visualization that shows the relationship between departure date, arrival date and required energy at departure and arrival. It is very helpful in case of long interplanetary missions, because then the geometry of the problem repeats only after long periods.

In this case the period of the system allows many launch windows per year and it matches the requirement of having many launches per year. In order to verify it, this mode has been run every two months for the year 2015. Then it has been launched all along the year 2016 to check if there are significant variations in the total ΔV computed. In the next table and in the next figure all results have been collected.

| Lower Limit | Upper Limit | Total ΔV (km/s) | TOF (days) |
|-------------|-------------|-------------------------|------------|
| 01/01/2015 | 28/02/2015 | 3.969 | 5.32 |
| 01/03/2015 | 30/04/2015 | 3.969 | 5.53 |
| 01/05/2015 | 30/06/2015 | 3.960 | 5.12 |
| 01/07/2015 | 31/08/2015 | 3.960 | 5.62 |
| 01/09/2015 | 31/10/2015 | 3.967 | 5.80 |
| 01/11/2015 | 31/12/2015 | 3.959 | 5.67 |
| 01/01/2016 | 31/12/2016 | 3.966 | 5.57 |

Table 5-B Results LW simulations

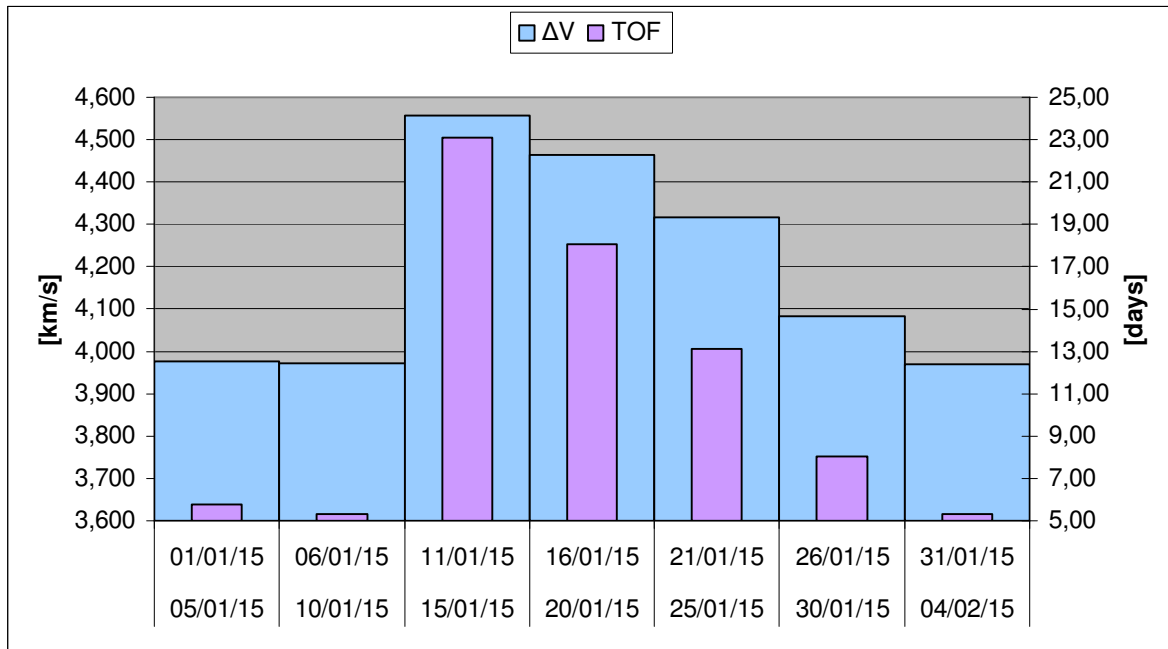
Fig 5.2 ΔV and TOF functions of two months periods in 2015

Then a second more detailed analysis has been done in order to check if there are differences within the same launch window identified in the last simulation. Therefore the first two months period has been split again in smaller periods.

First a simulation per month has been launched. Then, since the geometry of the system should repeat every 29 days (lunar period), due to the particular geometry of the problem, the first month has been split in periods of 5 days, and the results have been compared in the next table and in the next figure:

| Lower Limit | Upper Limit | Total ΔV (km/s) | TOF (days) |
|-------------|-------------|-------------------------|------------|
| 01/01/2015 | 31/01/2015 | 3.971 | 5.62 |
| 01/02/2015 | 28/02/2015 | 3.969 | 5.32 |
| 01/01/2015 | 05/01/2015 | 3.977 | 5.76 |
| 06/01/2015 | 10/01/2015 | 3.971 | 5.32 |
| 11/01/2015 | 15/01/2015 | 4.556 | 23.11 |
| 16/01/2015 | 20/01/2015 | 4.463 | 18.06 |
| 21/01/2015 | 25/01/2015 | 4.316 | 13.11 |
| 26/01/2015 | 30/01/2015 | 4.083 | 8.06 |
| 31/01/2015 | 04/02/2015 | 3.969 | 5.32 |

Table 5-C Results LW simulation to further reduce the launch window

Fig 5.3 ΔV and TOF functions of five days periods in January 2015

The total ΔV presented just small differences in the order of few m/s from month to month, but within the same lunar period there are not negligible differences. It means that many different launches are possible within the same month, but they are concentrated in a period of 10-15 days (01-10/01 and 26-30/01). In the other two weeks the total ΔV strongly increases as well as the TOF.

It's not required to specify any launch date in case this option will be selected, since at least every month there are two weeks suitable. Then it's assumed that at least every month it is possible to launch a S/C following a high-thrust trajectory with the same total ΔV and the same payload mass.

Therefore in the numerical targeting mode, that requires high computational efforts, only the best case (smallest total ΔV) will be considered. The optimal departure and arrival epochs obtained for the period 01/11/2015-31/12/2015 are here reported:

| Departure Epoch | Arrival Epoch |
|-----------------|---------------|
| 29/11/2015 | 05/12/2015 |

Table 5-D Optimal departure and arrival Epochs

5.3 Numerical Targeting Mode

The numerical targeting mode provides the user with the required starting condition around the departure planet in order to arrive at the target planet within a desired accuracy. Using the optimal departure and arrival dates, derived from the previous mode, as inputs to the program Table 5-A, optimization will be done in order to minimize the distance to the target altitude

and arrive at a preferred inclination or RAAN (w.r.t. the ecliptic plane) around the target body. In this case a quasi-polar orbit is required, therefore an inclination of 89° will be specified (see section 3.2.2), leaving free the RAAN.

In the GUI the target inclination is referred to the ecliptic plane. Because of the particular geometry of the system (shown in Fig 5.4), the inclination to the ecliptic as well as the axial tilt of the Moon have to be taken into account, depending on the phase in orbit considered (here it becomes 110.82°).

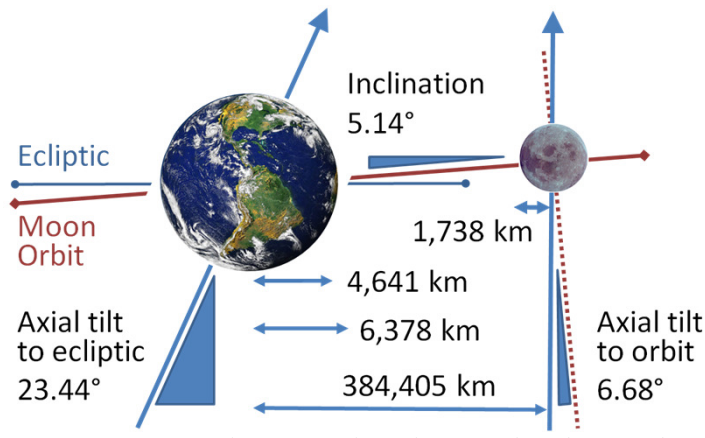


Fig 5.4 Moon inclination to the Ecliptic [Wikipedia, 2009b]

The GUI window for the numerical targeting mode is given in Fig 5.5. As can be observed, the user will be asked to define the departure and arrival time with the respective central bodies. The pericenter and apocenter altitudes of the departure and arrival orbits need to be specified in order to determine the required ΔV and target altitude. The altitude of the lunar orbit will be 100 km (as already specified in section 3.2.2).

Furthermore the user can select which perturbing body should be taken into account. As explained in section 4.4, only the solar third-body effect is considered. Many different trials have been done in order to include also the Moon effect, but either the computational time became very long (in the order of days!!!) or the software simply crashed. Also a look at the code has been taken in order to find the error, but it has not been found. Since the time required to check the code written and implemented by someone else usually takes a lot of time, for this first approximate orbit that perturbation has not been included.

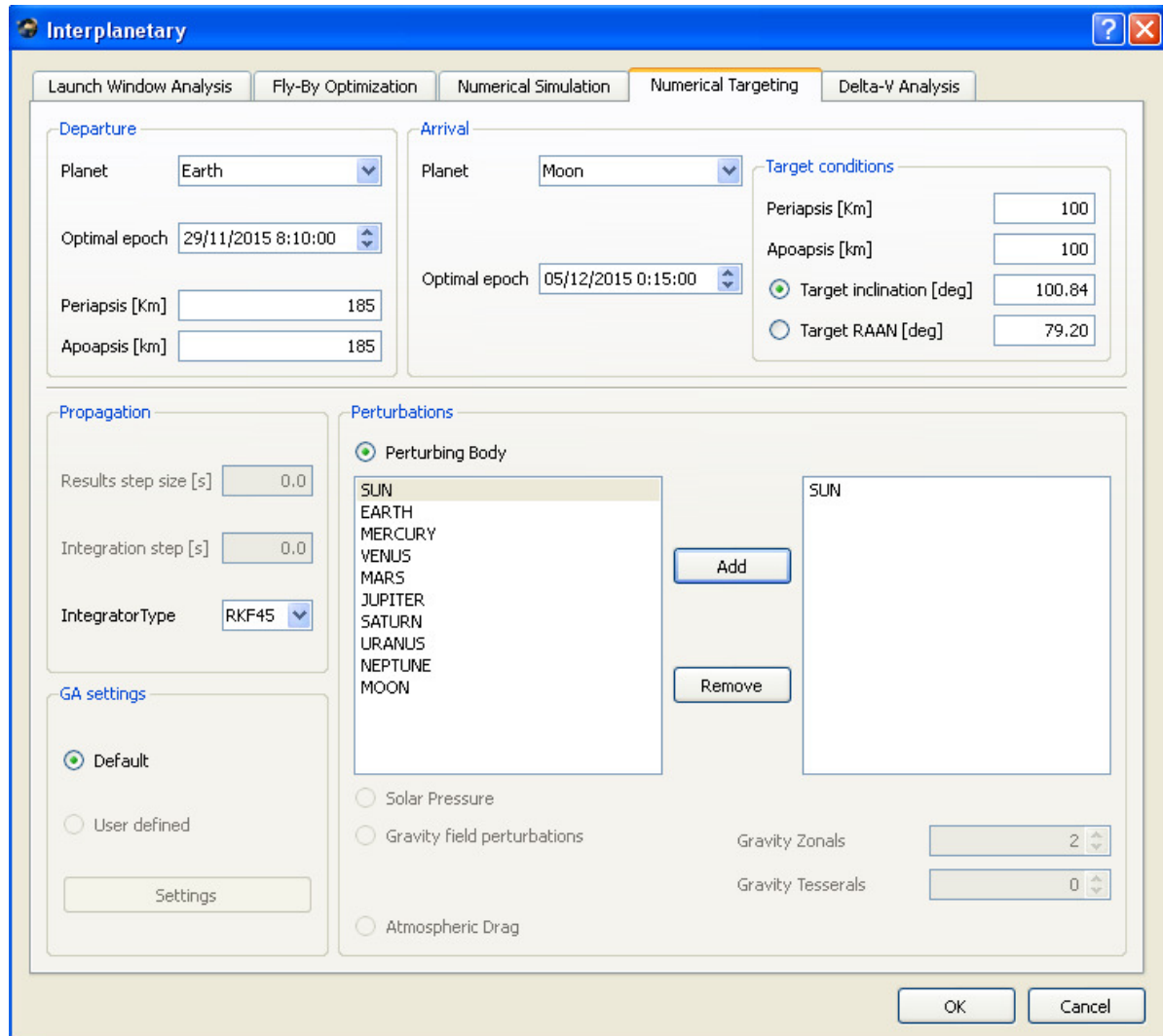


Fig 5.5 Interplanetary module: TARG mode GUI

The outputs obtained (as explained in Table 5-A) are the initial conditions around the Earth, actually the initial orbit, given in Keplerian elements; the final orbit obtained and the total ΔV required to inject into the transfer orbit and to leave it, once the S/C will have reached the Moon.

In the following table these results are summarized:

| Initial orbit | | Lunar parking orbit | |
|-------------------------------|------------|-------------------------------|------------|
| Altitude (km) | 185 | Altitude (km) | 105 |
| Inclination ($^{\circ}$) | 18.1 | Inclination ($^{\circ}$) | 88.79 |
| RAAN ($^{\circ}$) | 10.84 | RAAN ($^{\circ}$) | 46.38 |
| Departing epoch | 30/11/2015 | Arrival epoch | 04/12/2015 |
| ΔV_2 to escape (km/s) | 3.390 | ΔV_3 to inject (km/s) | 0.695 |

Table 5-E Results TARG simulation

The TOF obtained is 5.18 days.

Since the obtained inclination of the initial orbit is different from those specified for the parking orbits (see section 3.2.1), a manoeuvre to change only inclinations is required (since the altitude has been matched). By using equations 4.26, the ΔV 's required to change the inclination are combined with ΔV 2 for each inclination:

| Initial inclination ($^{\circ}$) | $\Delta V_1 + \Delta V_2$ (km/s) |
|------------------------------------|----------------------------------|
| 5 | 4.004 |
| 28.5 | 3.789 |
| 51.6 | 6.362 |

Table 5-F ΔV required to correct the initial inclination

As already explained, that is not the way to fully optimize the transfer trajectory, since this last manoeuvre is not part of the optimization process. By the way, all this work has to be assessed within the STA framework, therefore this module had to be used as it was, since this change would have required too much time.

Anyway, by using the Tsiolkovsky law (see section 4.6.5), considered the engine selected in section 4.6.6, now it's possible to compute the LLO mass and then the Moon payload delivered on the Moon, since all manoeuvres have been quantified:

| Launcher | $\Delta V_1 + \Delta V_2$ (km/s) | ΔV_3 (km/s) | Total ΔV (km/s) | LEO mass (tons) | LLO mass (tons) | Moon Payload (tons) |
|----------|----------------------------------|---------------------|-------------------------|-----------------|-----------------|---------------------------------------|
| Ariane V | 4.004 | 0.695 | 4.699 | 22.6 | 8.189 | 2.289 |
| Proton | 6.362 | 0.695 | 7.057 | 21 | 4.920 | 0 |
| Ares V | 3.789 | 0.695 | 4.484 | 130 | 49.341 | 2.341 (M) 29.341 (U) |
| Ares I | 3.789 | 0.695 | 4.484 | 25 | 9.489 | 3.589 |
| Atlas V | 3.789 | 0.695 | 4.484 | 20.25 | 7.686 | 1.786 |

Table 5-G Final Moon payload deliver per each launcher

From the last table and from section 2.5 it is clear that the only launcher able to build the lunar base by using this kind of trajectory is Ares V. The values in the last column have been computed from the previous one considering the corrections shown in Table 2-F and in Table 2-G. In order to use other launchers to carry a module of the base, at least 10.9 tons of LLO mass should be delivered. Therefore only Ares V is considered suitable for this mission by means of this trajectory. Furthermore Ares V is also suitable for manned missions, since the minimum LLO mass required was 47 tons, assuming zero the Moon payload (see section 2.5).

The transfer trajectory will be shown in the next paragraph.

The value found for the total ΔV from Cape Canaveral seems reasonable, since the Apollo 11 mission had a total ΔV of 3.943 (see section 3.1.1), but the final orbit was not a lunar polar orbit. In order to have a transfer orbit able to inject into such a polar orbit, an extra ΔV has been required at the beginning of the transfer orbit, in order to match the proper inclination of the trajectory (Table 5-F).

5.4 Numerical Simulation Mode

The numerical simulation mode is able to construct trajectories by using numerical integration. First, the user should define the initial state of the S/C, by setting the initial time and by selecting the central body, and by giving the initial state vector in Cartesian or Keplerian elements.

At the initial position, in case the Keplerian elements have been provided, the user has to insert a ΔV manoeuvre in terms of a vector.

The maximum flight time (in days) defines the stopping condition of the propagated trajectory. The implemented integrator is the Runge-Kutta-Fehlberg method of the 4(5th) order.

Finally, the user has to select the perturbations that have to be taken into account during trajectory propagations. At this moment, only third body perturbations can be selected. In this case the Sun has been selected as cause of third body perturbations. The perturbations due to solar radiation, gravity field perturbations and aerodynamic drag still have to be implemented into the program, but anyway, as already explained in section 4.5, they are not required for this mission.

All these inputs come from the computation done in the previous mode, therefore a simple numerical integration is performed starting by specified initial conditions.

The output of this mode is such that the Cartesian state vectors are given with respect to the ecliptic heliocentric reference frame. With the use of this output file, the trajectory can be visualized in a heliocentric reference frame, and it's shown in next two figures:

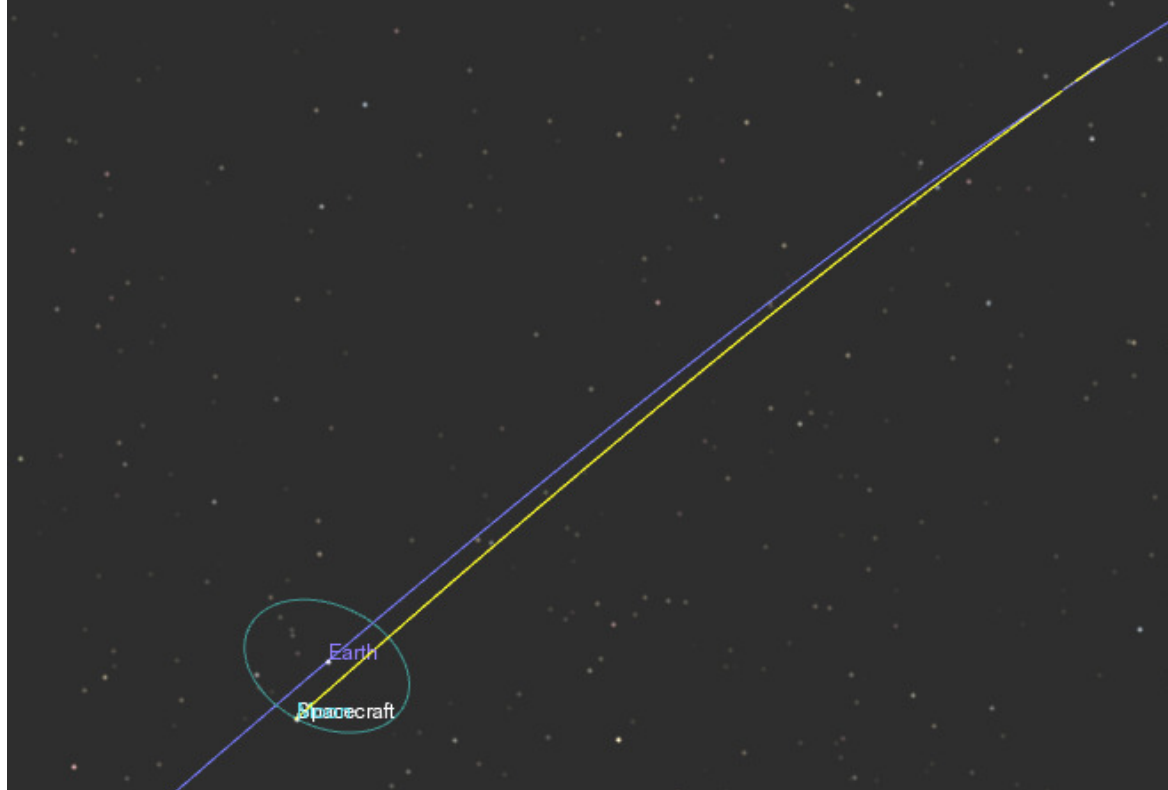


Fig 5.6 Earth-Moon high-thrust trajectory screenshot 1

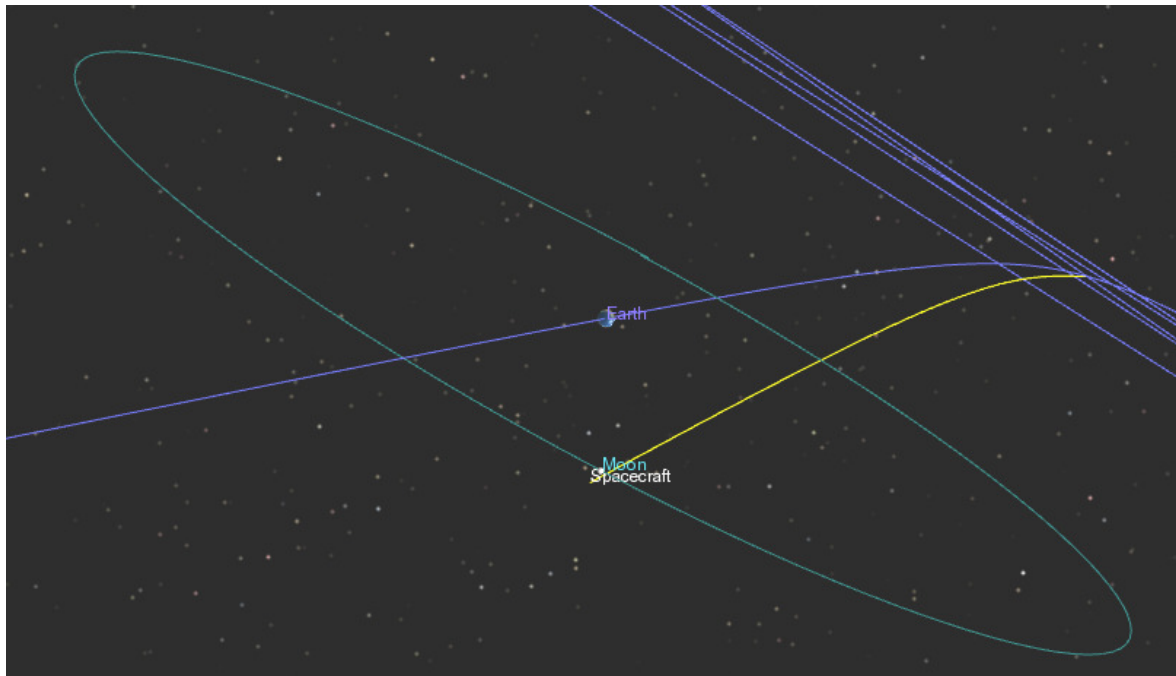


Fig 5.7 Earth-Moon high-thrust trajectory screenshot 2

CHAPTER 6

6. Three-Body Trajectories: Theory

In this chapter, the theory of the 3BP will be explained in order to give some basic knowledge to the reader. Therefore the equations of motion, the definition of Lagrangian points, the computation of Halo orbits and manifolds trajectories will be addressed here.

In parallel with these theoretical explanations, also the software used to do all the computations will be presented and discussed in detail. As a requirement for this work, all the computations have to be executed by using STA. At this purpose, the author of this work developed the STA 3-Body Module (3BM), during his internship at ESA ESTEC.

6.1 Introduction to 3BP and 3BM

The most used model for trajectories design is the 2-body problem (already explained in Chapter 4), where a satellite, with negligible mass, is gravitating around a central body. In order to improve this simple model, usually some perturbations are considered (drag, effects due to gravity field asymmetry, third-body effect, radiation pressure, etc.). Amongst them, for interplanetary trajectories, the third-body effect becomes very relevant. This perturbation is determined by the gravity field of another main body disturbing the motion around the first body. In this way the attraction by the third body is considered just as a perturbation, while its gravity field creates a complete different environment for the satellite.

Therefore the idea is to include this third body directly within the model in order to use the advantages given by this adjunctive mass. This model (called 3-body problem) becomes very important when a S/C moves far away its main body, actually for interplanetary trajectories.

The deep space can be considered as divided in spheres of influence (as explained in section 4.4). For each of them the centre is occupied by a main body and the main force acting on a S/C is given by its gravity field. As a first approximation, interplanetary trajectories can be computed by using the 2-body model, switching the central body when transiting from one sphere of influence to another. Typically, spheres of influence are located within other spheres of influence and frequently the effect of the outer main body spheres is not negligible at all. It is the case of the Earth-Moon system, where the effect of the Sun is quite relevant.

Therefore an STA module has been developed, in order to deal with this “advanced” model, and to improve designs of those missions relevant for this problem. For this reason this new module allows the user to propagate a trajectory within the 3-body problem.

Besides, the use of such a model brings new fancy features, not present in the 2-body problem. The most evident one is the availability of new trajectories. Amongst them the Halo orbits are the most attractive for space missions, they are quasi-stable orbits around the Lagrangian points. Actually if a S/C is sent to one of them it could remain there for many orbits requiring just very small corrective manoeuvres to keep the initial orbit. It is clear that applications for these orbits are numerous and for this reason, in the last few years, many missions focused on these trajectories have been planned and already started (as the SOHO mission, launched in 1995 and shown in Fig 6.1).

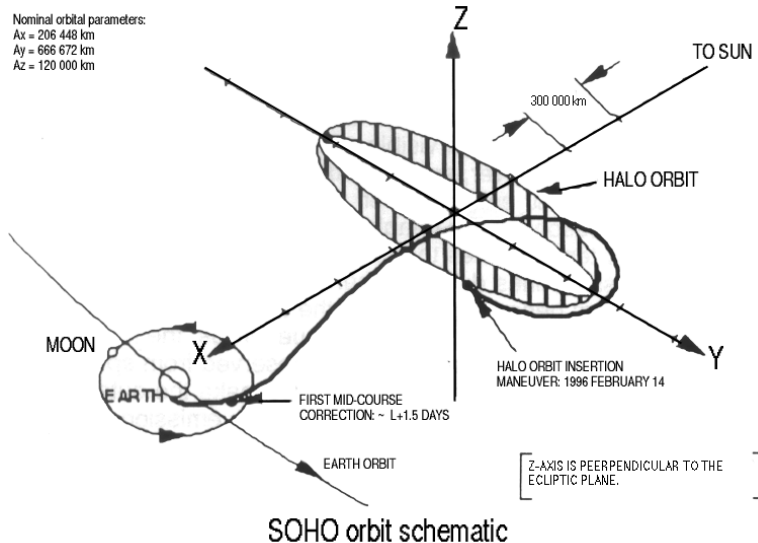


Fig 6.1 SOHO trajectory [MSU Polar Physics website, 2009]

Moreover these orbits have another interesting property. If the S/C is a bit perturbed from the reference orbit, it can escape from the Halo orbit and can follow a trajectory guiding the S/C toward one of the main bodies, or outward of the system. All these trajectories can be seen as a stream of trajectories (because from each point of the Halo orbit departs a different trajectory in both directions), and together they are combined in so-called manifolds. On the other way around it could be possible to follow them in the opposite way, from outside the system toward the Halo orbit itself.

It is intuitive that it could be possible to use these manifold trajectories in order to get to these Halo orbits from a parking orbit around a main body, or to jump from one system to another one.

All these “special” features belong to the 3BP, and they will be analyzed in this chapter.

The 3BM allows the user to compute these particular orbits and to optimize the transfer between a parking orbit around a main body and the Halo orbit desired, minimizing the propellant consumption. This functionality could be used to send communication satellites in the L2 point of the Earth-Moon system, as required for this mission (see sections 2.3-2.6).

Moreover the 3BM also allows the user to design a transfer trajectory able to connect a parking orbit around the Earth and another one around the Moon by patching two different 3-body systems: Sun-Earth and Earth-Moon. In this way, manifolds are used as a highway able to link the Earth and the Moon, and that is the most interesting application of the 3BM for this work. This functionality could allow to find a new transfer trajectory, hopefully cheaper than the usual ones (see Table 3-A).

| 3BM Mode | Theory required |
|---|---|
| 1) Trajectory propagator | CR3BP Equations of Motion, Jacobi's constant |
| 2) Halo orbit and manifolds computation | Numerical computation of Halo orbits and manifolds trajectories |
| 3) Transfer orbit optimization | As above |
| 4) Earth-Moon transfer orbit | 3-body systems patching |

Table 6-A 3BM functionalities scheme

The 3BM presents four different main functionalities (modes, as shown in Table 6-A). All of them will be used during this work. Therefore they will be explained in parallel with the theory behind each of them. First the basic theoretical knowledge will be given to the reader, then the relative 3BM mode will be shown (next chapter).

6.2 Mode 1: Trajectory Propagator

This mode is for the simple simulation of trajectories, knowing the initial conditions (the three components of position and velocity) given by the user. This mode requires the implementation of the equations of motion, the definition of the reference frame and of Jacobi's constant. Therefore these theoretical topics will be explained. Actually it will be not used for computations, but all other modes are based on the trajectory propagator, so it is important to understand how it has been developed.

6.2.1 Circular Restricted 3-Body Problem

The CR3BP is just a particular case of the n-problem (treated in section 4.1). It regards the motion of a body with negligible mass (m_3) within the gravitational field generated by two massive bodies (called primaries, with $m_1 > m_2 \gg m_3$). Since one of the masses is negligible, it's called *restricted*. Besides, the two primaries are moving on circular orbits around the centre of mass. For this reason it's called *circular*.

In the next paragraph, the reference frames used to describe this mathematical problem are explained.

6.2.2 Reference Frames

The reference frame used to analyze the CR3BP is a co-rotating normalized reference frame. In this framework the equations of motion can assume a more simple expression.

The system will be normalized by using the following units of mass, length and time:

- unit of mass = $m_1 + m_2$
- unit of length = mean distance between the primaries (L)

- unit of time = $\frac{1}{\omega} = \frac{T}{2\pi}$ (the inverse of constant angular velocity)

By using these new units the Gravitational constant and the angular velocity become equal to one.

To reconvert the adimensional quantities into the dimensional ones, it is necessary to apply the following transformation:

| | |
|----------|---|
| Length | $d[\text{km}] = L[\text{km}] \cdot d[-]$ |
| Velocity | $v[\text{km/s}] = V[\text{km/s}] \cdot v[-]$ |
| Time | $t[\text{s}] = \frac{T[\text{s}]}{2\pi} t[-]$ |

Table 6-B Conversion between adimensional and dimensional quantities

where V is the mean orbital velocity of m_2 (29.783 km/s for the Sun-Earth system) and T is the mean orbital period of m_1 and m_2 .

A fundamental parameter has to be introduced in order to define a three-body problem. The mass parameter is able to uniquely identify every three-body problem and is defined in the following way [Wakker, 2007a]:

$$\mu = \frac{m_2}{m_1 + m_2} \quad \mu \in \left[0, \frac{1}{2} \right] \quad (6.1)$$

With the previous assumptions the masses of the primaries can be expressed:

$$m_1 = 1 - \mu \quad m_2 = \mu \quad (6.2)$$

Now it is possible to introduce the inertial r.f. (XYZ) w.r.t. the co-rotating one (xyz) considered, as shown in the next figure.

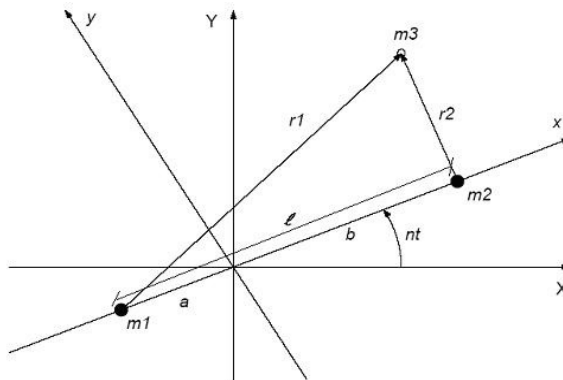


Fig 6.2 Inertial and rotating reference frames [Wiesel, 1989]

From the previous figure and the assumptions already done, some relations can be formulated:

$$a = \mu \quad b = 1 - \mu \quad l = 1 \quad n = 1 \quad (6.3)$$

The integration of the equations of motion has to be executed in this co-rotating r.f., but the results of this process should be given in a geocentric or heliocentric inertial r.f. in order to be

analyzed and plotted by using the STA 3BM (software requirement). Therefore a transformation between these two r.f.'s has to be performed. On the other hand, also the opposite transformation will be used in order to transform initial conditions given in the inertial body-centred r.f. to the co-rotating one.

These r.f.'s are shown in Fig 6.3. The XYZ r.f. is a body-centred inertial r.f., while the xyz-frame is the co-rotating r.f. The plane xy is the orbital plane of the second body relative to the first one (XY) and generally it has a certain inclination i . Besides it is rotated over a certain angle (α) determining the ascending node of the second body, while its position along the orbit is determined by the true anomaly β .

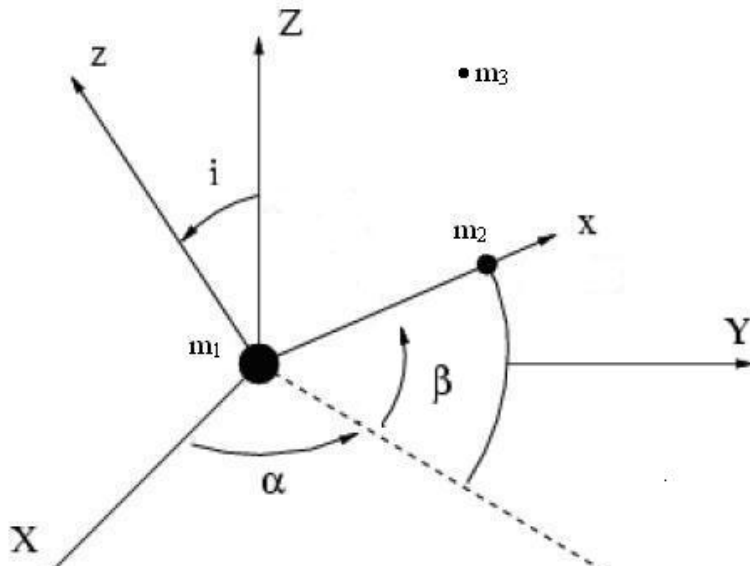


Fig 6.3 First body-centred inertial r.f. (XYZ) and co-rotating r.f. (xyz)

By using the general rotational matrices [Wikipedia, 2009c] and applying the $Z \rightarrow X \rightarrow Z$ series of rotations (respectively around α , i and β), the following transformation matrix is to be used for transformation between the two frames:

$$A_{XYZ \rightarrow xyz} = \begin{bmatrix} \cos \alpha \cos \beta - \sin \alpha \sin \beta \cos i & -\sin \alpha \cos \beta \cos i - \cos \alpha \sin \beta & \sin \alpha \sin i \\ \sin \alpha \cos \beta + \cos \alpha \sin \beta \cos i & \cos \alpha \cos \beta \cos i - \sin \alpha \sin \beta & -\cos \alpha \sin i \\ \sin i \sin \beta & \cos \beta \sin i & \cos i \end{bmatrix} \quad (6.4)$$

Then the rotations are accomplished by:

$$\begin{bmatrix} x \\ y \\ z \end{bmatrix} = A_{XYZ \rightarrow xyz} \begin{bmatrix} X \\ Y \\ Z \end{bmatrix} \Rightarrow \begin{bmatrix} X \\ Y \\ Z \end{bmatrix} = A_{XYZ \rightarrow xyz}^{-1} \begin{bmatrix} x \\ y \\ z \end{bmatrix} \quad (6.5)$$

Since the co-rotating r.f. is not centred in the center-of-mass of the first body, but in the center-of-mass of the 3-body system (as shown in Fig 6.2), a translation along the x-axis is also required before applying the transformation matrix:

$$\begin{aligned} x' &= x + \mu \\ y' &= y \\ z' &= z \end{aligned} \quad (6.6)$$

6.2.3 Circular Restricted 3-Body Problem: Equations of Motion

By using the previous assumptions and by using the 2nd Newton's law, the equations of motion can be written, in the co-rotating reference frame, in the following way [Wakker, 2007a]:

$$\begin{aligned}\ddot{x} - 2\dot{y} &= x - \frac{(1-\mu)(x+\mu)}{r_1^3} + \frac{\mu(1-x-\mu)}{r_2^3} = \frac{\partial U}{\partial x} \\ \ddot{y} + 2\dot{x} &= y - \frac{(1-\mu)y}{r_1^3} - \frac{\mu y}{r_2^3} = \frac{\partial U}{\partial y} \\ \ddot{z} &= -\frac{(1-\mu)z}{r_1^3} - \frac{\mu z}{r_2^3} = \frac{\partial U}{\partial z}\end{aligned}\tag{6.7}$$

where $r_1 = \left[(x+\mu)^2 + y^2 + z^2 \right]^{\frac{1}{2}}$ and $r_2 = \left[(x-1+\mu)^2 + y^2 + z^2 \right]^{\frac{1}{2}}$ are the distances of the third body from the respective primaries;

$U = \frac{1}{2} \left(x^2 + y^2 \right) + \frac{1-\mu}{r_1} + \frac{\mu}{r_2}$ is a scalar function of the spatial coordinates, defined as the potential accounting both the gravitational forces and the centrifugal force.

6.2.4 Jacobi's Integral and Hill's Surfaces

By manipulating the previous relations, it is possible to find the following equation [Wakker, 2007b]:

$$\dot{x}^2 + \dot{y}^2 + \dot{z}^2 = 2U - C = V^2\tag{6.8}$$

where C is an integration constant, determined by position and velocity of the third body at time t=0. This formula is the famous Jacobi's integral, and it represents the only integral known for the CR3BP.

A special case occurs when the velocity of the negligible mass is zero, then it follows [Wakker, 2007b]:

$$\begin{aligned}2U &= x^2 + y^2 + \frac{2(1-\mu)}{r_1} + \frac{2\mu}{r_2} = C \\ r_1^2 &= (\mu + x)^2 + y^2 + z^2 \\ \text{where again } r_2^2 &= (1-\mu - x)^2 + y^2 + z^2\end{aligned}\tag{6.9}$$

This equation describes the Surfaces of Hill. These are defined in the xyz-space. Along these surfaces the velocity of the third body is zero.

Since for any real body $V^2 \geq 0$, the region where the third body can move is given by [Wakker, 2007b]:

$$2U = x^2 + y^2 + \frac{2(1-\mu)}{r_1} + \frac{2\mu}{r_2} \geq C \quad (6.10)$$

For the planar case ($z=0$), the previous equation determines the part of the xyz-space that is accessible to the negligible mass, for a given value of C . By varying this value, that indeed is a measure of the orbital energy, in fact [Kumar, 2008]:

$$E = -\frac{1}{2}C = \frac{1}{2}V^2 - \Omega \quad (6.11)$$

$$\text{where } \Omega = \frac{1}{2}(x^2 + y^2) + \frac{1-\mu}{r_1} + \frac{\mu}{r_2}$$

it is possible to obtain different cases, depending on the C value. As shown by Fig 6.4, increasing the Jacobi's constant (C) and indeed decreasing the orbital Energy (equation 6.11), the accessible area decreases. Moreover it is interesting to observe the particular shape of this zone. Actually for higher values of C , it consists in two small circles about the primaries. By decreasing that value, the two circles become bigger up to a point where they meet each other. The point of contact is defined as the first Lagrangian point (L_1). Decreasing further the constant C , the inner accessible area increases again, until it touches the outer circle, defining in this way the point L_2 .

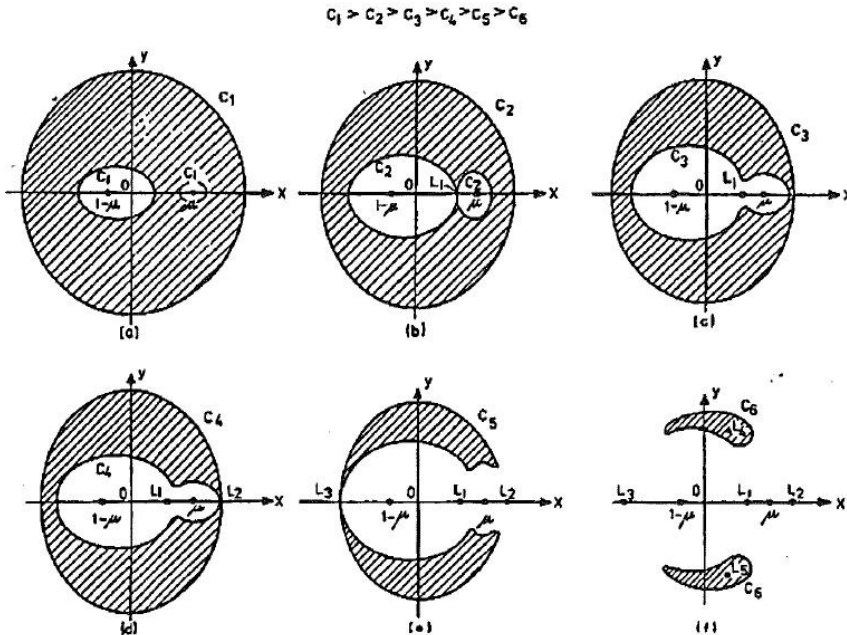


Fig 6.4 Hill's surfaces[Wakker, 2007a]

This value of C is particularly important, because it determines the value for which the entire space is accessible to the spacecraft.

Therefore, applying this theory to the Earth-Moon system, there should exist a particular value (C_2), that makes impossible to go from the Earth to the Moon, because the forbidden area avoids the passage between the two bodies. Actually that is the value at which the first Lagrangian point L1 appears.

On the other hand, for the value (C_4), that fits with the L2 point, the inner region (allowed) becomes open, so it is possible to escape from the Earth-Moon system. Then it would be possible to let a spacecraft come back to the Earth even in case of an engine failure, that would not allow it to enter in a parking orbit about the Moon. This condition ($C_3 > C > C_4$) is called free-return and if this condition is matched, then the spacecraft can come back to the Earth, because its energy will be not high enough to escape from the Earth-Moon system.

In order to obtain the free-return condition, the energy of the spacecraft must be below this value, and of course the Jacobian constant must be higher than C_4 .

These important values are listed in the following table:

| Lagrangian point | x-position | C value |
|------------------|------------|------------------|
| L1 | 0.836914 | 3.1883 (C_2) |
| L2 | 1.155682 | 3.1724 (C_4) |

Table 6-C Position of the Libration points and boundary value of C for the Earth-Moon system

For these reasons, to reach the Moon, the L1 point has to be “open” ($C < C_2=3.1883$), on the other hand, to obtain the free-return condition, the L1 point has to be “closed” ($C > C_4=3.1724$).

The formula to compute the Jacobi's constant in a non-rotating inertial reference frame is given by [Wakker, 2007a]:

$$\frac{1}{2}V_a^2 - \left(\frac{\mu_E}{r_1} + \frac{\mu_M}{r_2} \right) - n_M (\xi\dot{\eta} - \eta\dot{\xi}) = -\frac{1}{2}r_M^2 n_M^2 C \quad (6.12)$$

where V_a is the magnitude of the velocity of the spacecraft relative to the non-rotating inertial reference frame (centred in the center of mass), ξ and η correspond respectively to x and y, but in the inertial reference frame (so X and Y), μ_E and μ_M are the gravitational parameters of the Earth and the Moon, n_M is the mean motion of the Moon ($2.6617 \cdot 10^{-6}$ rad/s) and r_M is the radius of the Moon's orbit.

This formula could be applied just within the 3BP, because the Jacobian constant is an integral of motion just in that model. Nonetheless this condition has been considered here for completeness.

6.2.5 Mode 1 Implementation

The implementation of this mode has been quite straightforward. It required only the integration of the equations of motion, by giving initial conditions (state vector or Keplerian elements). The integrator adopted is Runge-Kutta-Fehlberg 4-5, and the user can select the step size. In order to check the correctness of the integration process, the Jacobi's constant has been checked at each step.

No other details about this mode will be given here, because it will be not used directly for computations, but only as framework for the other modes.

6.3 Mode 2: Halo Orbit and Manifolds Computation

This mode is for the design of Halo orbits and their relative manifold systems. The user can construct the desired Halo orbit selecting proper initial conditions. Moreover the user is able to design also manifold systems departing from the designed Halo orbit.

Therefore in this section, the concepts of Halo orbits and manifolds will be analyzed.

6.3.1 Numerical Approach for Halo orbits

Three-dimensional halo orbits are a particular kind of periodic orbits. In fact, they have the same frequency in the in-plane and out-plane motions and also for this reason they have been already used for several mission (SOHO, ISEE-3, ACE and Genesis [Russell, 2006]).

Besides by using those orbits, trajectories can exploit natural unstable dynamics to efficiently navigate through chaotic regions. The perturbing effects of a secondary gravitating body in the vicinity of a spacecraft and a primary body can be utilized to capture or escape the primary using little or no fuel. These attracting or repelling trajectories comprise a stable or unstable manifold of orbits, respectively. The set of these manifolds extended to all the bodies in the solar system comprises what is referred to as the Interplanetary Superhighway. The paths of these manifolds trace chaotically through the solar system, and interconnections of two manifolds provide mechanisms to ballistically connect two seemingly isolated regions.

In order to obtain and indeed study the connections between different manifolds, it is necessary to find periodic orbits and then it will be possible to design their respective manifolds. For this reason a numerical method will be explained and then applied.

The used numerical approach was developed by [Howell, 1983]. The purpose is to find periodic orbits in the CR3BP and for this scope some of their properties will be used. Actually these orbits must be symmetric w.r.t. the xz-plane ($y=0$), following from simple geometric considerations. Moreover they must intersect the xz-plane perpendicularly ($\dot{x}=\dot{z}=0$). Therefore these properties can be used for the initial vector:

$$\bar{x}_0 = (x_0 \ 0 \ z_0 \ 0 \ \dot{y}_0 \ 0)^T \quad (6.13)$$

Not only the initial vector, but also the solution at the final state must have the same form:

$$\bar{x}_1 = \bar{x} \left(\frac{T}{2} \right) = (x_1 \ 0 \ z_1 \ 0 \ \dot{y}_1 \ 0)^T \quad (6.14)$$

Due to the symmetry w.r.t. the xz-plane, it is correct to consider only half of the orbit period. Of course the sign of \dot{y}_1 has to be opposite to that of \dot{y}_0 . Because the initial vector is chosen arbitrarily, at the first crossing with the x-axis \dot{x}_1 and \dot{z}_1 will be not equal to zero, therefore the trajectory will be not periodic yet. The idea is to manipulate the initial vector in order to reach a periodic orbit, by using a differential corrector.

The main role in this method is played by the State Transition Matrix (STM: $\Phi(t, t_0)$), in fact it relates changes in the initial state with those in the final state of a trajectory. It is a linear approximation of the sensitivity of the final state to changes in the initial one. Before starting to explain how it will be used, it has to be found out. For this reason the following differential system will be solved numerically:

$$\begin{aligned}\dot{\Phi}(t, t_0) &= \mathbf{F}(t)\Phi(t, t_0) \\ \Phi(t_0, t_0) &= \mathbf{I}\end{aligned}\tag{6.15}$$

The matrix \mathbf{F} is defined by [Kumar, 2008]:

$$\mathbf{F} = \begin{pmatrix} \mathbf{0} & \mathbf{I} \\ \boldsymbol{\Omega}_{xx} & 2\mathbf{A} \end{pmatrix}\tag{6.16}$$

$$\text{where } \mathbf{A} = \begin{pmatrix} 0 & 1 & 0 \\ -1 & 0 & 0 \\ 0 & 0 & 0 \end{pmatrix}$$

$$\Omega_{xx1,1} = 1 - \frac{1-\mu}{r_1^3} + 3 \frac{(1-\mu)(x+\mu)^2}{r_1^5} - \frac{\mu}{r_2^3} + 3 \frac{\mu}{r_2^5} (x+\mu-1)^2$$

$$\Omega_{xx2,2} = 1 - \frac{1-\mu}{r_1^3} + 3 \frac{(1-\mu)y^2}{r_1^5} - \frac{\mu}{r_2^3} + 3 \frac{\mu}{r_2^5} y^2$$

$$\Omega_{xx3,3} = -\frac{1-\mu}{r_1^3} - \frac{\mu}{r_2^3} + 3z^2 \left[\frac{1-\mu}{r_1^5} + \frac{\mu}{r_2^5} \right]$$

$$\Omega_{xx1,2} = \Omega_{xx2,1} = 3y \left(\frac{(1-\mu)(x+\mu)}{r_1^5} + \frac{\mu(x+\mu-1)}{r_2^5} \right)$$

$$\Omega_{xx1,3} = \Omega_{xx3,1} = 3z \left(\frac{(1-\mu)(x+\mu)}{r_1^5} + \frac{\mu(x+\mu-1)}{r_2^5} \right)$$

$$\Omega_{xx2,3} = \Omega_{xx3,2} = 3yz \left(\frac{1-\mu}{r_1^5} + \frac{\mu}{r_2^5} \right)$$

In this way the equations of motion are integrated until y changes sign. Then the step-size is reduced and the integration goes forward again, until $|y| < 10^{-11}$ and the time could now be defined as $T/2$.

The orbit is considered periodic if $|\dot{x}|$ and $|\dot{z}| < 10^{-8}$ at $T/2$. Otherwise those values should be corrected playing with the initial vector. If they effectively result too large, the correction to be applied at the initial vector should be:

$$\delta\bar{x}_0 = (\delta x_0 \ 0 \ \delta z_0 \ 0 \ \delta \dot{y}_0 \ 0)^T \quad (6.17)$$

The corrections can be computed by keeping \dot{x}_0 constant:

$$\begin{bmatrix} \delta z_0 \\ \delta \dot{y}_0 \end{bmatrix} = \left(\begin{bmatrix} \Phi_{43} & \Phi_{45} \\ \Phi_{63} & \Phi_{65} \end{bmatrix} - \frac{1}{\dot{y}} \begin{bmatrix} \ddot{x} \\ \ddot{z} \end{bmatrix} \begin{bmatrix} \Phi_{23} & \Phi_{25} \end{bmatrix} \right)^{-1} \begin{bmatrix} \delta \dot{x} \\ \delta \dot{z} \end{bmatrix} \quad (6.18)$$

or by keeping \dot{z}_0 constant:

$$\begin{bmatrix} \delta x_0 \\ \delta \dot{y}_0 \end{bmatrix} = \left(\begin{bmatrix} \Phi_{41} & \Phi_{43} \\ \Phi_{61} & \Phi_{63} \end{bmatrix} - \frac{1}{\dot{y}} \begin{bmatrix} \ddot{x} \\ \ddot{z} \end{bmatrix} \begin{bmatrix} \Phi_{21} & \Phi_{23} \end{bmatrix} \right)^{-1} \begin{bmatrix} \delta \dot{x} \\ \delta \dot{z} \end{bmatrix} \quad (6.19)$$

where all the quantities are computed at $t=T/2$.

Using this method, the convergence to a periodic halo orbit is rapid and in most cases three or four iterations are sufficient.

In order to verify all these computations and to check if the numerical method will converge to a correct halo orbit, the database present in [Howell, 1983] has been used, as it will be shown in section 7.1.

6.3.2 Stability of Halo orbits

In order to evaluate the stability of these orbits, the monodromy matrix will be used. It is the STM associated with the periodic orbit after an integration of one cycle ($\Phi(T, t_0)$). For any point \bar{x} along the periodic orbit, the monodromy matrix serves as a linearization. The characteristics of the local geometry can be determined from the eigenvalues and eigenvectors of this matrix.

The monodromy matrix is given by [Howell, 1983]:

$$\Phi(T, t_0) = \mathbf{B} \begin{pmatrix} \mathbf{0} & -\mathbf{I} \\ \mathbf{I} & -2\mathbf{A} \end{pmatrix} \Phi^T \left(\frac{T}{2}, t_0 \right) \begin{pmatrix} -2\mathbf{A} & \mathbf{I} \\ -\mathbf{I} & \mathbf{0} \end{pmatrix} \quad (6.20)$$

where $\mathbf{B} = -\mathbf{I}_{6 \times 6}$.

Analyzing the eigenvalues of this matrix, because of the periodicity, two of them must have a modulus of one. Besides Φ , Φ^{-1} and Φ^T have the same eigenvalues. Moreover the determinant is one, so zero eigenvalues are excluded.

However it is possible to demonstrate the eigenvalues of this matrix turn out to be of the form:

$$\lambda_1 > 1, \lambda_2 = \frac{1}{\lambda_1}, \lambda_3 = \lambda_4 = 1, \lambda_5 = \bar{\lambda}_6 = \frac{1}{\lambda_6} \quad (6.21)$$

The last two eigenvalues are complex conjugates, while the first two are real.

In [Koon et al., 2006] a more in-depth analysis of the eigenvalues is furnished. A few indicative and useful guidelines are given here:

- λ_1, λ_2 : these are associated with the stable and unstable characteristics of the periodic orbit. They reflect the hyperbolic nature of the dynamics in the neighbourhood of the periodic orbit. Using this, approximations to the full stable and unstable manifolds can be generated.
- λ_3, λ_4 : these are neutral values, associated with motion tangent to the orbit.
- λ_5, λ_6 : these eigenvalues are associated with a rotation and is related to the existence of quasi-periodic orbits in the neighbourhood of the periodic orbit.

Therefore to generate stable and unstable manifolds, it will be necessary to use the first two, as it will be shown in the next section.

6.3.3 Manifolds

The first two eigenvalues will be used. The eigenvalues λ_1 and its eigenvector v_1 are used to generate the unstable manifold, and the eigenvalues λ_2 and its eigenvector v_2 for the stable manifold. The manifold will be generated by using the following initial guess [Kumar, 2008], [Russell, 2006]:

$$x^s(x_0) = x_0 \pm \epsilon v_2(x_0) \quad (6.22)$$

$$x^u(x_0) = x_0 \pm \epsilon v_1(x_0) \quad (6.23)$$

The eigenvector is generated with the classical procedure that briefly is now reported:

$$\Phi(T, t_0) \begin{bmatrix} x \\ y \\ z \\ \dot{x} \\ \dot{y} \\ \dot{z} \end{bmatrix} = \lambda_i \begin{bmatrix} x \\ y \\ z \\ \dot{x} \\ \dot{y} \\ \dot{z} \end{bmatrix} \quad (6.24)$$

The choice of the parameter ϵ is crucial. It gives a small displacement from the point x_0 along the periodic orbit. Therefore it perturbs the initial position and velocity from those of the

periodic orbit along the direction given by the eigenvector. It is problematic to find the proper value, because if it is too small the TOF to leave the reference orbit becomes too large. On the other hand it can't be chosen too big, because the linearization is valid just in the neighbourhood of the periodic orbit.

By the way, Perturbing the initial orbit by using the parameter ϵ allows the computation of manifolds. Those manifold trajectories leaving the Halo orbit are called unstable, on the other hand those manifold trajectories going from external regions toward the Halo orbit are called stable. In order to compute the stable ones the smallest eigenvalue (<1) is used and a backward integration from the perturbed condition around the Halo orbit is required, while for unstable manifolds the other real eigenvalues (>1) and a normal forward integration is required.

By integrating the estimate for the unstable manifolds forward in time and the estimate for the stable manifolds backwards in time, it is possible to generate approximations that shadow the manifolds. Because the equations of the CR3BP are invariant under the transformation $\{t=-t, y=-y$ and $z=-z\}$, if an arbitrary initial condition $(x_0, y_0, z_0, v_{x0}, v_{y0}, v_{z0})$ is integrated forwards in time, the resulting trajectory will be a mirror-image (w.r.t. the x-axis) of the trajectory integrated backwards in time starting from the initial conditions $(x_0, -y_0, -z_0, v_{x0}, -v_{y0}, -v_{z0})$ [Russell, 2006], as shown in the previous figure. The sign in front of the parameter ϵ gives the direction of the approaching orbit. If it is positive the approaching orbit comes from the right side, and vice versa.

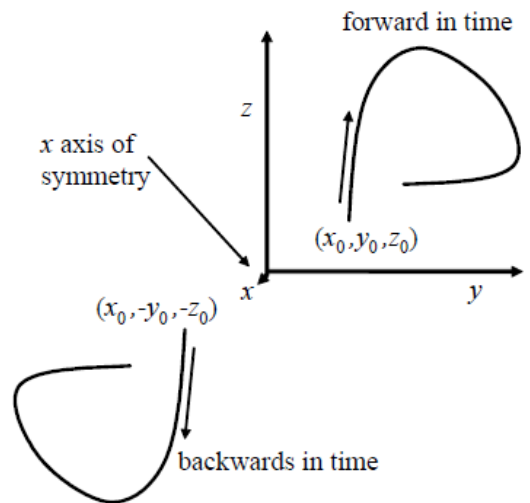


Fig 6.5 Symmetry with the xz-plane [Russell, 2006]

These manifolds could be very useful in order to reach the Moon, by using periodic orbits around the Lagrangian points as gateways of the different branches of manifolds.

6.4 Mode 3: Transfer Orbit Optimization

This mode is for the design of a complete mission from a main body of the 3-body system to a designed (by using the previous mode) Halo orbit. This kind of transfer orbit is called homoclinic connection, because the spacecraft remains for all the time in the same 3-body system. A global optimization process will be used in order to optimize the mission (TOF and/or total ΔV).

It makes use of the theory already explained in the previous paragraphs: a certain Halo orbit is selected and then a stable manifold system is generated from the perturbed Halo orbit by backward integrating. Then an intersection between a parking orbit around a main body (for instance the Earth) and this manifold system is searched for, so it is possible to create a transfer orbit from that body to a certain Halo orbit. Once the spacecraft reaches the perturbed

condition of the Halo orbit, the Halo orbit itself is assumed acquired. That is because the deviation ε in order to compute manifolds should be very small, otherwise the linearization used to derive this theory can't be applied. Therefore the difference in velocity and position between the real Halo orbit and the perturbed condition acquired would be reasonable small and it can be considered as covered by midcourse corrective manoeuvres (not considered in this work).

6.5 Mode 4: Earth-Moon Transfer Orbit Theory

This mode is for the design of a transfer orbit from the Earth to the Moon, by using a connection between the L2 points of the Earth-Sun and the Earth-Moon systems. This transfer orbit is called a heteroclinic connection, because two different 3-body systems are involved. In the following paragraphs the way to patch different manifolds systems and the way to find the proper geometry in order to guarantee this connection will be explained.

A reference paper [Parker and Lo, 2006] will be analyzed to explain this theory, then the specific procedure to compute this transfer orbit will be reported.

6.5.1 Heteroclinic Connection

In [Parker and Lo, 2006] the specific case of the Moon has been treated in 3D. This study shows how it is possible to use Lagrangian points and their manifolds, in order to reach the Moon.

In this case two different staging orbits are set. The satellite departs from a LEO orbit around the Earth. Hereafter it is sent to L2 of the Earth-Sun three-body system (EL2), by using the stable manifold of this point (Fig 6.6). If it was put within the stable manifold, it would have reached the Halo orbit around the EL2 point and then, after some revolutions, it would have passed by, because it is a transit orbit. It is known that points outside the manifold are pushed away, but the closer they are to the manifold the longer they remain in its neighbourhood [Koon et al., 2000]. For this reason the spacecraft will be launched in such a way that it skims the stable manifold (as shown in Fig 6.10) and then it will be pushed away periodically along the unstable manifold (Fig 6.6). Now it can go toward the L2 point of the Earth-Moon system (LL2), after that it is “captured” by its stable manifold (Fig 6.8). Finally the spacecraft will escape again by using the unstable manifold of LL2 (Fig 6.8), and choosing the proper conditions it can reach the desired three-dimensional final orbit around the Moon. The entire manoeuvre is summarized in Fig 6.10.

Two different aspects have to be emphasized about heteroclinic connections.

First, because the manifolds of two different Lagrangian points have different energies (and indeed different values for the Jacobi's constant), a ΔV has to be provided in order to allow the spacecraft to switch from one to another one. The magnitude of this manoeuvre depends on the two Halo orbits selected.

Second, due to the heteroclinic connection, this problem is indeed a four-body problem, very difficult to solve. For this reason the solution proposed is splitting it in two parts. Therefore the complex four-body system is decoupled in two three-body systems.

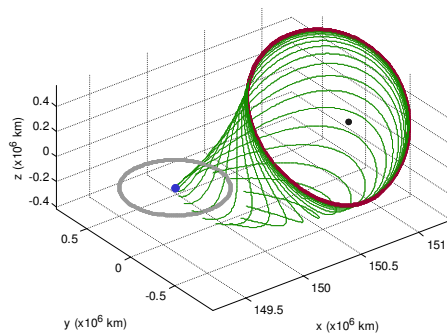


Fig 6.6 EL₂ halo orbit and its stable manifold

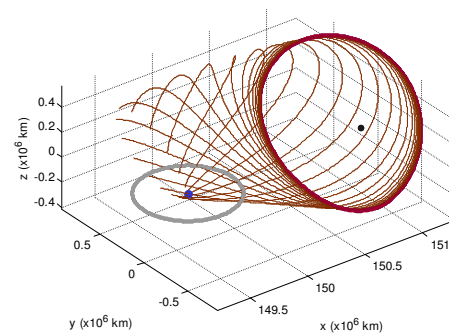


Fig 6.7 EL₂ halo orbit and its unstable manifold

[Parker and Lo, 2006]

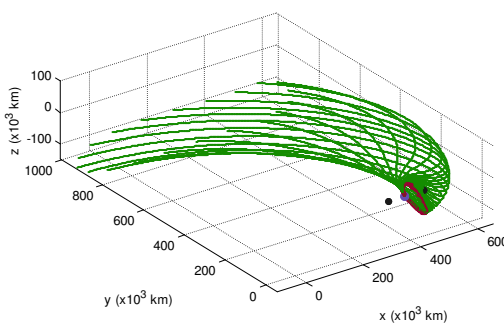


Fig 6.8 LL₂ halo orbit and its stable manifold

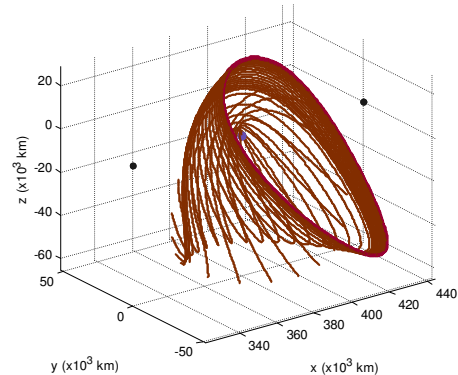


Fig 6.9 LL₂ halo orbit and its unstable manifold

[Parker and Lo, 2006]

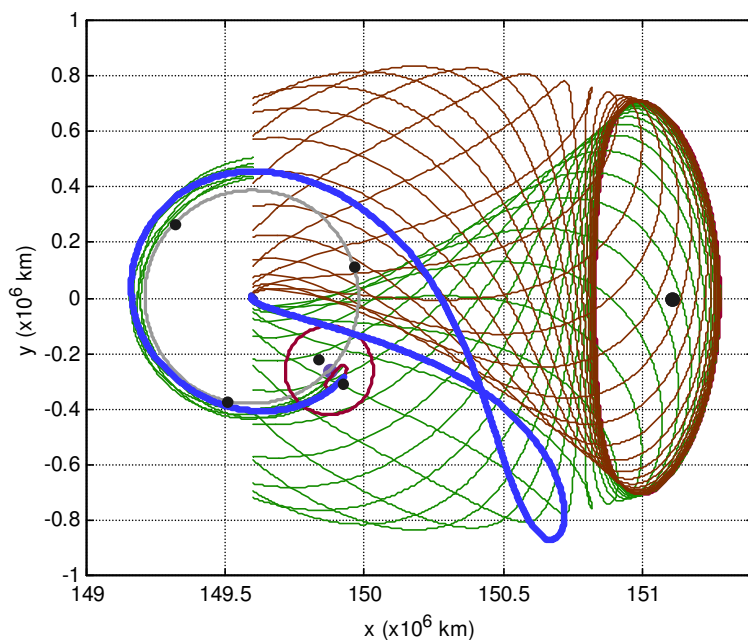


Fig 6.10 The 3D Shoot the Moon transfer plotted alongside the stable and unstable manifolds of the EL₂ halo staging orbit and the stable manifold of the LL₂ halo staging orbit [Parker and Lo, 2006]

6.5.2 Technique to Guarantee Heteroclinic Connection

In order to find good transfers between the Earth and the Moon, in literature the previous option is one of the most used. The reference papers consulted suggest to use periodic orbits and respective manifolds around EL2 and LL2 points, as shown in the last subsection.

In this thesis work some assumptions have been done in order to simplify the computation of the transfer trajectory:

- the first leg of the trajectory will be within the stable manifold until the S/C will get into the SE Halo orbit, as explained in section 6.4;
- from the SE Halo orbit, the initial conditions will be perturbed in order to escape from it through unstable manifolds until a patching section will be reached;
- from the patching section the S/C will enter into a stable manifold in order to get into the EM Halo orbit, as explained in section 6.4;
- from the EM Halo orbit, the initial conditions will be perturbed in order to intersect the final lunar parking orbit.

Therefore no ballistic captures and no corrective manoeuvres to avoid Halo orbits will be considered, reducing in this way the total TOF. That means the TOF will be quite long, because the S/C will last in the neighbourhood of the Halo orbits for quite a long time, instead of coming back immediately as in Fig 6.10. That is because including manoeuvres and ballistic captures would have increased the implementation efforts for the 3BM too much. Anyway the ΔV required for them usually is very small (in the order of m/s), therefore the total ΔV computed in this work represents an excellent approximation of a real transfer trajectory. Another difference will be at the patching section, where an adjunctive ΔV should be given to avoid Halo orbits, selecting faster transfer trajectories. As already explained, also this term would be very small, therefore it should not affect the final total ΔV .

For this reason, without including corrective manoeuvres and ballistic captures, the total TOF will not be reliable and will not be optimized, since the time to end up in a perfect Halo orbit is very long, in particular for the part closest to the Halo orbit itself (that is the part avoided by the other faster transfers). Therefore a real launch epoch will be not provided at the end of the computations. The main focus will be put on the minimization of the total ΔV to understand the competitiveness of such a complex trajectory.

Now the geometry of the problem will be defined. First the position of the Moon will be expressed relative to the Earth, then a patching section for the two manifold systems will be defined as well.

Patching these two different systems is the most difficult problem to solve due to their particular geometry. Actually the EL2 point is fixed w.r.t. the Earth, because they are moving around the Sun, but in the mean time the LL2 point is rotating around the Earth. For these reasons a connection point has to be found, and in order to obtain it, the coordinates of the “lunar” manifolds have to be converted into the Sun-Earth reference frame [Howell and Kakoi, 2006]. Generally moments, during the lunar orbit, do exist in which the two manifolds will not be in the correct geometry. Because the unstable manifold of EL2 has to intersect the stable manifold of LL2, the proper geometry has to be defined [Correia et al., 2004]. Once a connection point has been located, then it will be possible to integrate backwards and forwards in time in order to obtain the complete orbit and the proper time to launch the spacecraft. Therefore many trials will be needed in order to obtain this condition and also an optimization process will be necessary in order to minimize the propellant consumption.

The position of the Moon is given by three different angles (as shown in Fig 6.11, where xyz is the Earth-Moon co-rotating r.f., while XYZ is co-rotating with the Sun, both centred in the Earth): i is the inclination of the Moon's orbit relative to the ecliptic and it is fixed (5.145°); α is the angle defined by the line of Nodes (it rotates at a rate of 0.053° per day) and β defines the position of the Moon within its orbit. These last two angles can be varied in order to minimize the propellant consumption.

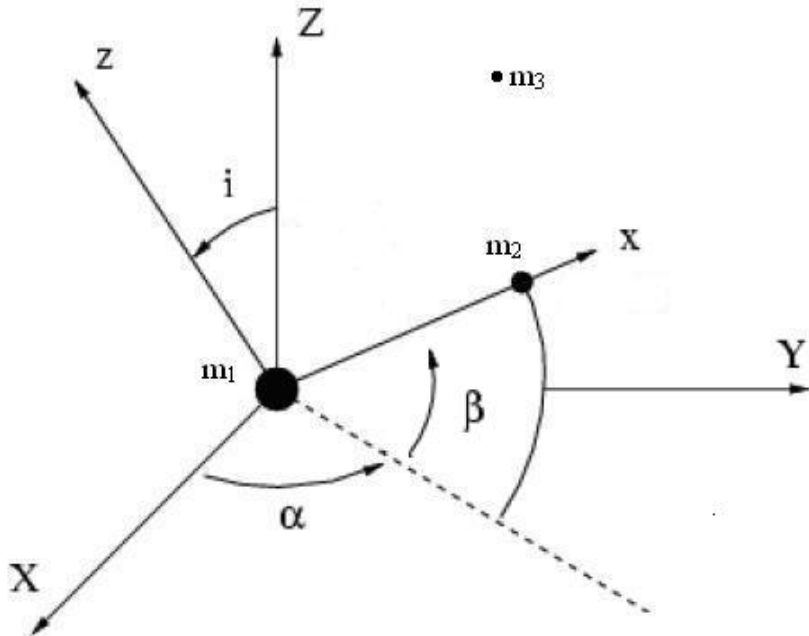


Fig 6.11 Earth-Moon and Sun-Earth reference frames [Howell and Kakoi, 2006]

Another important parameter that can be varied is the position of the connecting section between the two different orbits, that can be defined by the angle ψ , shown in the next figure.

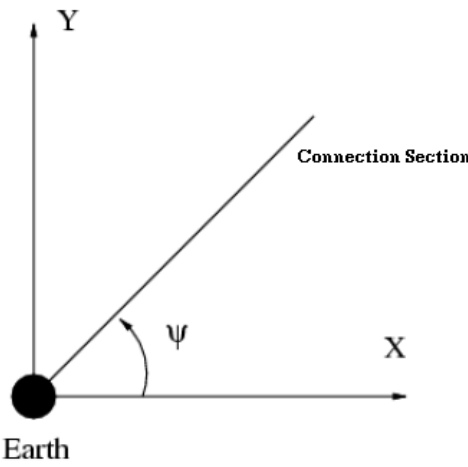


Fig 6.12 Connection section in the Sun-Earth reference frame [Howell and Kakoi, 2006]

Of course other variables are the sizes of the periodic orbits. Because in case of a Lissajous orbit it is more difficult to compute such a orbit, just halo orbits will be considered, otherwise a specific study is required and it is beyond the purposes of this work.

All these parameters should be varied in order to minimize the four ΔV 's that have to be given (the first to reach the injection point, the second one at the injection, the third one to

change the manifold and the last one to get into the final lunar orbit). Moreover the entire problem is time depending, therefore also the time takes part into the optimization process.

Therefore the crucial “geometric” parameters are:

- **Ψ** , angle between the Earth-Moon connecting line and the patch section in the Sun-Earth r.f.;
- **α** , angle between the Earth-Moon connecting line and the line of Nodes;
- **β** , angle defining the position of the Moon within its orbit.

In [Howell and Kakoi, 2006], the following relations are given;

$$\theta = \alpha + \beta \quad (6.25)$$

$$\theta = a\Psi + b \quad (6.26)$$

The angle θ defines the relation between α and β . It can be computed by using the relation (6.26), where the coefficients a and b depend on the amplitudes of the two Halo orbits (all these values are provided in [Howell and Kakoi, 2006]). Knowing θ , after having computed also the angle α just by using the ephemerides of the Moon, it is possible to compute the angle β too. It means that every month it changes value.

Once those three angles are known, it is possible to forward integrate (we are escaping from that orbit) the first manifold system from the SE Halo orbit until the patching section is reached (defined by Ψ) and then it is possible to backwards integrate (we want to go from the patching section to that orbit) the second manifold system from the EM Halo orbit to the patching section (defined by α and β). On that section, the coordinates are transformed from the EM r.f. into the SE r.f. and the patch is verified. There will be many different manifolds trajectories patching on that section, so only the best patch (smallest ΔV required) will be taken. By using a complete ephemerides model, this patching ΔV could be avoided as explained in [Howell and Kakoi, 2006], but this model is too complicated to be treated here. In the next chapter a list of Halo orbits and of the respective geometric parameters will be provided.

CHAPTER 7

7. Three-Body Trajectories: Results

In this chapter, the results of all computations done by using the 3BM and based on the theory of the previous chapter will be provided and analyzed.

First, the 3BM will be briefly verified and validated. Then, in the following section, all those Halo orbits obtained with mode 2 and then used for the optimization of the transfer orbit (mode 4) will be listed.

Moreover also an additional Halo orbit around LL2 and the optimized transfer trajectory to get it will be shown. That particular orbit will be used to send two satellites to guarantee communications with the Moon, as explained in sections 2.3 and 2.6.

7.1 3BM Implementation and Validation

Before starting computations with the 3BM, a brief overview about the verification and validation process will be given. For the complete documentation it is possible to refer to [ESA Technical Note, 2009a].

Actually every mode has been verified and validated.

For the first one other benchmarking software like STK or ASTOS and the Jacobi's constant, that by definition has to be kept constant along the trajectory, have been used.

The second mode has been verified by using two test cases, reported in this paragraph.

The last two modes have been verified and validated by using the previous tests. Actually these two modes make use of the same mathematical subroutines of the other two, like coordinates transformations, integration of the equations of motion, changes of r.f., etc. Therefore if the first two modes work properly, then also the last ones do.

The GUI of mode 2 is reported here to show how mode 2 has been properly integrated and validated:

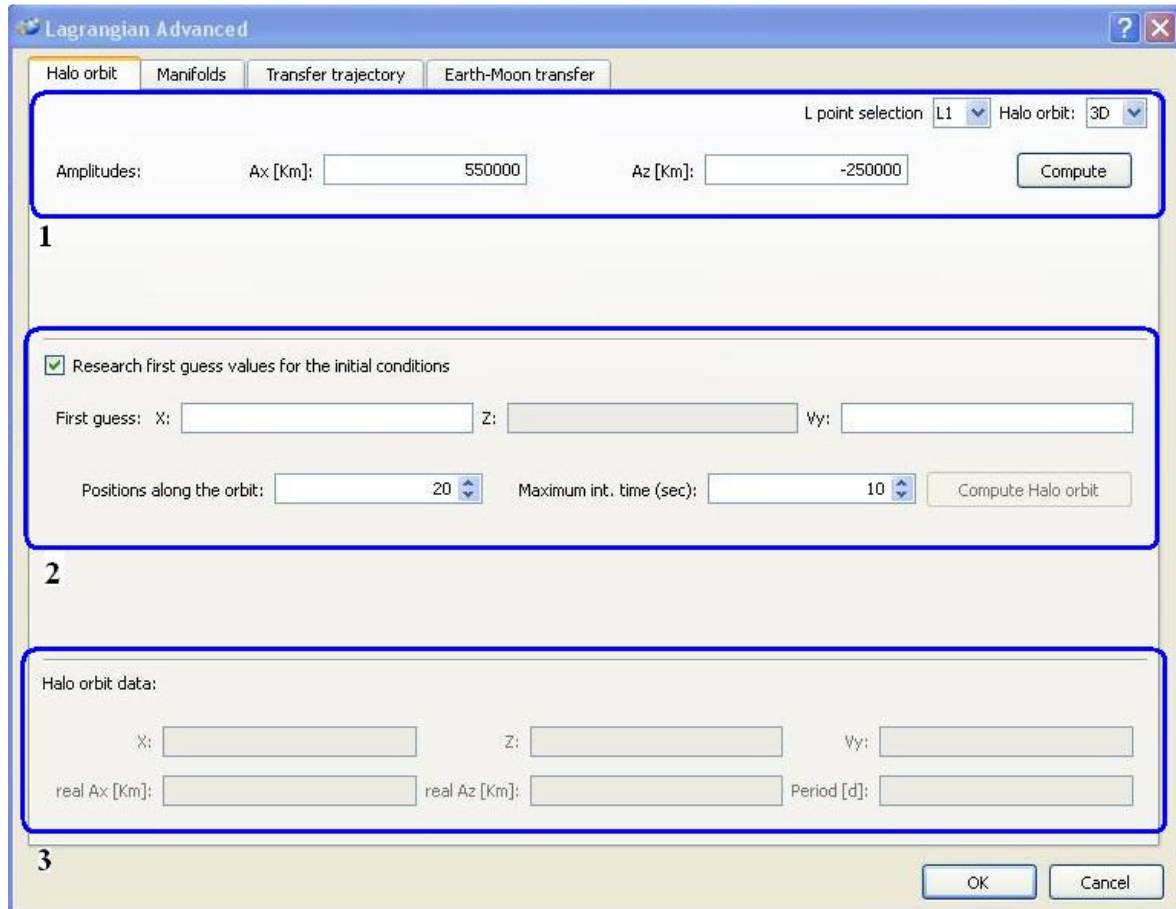


Fig 7.1 3BM GUI for mode I

For the computation of Halo orbits, a first guess is required to let the computation start (section 6.3.1). Thereto the user can insert directly this first guess by using panel 2 of Fig 7.1. The initial guess has the following layout:

- x-position (given by the user)
- y-position = 0
- z-position (given by the user)
- x-velocity = 0
- y-velocity (given by the user)
- z-velocity = 0

It could happen that the user doesn't know any information about the Halo orbit. In this case, by selecting the check box "research first guess values for the initial conditions", the user can design an orbit just specifying the location (in the L point selection box the user can select the Lagrangian point where the Halo orbit will take place) and the amplitudes (only in the x and z-direction, because for Halo orbits the y one is determined by the x amplitude). Therefore by using the first panel the user can get the first guess required to start the computation.

Once a first guess has been given/computed, the user should select how many positions he wants to know and the maximum computational time for the Halo orbit.

When the computation has been completed, the results are shown in panel 3. The real initial conditions are printed as well as the real amplitudes and the period of such orbit. It could happen that the orbit computed is too different from the one which is required, in this case an error box communicates it to the user.

The two different test cases used are here reported [Howell, 1983]:

| Parameter | Expected | Computed |
|-------------------|----------|----------|
| X-position | 0.723268 | 0.723268 |
| Z-position | 0.040000 | 0.040000 |
| Y-velocity | 0.198019 | 0.198019 |
| Semi-period | 1.30177 | 1.3002 |
| Jacobi's constant | 3.329168 | 3.32917 |

Table 7-A Initial conditions and results for test case I around L1 point

| Parameter | Expected | Computed |
|-------------------|-----------|-----------|
| X-position | 1.057222 | 1.057222 |
| Z-position | 0.300720 | 0.300721 |
| Y-velocity | -0.238026 | -0.238026 |
| Semi-period | 1.019032 | 1.0190 |
| Jacobi's constant | 3.001826 | 3.00183 |

Table 7-B Initial conditions and results for test case I around L2 point

For these test cases, not a real 3-body system has been used, indeed the gravitational parameter equal to 0.04 doesn't match with any combination of bodies within the solar system. Anyway it doesn't affect the test itself, since the gravitational parameter is just an input that can be changed in the 3BM.

The results completely match the expected values, therefore mode 2 has been validated and verified. Since also the Jacobi's constant along the Halo orbit is kept constant (not reported here), this is also a proof that mode 1 (trajectory propagator) works properly too.

7.2 Halo orbits computations

In this paragraph a list of SE and EM Halo orbits suitable to guarantee a transfer orbit from the Earth to the Moon will be provided. Therefore they will be inputs for the optimization process, that takes place in mode 4 and it will be shown in one of the next paragraphs. These orbits have been computed by using mode 2 of the 3BM.

Since the theory behind Halo orbits has been explained already (see section 6.3), now only the results of computations will be addressed.

Following [Howell and Kakoi, 2006], for the SE Halo orbit around L2, a range between 120,000 km and 200,000 km has been selected for the amplitude along the z-axis (Az). This is the driving parameter in the Halo orbit design.

Therefore nine different orbits have been computed, and their initial conditions (in normalized units) are listed here:

| SE-Az (km) | x | z | Vy |
|------------|--------------|--------------|--------------|
| 200,000 | 1.0082250205 | 0.0011850224 | 0.0102775333 |
| 190,000 | 1.0082403854 | 0.0011265286 | 0.0102263950 |
| 180,000 | 1.0082548776 | 0.0010679072 | 0.0101782843 |
| 170,000 | 1.0082685948 | 0.0010092508 | 0.0101326490 |
| 160,000 | 1.0082815391 | 0.0009503705 | 0.0100895604 |
| 150,000 | 1.0082937164 | 0.0008914432 | 0.0100489333 |
| 140,000 | 1.0083050966 | 0.0008324675 | 0.0100109338 |
| 130,000 | 1.0083157258 | 0.0007732952 | 0.0099753838 |
| 120,000 | 1.0083255618 | 0.0007141843 | 0.0099424236 |

Table 7-C SE Halo orbits initial conditions

The same has been done for the EM Halo orbit around L2. In this case the range selected was between 16,000 km and 30,000 km and again this interval has been discretized obtaining eight different Halo orbits.

In Table 7-D their initial conditions (in normalized units) have been reported:

| EM-Az (km) | x | z | Vy |
|------------|--------------|--------------|--------------|
| 30,000 | 1.0891503304 | 0.0600409940 | 0.2634447487 |
| 28,000 | 1.0932424164 | 0.0567677353 | 0.2522307546 |
| 26,000 | 1.0970414455 | 0.0533085711 | 0.2417893247 |
| 24,000 | 1.1004876383 | 0.0497539199 | 0.2322790181 |
| 22,000 | 1.1036592196 | 0.0460559141 | 0.2234838791 |
| 20,000 | 1.1065617347 | 0.0422241380 | 0.2153911054 |
| 18,000 | 1.1094258180 | 0.0378986959 | 0.2073573381 |
| 16,000 | 1.1115191716 | 0.0342811248 | 0.2014511208 |

Table 7-D EM Halo orbits initial conditions

All these orbits are suitable for the Earth-Moon transfer orbit. The choice of the best combination will be left to the optimization process.

All these orbits have been checked by plotting them in the 3BM. Only the first one of the SE Halo orbits computed will be shown here. First the GUI with the inputs used has been reported (Fig 7.2) and then the trajectory obtained (Fig 7.3):

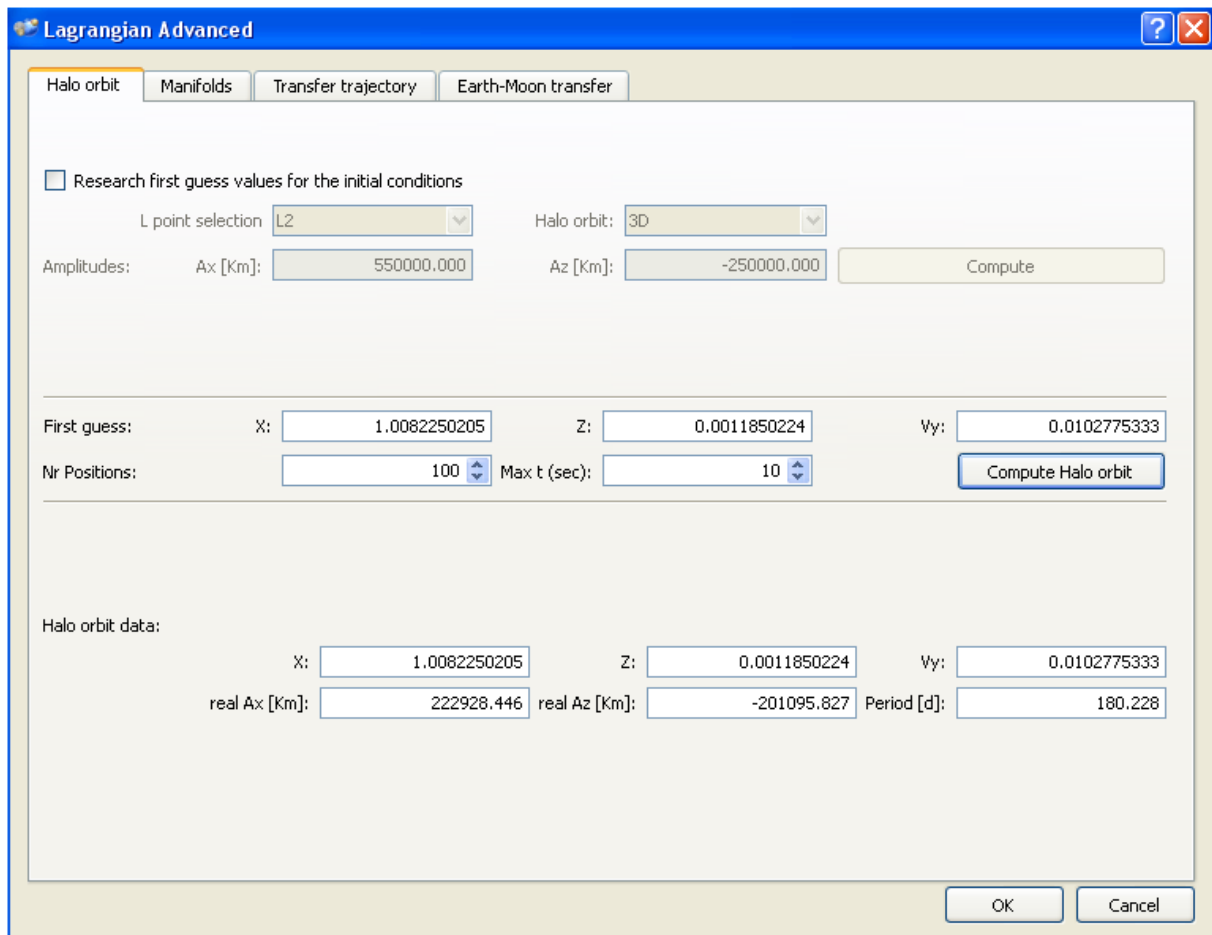


Fig 7.2 SE Az=200,000 km Halo orbit GUI

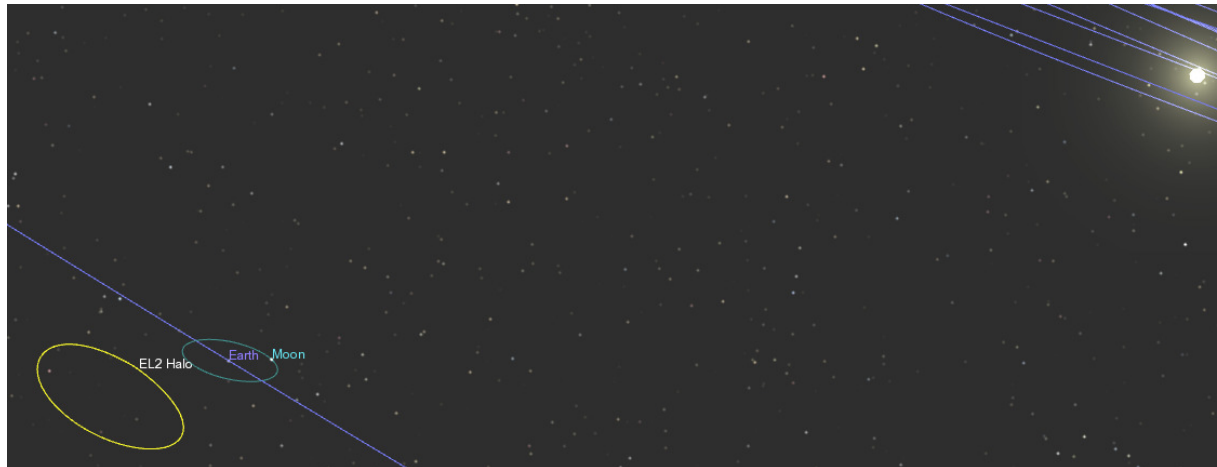


Fig 7.3 SE Az=200,000 km Halo orbit

7.3 Earth-Moon Transfer Orbit

In this paragraph, the procedure explained in section 6.5.2 will be followed.

The first step is to compute the geometric parameters Ψ , α and β , in order to define the relative geometry of the two different 3-body systems.

From [Howell and Kakoi, 2006], the suggested value for Ψ is 110° , therefore this value will be used for all the following computations.

The angle α can be computed by integration of the Moon motion around the Earth, until it intersects the Earth-Sun plane. The year 2015 has been selected, since most likely four years should be required to build the base (as shown in section 2.6).

For the angle β , two other parameters (a, b) have to be computed. In [Howell and Kakoi, 2006] these values are given in two plots as function of z-amplitudes of the SE and EM orbits. These plots are here reported respectively for a (Fig 7.4) and b (Fig 7.5):

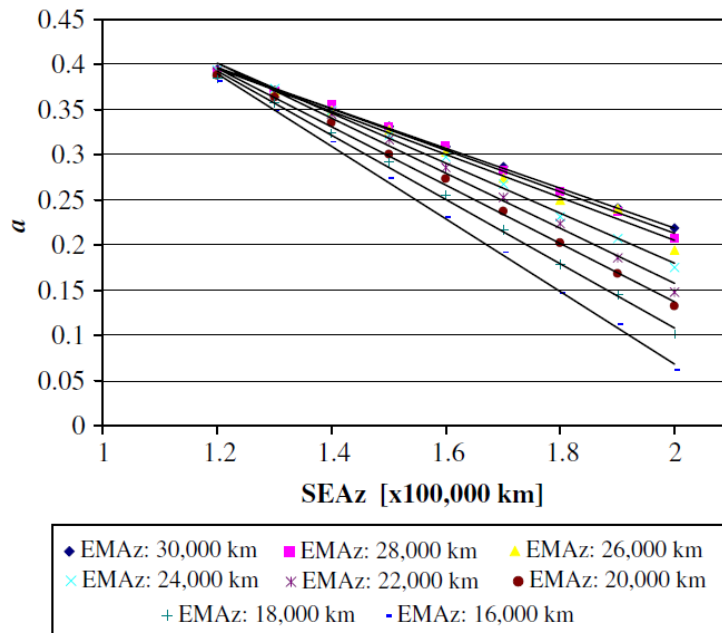


Fig 7.4 Relationship between a and SE Az for each EM Az [Howell and Kakoi, 2006]

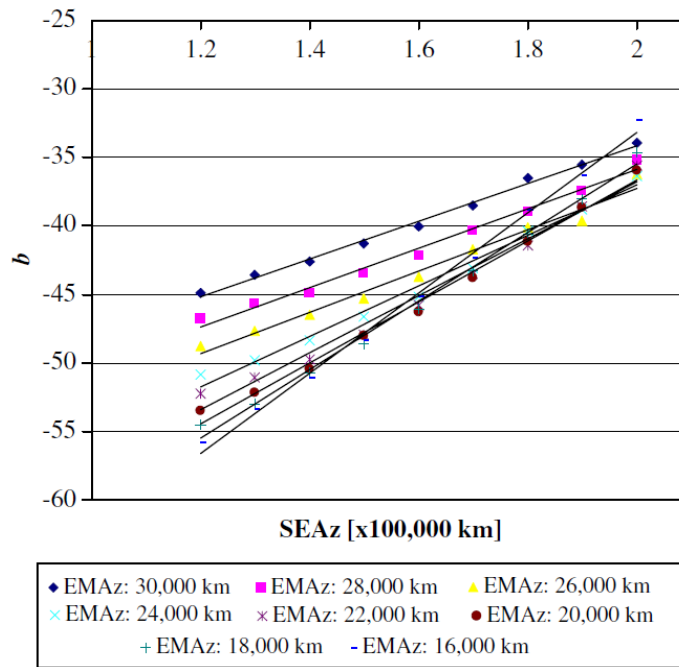


Fig 7.5 Relationship between b and SE Az for each EM Az [Howell and Kakoi, 2006]

Now all parameters are known, therefore the exact geometry of the two systems can be computed. The computed value of the angle β is reached once per month, because it

represents a certain position of the Moon relative to the ascending node. It means once per month it is possible to have connections between those two 3-body systems.

The optimization process (that makes use of a Non-dominated Sorting Genetic Algorithm: NSGA-II, improvement of the previous version presented by [Srinivas and Deb, 1994]) will regard one year, with 13 possible intersections epochs, because over one year the geometry of the system is repeated in the same way. Amongst them, only that one requiring the smallest ΔV to patch manifolds will be used. It doesn't ensure the global optimization of the problem, because three other terms contribute to the total ΔV : the first two to escape from the parking orbit around the Earth and another one to get into the lunar orbit. But, as it will describe, they are evaluated in two other optimization processes, therefore these four different terms are optimized separately. That guarantees the global optimization of the process.

It is worth emphasizing that also here the optimization process has to be run several times in order to find the best solution. Therefore all simulations been repeated many times (3-5 times depending on the discrepancy of the results) and only the best result has been considered. Therefore, at the end of it, just one trajectory will be provided, actually the best one that is possible to achieve during one year, and due to the geometry of the problem, it can be reproduced at least once per year. From this optimization process, there are no information about other “good” trajectories, that could reach a total ΔV similar to the best one, in the same year. So it is not possible to determine how many missions per year can follow this kind of trajectory, delivering the “same” payload on the Moon.

Actually it is worth noticing two different behaviours of this kind of trajectory:

- a change of the best intersection epoch doesn't strongly influence the total ΔV of the mission. The total ΔV doesn't increase very much w.r.t. the best value. Anyway **every year just one intersection epoch** (the best one) is selected in order to speed up the computations made by the 3BM (computing all intersections at each epoch would mean elaborating a huge amount of data);
- since in this work the TOF is not an optimization object (as explained in section 6.5.2), it is not possible to compute a real launch epoch. The way used to compute the TOF doesn't take into account the launch phase, ballistic captures and corrective-manoeuvres that can be used to speed up the transfer with a very small additional propellant consumption. Using them, the same intersection epoch can be obtained from different trajectories, that would allow more missions per year with almost the same total ΔV .

Therefore in this work many different “3-body” trajectories per year with the same total ΔV will be assumed feasible, without specifying any launch epochs.

The next step is to specify the initial and final orbits respectively around the Earth and the Moon. They have been already discussed and given respectively in sections 3.2.1, 3.2.2 and are reported in Table 7-E and in Table 7-F:

| Launcher | Inclination ($^{\circ}$) | Altitude (km) |
|----------|----------------------------|---------------|
| Ariane V | 5 | 185 |
| Proton | 51.6 | 185 |
| Ares V | 28.5 | 185 |
| Ares I | 28.5 | 185 |
| Atlas V | 28.5 | 185 |

Table 7-E Initial orbit

| Altitude (km) | Inclination ($^{\circ}$) |
|---------------|----------------------------|
| 100 | 89 |

Table 7-F Final lunar orbit

Now the initial and final orbits and the “intermediate” Halo orbits are known. So the way to connect them using manifolds and to optimize the entire transfer trajectory will be explained here.

The entire transfer orbit can be divided in four different legs as shown in Fig 7.6 (where the parking orbits are indicated in yellow with arbitrary inclination, the stable manifolds in green, the unstable manifolds in red, and the patching section and the Halo orbits in blue):

- Earth parking orbit-SE Halo orbit
- SE Halo orbit-Patching section
- Patching section-EM Halo orbit
- EM Halo orbit-Lunar parking orbit

Each of them will be described and shown in the next paragraphs. Then in the last section, the obtained results will be summarized.

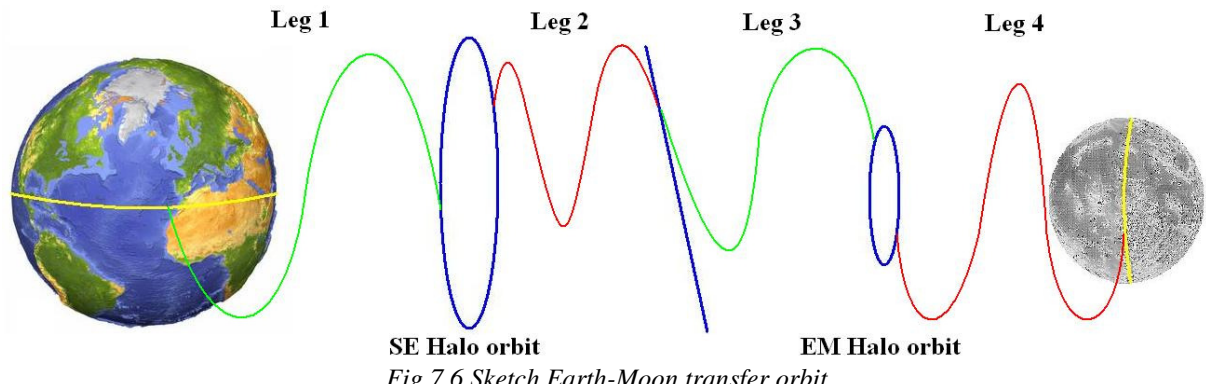


Fig 7.6 Sketch Earth-Moon transfer orbit

Fig 7.6 is just a sketch of the transfer orbit, used to show the different legs of the trajectory. For this reason the dimensions and orientations of the orbits, and the distances are not to scale.

7.3.1 Earth Parking Orbit-SE Halo Orbit

Along the SE-Halo orbit a **certain point** is selected randomly by the optimizer in order to compute a manifold trajectory. The choice of this point is left to the optimization process, because the most suitable one to guarantee the best connection can't be known a priori.

Then it is perturbed by using a **deviation parameter ϵ** (see section 6.3.3) selected by the optimizer within a certain specified range. At each iteration of the optimization process the deviation changes value, because it is a variable to optimize.

Then all these trajectories are backwards integrated, because the S/C will follow the stable manifold in order to get into the SE Halo orbit (see sections 6.3.3 and 6.5). The integration is stopped once the S/C will have intersected a sphere around the Earth with a radius of four times the parking orbit (if an intersection is reached, otherwise that trajectory is discarded), that has to be linked with the manifold trajectory. All the points of that trajectory inside the sphere are suitable for this intersection. For this reason that part of the trajectory is discretized in 100 different points, in order to compute the best intersection with the Earth.

So far all the computations have been performed in the co-rotating r.f. Now position and velocity of the intersection point are transformed in the inertial geocentric r.f. (by using equation 6.5). The **Julian date** has to be specified in order to perform this transformation, and this is the third variable left to the optimizer.

Generally, that position will be at a different altitude and inclination from the parking orbit, therefore some impulsive manoeuvres have to be executed. Since the initial RAAN has been left free, because it depends on the launch date and on the ascent trajectory, not treated in this work, only two kinds of manoeuvres are considered:

- change of inclination
- Hohmann transfer

The Hohmann transfer represents the cheapest way to raise the altitude of the trajectory, for this reason it has been selected to perform that task. Then a change of the inclination has been performed in order to reach the proper position to leave the Earth. A combined manoeuvre to raise the altitude and to change the inclination has been used [see section 4.6.3], since it results quite cheaper.

From that point the inclination required to transfer the S/C from its parking orbit is computed with the following formula [Wakker, 2007a]:

$$i = \arccos \frac{h_z}{|\vec{h}|} \quad (7.1)$$

where vector \vec{h} is the orbital momentum vector perpendicular to the orbital plane defined as the cross product of position and velocity vectors ($\vec{h} = \vec{r} \times \vec{v}$).

The manoeuvres required can be shown in the next figures. In Fig 7.7, the trajectory in the orbital plane is shown. The Hohmann transfer from the initial parking orbit (position A) to the circular higher orbit (position B) is clearly recognizable. Then after having changed the inclination, the third ΔV to enter into the escape trajectory is given (position C).

The change of inclination is performed along with the Hohmann transfer, as explained in section 4.6.3.

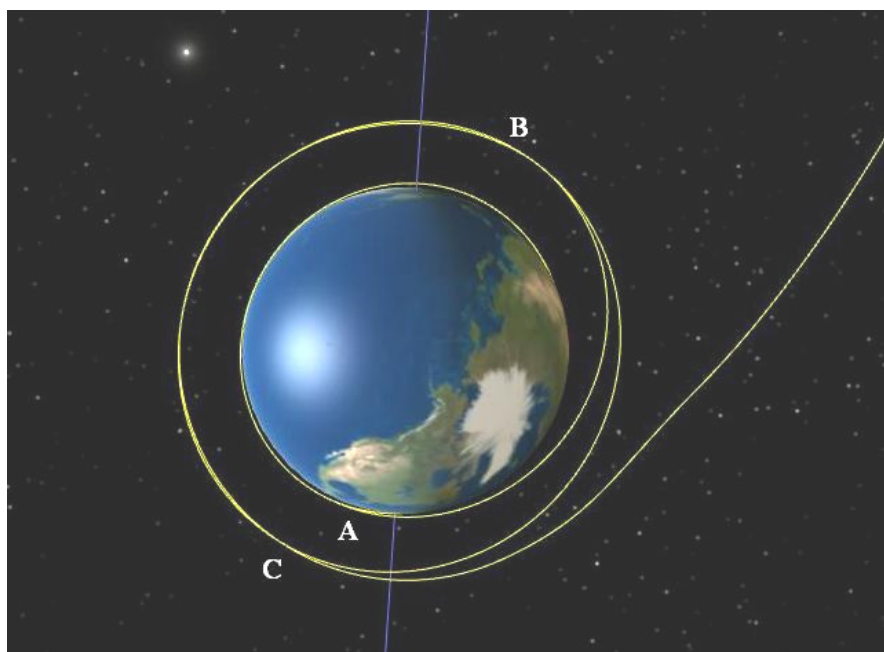


Fig 7.7 Leg 1 in the orbital plane

In Fig 7.8 the change of inclination can be easily noticed (position D). The manoeuvre given at the intersection point to escape from the Earth and to enter into the manifold trajectory is again shown (position C).

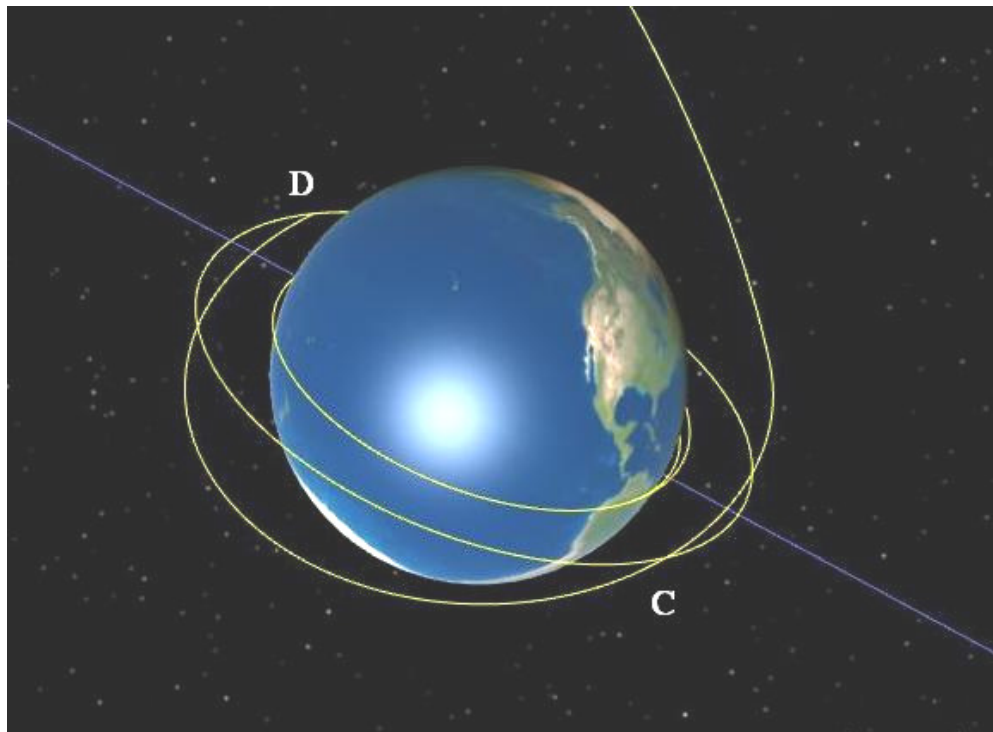


Fig 7.8 Leg 1 change of inclination around the Earth

Then the entire trajectory from the Earth until the SE Halo orbit is shown:

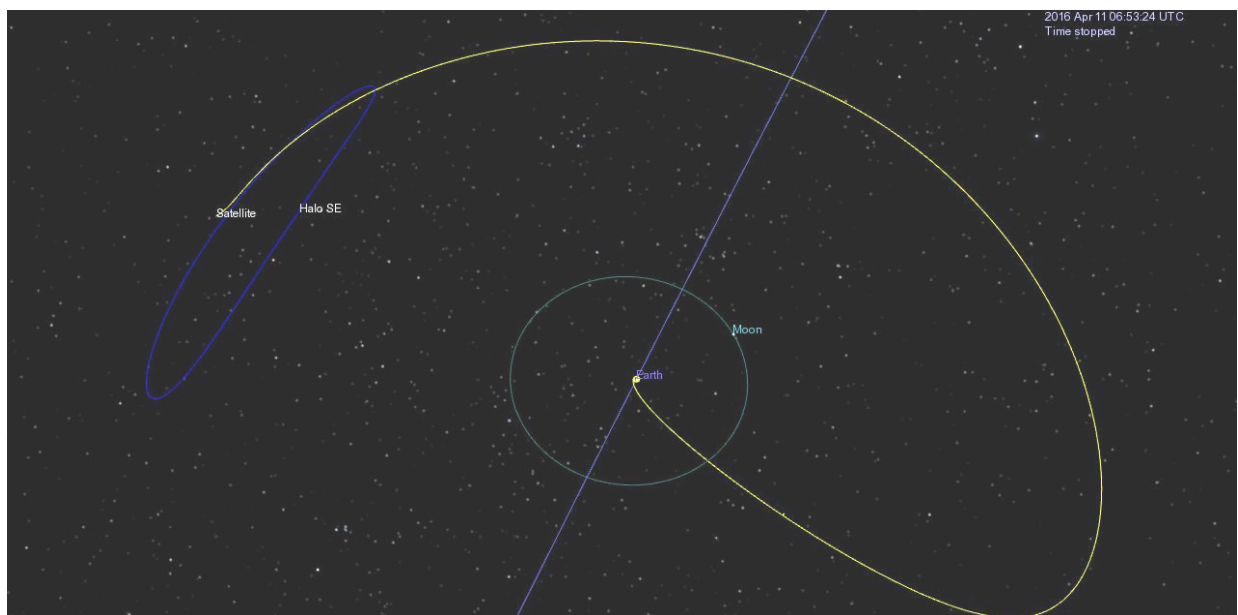


Fig 7.9 Leg 1 entire trajectory

7.3.2 SE Halo Orbit-Patching Section

The SE Halo orbit is discretized in 200 different points. For each of them a manifold trajectory is computed for 40 different values of the deviation parameter ε_1 (from 0.000025 to 0.001, with a step of 0.000025). All these trajectories are propagated until they reach an intersection with the patching section. An intersection is considered accomplished once a trajectory reaches a distance below 1,000 km from this section. That value is considered reasonable, since it can be easily covered by using corrective manoeuvres.

In this way, only those trajectories matching this condition are stored and considered suitable for an intersection with the manifold coming from the EM Halo orbit.

This part of the trajectory is shown in Fig 7.10:

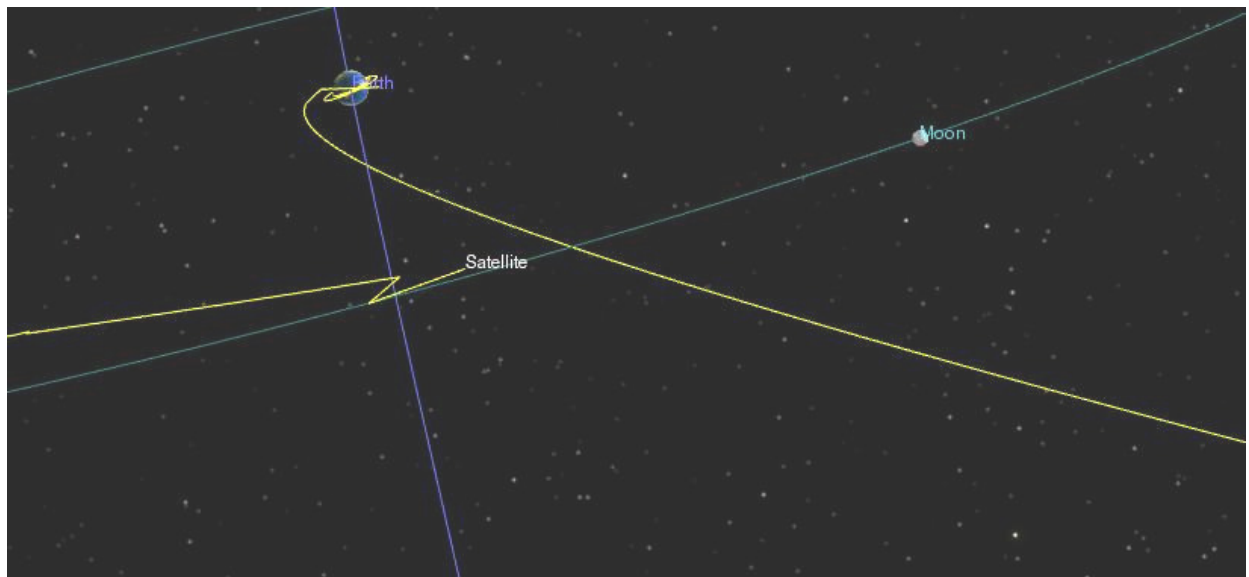


Fig 7.10 Leg 2–Leg 3 patching point

In the last figure the patching point is clearly recognizable. A discontinuity in position (as well as in velocity) of 7,853 km has been obtained for this trajectory. It will be explained in the next paragraph.

7.3.3 Patching Section-EM Halo Orbit

In this case, the EM Halo orbit is discretized in 100 different points. A smaller number has been considered, since this orbit is quite smaller than the previous one, so 100 points are enough to cover all the orbit.

Also in this case, from each point a manifold trajectory is computed for different values of the deviation parameter ε_2 (from 0.16 to 0.30, with a step of 0.2). This value is quite bigger than that used for the SE Halo orbit. That is because the trajectory followed in this leg is a stable trajectory (smaller eigenvalue), while the other one is unstable, therefore a bigger deviation is required to leave the orbit to compensate the smaller eigenvalue and obtain a similar trajectory.

Even though the deviation is quite big, the real deviation (given by the eigenvalue times initial condition times ε_2) in position and velocity is still very small (in terms of a few thousand of km and few m/s). Therefore, the resulted mismatch in position is similar to those obtained in

the previous case, and again it can be covered by using corrective manoeuvres, that could allow the user to get into this Halo orbit.

These trajectories are propagated until they reach the patching section. If the distance from one of the points stored and computed in the previous leg is smaller than a certain value of tolerance (10,000 km), the intersection is considered accomplished. Then the ΔV required is computed and the best combination of trajectory is selected. The difference in position is considered covered by using corrective manoeuvres.

This part of the trajectory is shown in Fig 7.11:



Fig 7.11 Leg 3 transfer orbit

7.3.4 EM Halo Orbit-Lunar Parking Orbit

In this last leg an optimization process involving the same parameters used in section 7.3.1 is performed. A new set of manifold trajectories is computed, departing from the EM Halo orbit and reaching the Moon. There a certain set of manoeuvres can be executed (as in section 7.3.1) in order to insert the S/C into the lunar parking orbit selected.

This part of the trajectory is shown in Fig 7.12 (where the “weird” spiralling trajectory obtained is due to the heliocentric r.f. used to plot the trajectory):

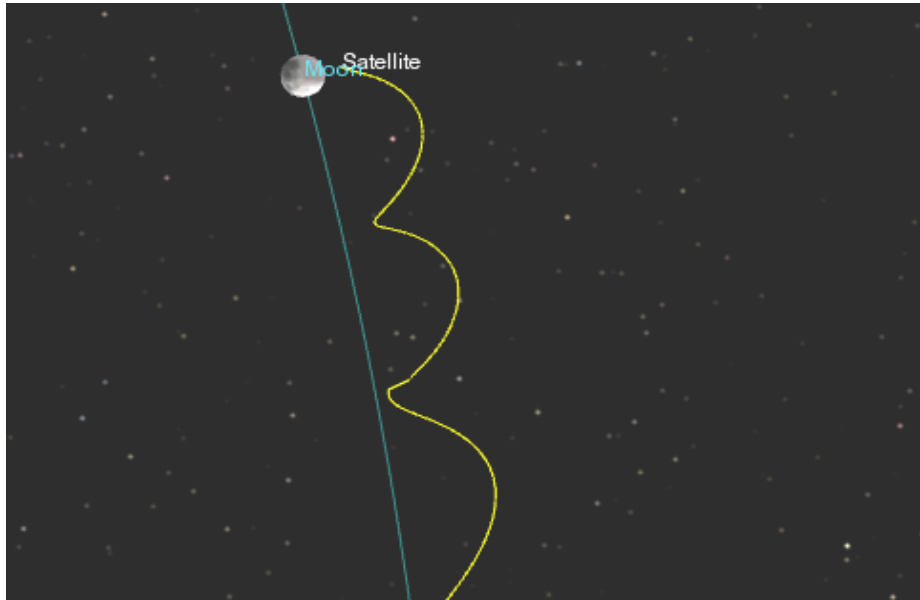


Fig 7.12 Leg 4 transfer orbit

7.3.5 Total ΔV and payload delivered

In the next table all results obtained from the optimization process are summarized.

| Launcher | $\Delta V1$ (km/s) | $\Delta V2$ (km/s) | $\Delta V3$ (km/s) | $\Delta V4$ (km/s) | Total ΔV (km/s) | LEO mass (tons) | LLO mass (tons) | Moon Payload (tons) |
|----------|-----------------------|-----------------------|-----------------------|-----------------------|----------------------------|-----------------------|-----------------------|---------------------------|
| Ariane V | 1.349 | 1.779 | 0.189 | 1.458 | 4.775 | 22.6 | 8.052 | 2.152 |
| Proton | 1.940 | 0.340 | 0.189 | 1.458 | 3.927 | 21 | 8.994 | 3.094 |
| Ares V | 1.813 | 0.792 | 0.189 | 1.458 | 4.252 | 130 | 51.896 | 4.896 (M) 31.896 (U) |
| Ares I | 1.813 | 0.792 | 0.189 | 1.458 | 4.252 | 25 | 9.974 | 4.074 |
| Atlas V | 1.813 | 0.792 | 0.189 | 1.458 | 4.252 | 20.25 | 8.079 | 2.179 |

Table 7-G Total ΔV and mass budget for the Earth-Moon transfer orbit

$\Delta V1$ regards the manoeuvre to change inclination and to execute a Hohmann transfer from the parking orbit around the Earth (see section 7.3.1);

$\Delta V2$ regards the manoeuvre to escape from the Earth, reaching EL2 (see section 7.3.1);

$\Delta V3$ regards the manoeuvre to patch leg 2 and leg 3 (see section 7.3.3);

$\Delta V4$ regards the manoeuvre to inject the S/C into a lunar orbit (see section 7.3.4).

The best feasible trajectories have been obtained for the following orbits:

| Launcher | SE-Az (km) | EM-Az (km) |
|----------|------------|------------|
| Ariane V | 190,000 | 28,000 |
| Proton | 190,000 | 28,000 |
| Ares V | 190,000 | 28,000 |
| Ares I | 190,000 | 28,000 |
| Atlas V | 190,000 | 28,000 |

Table 7-H Optimization parameters for the Earth-Moon transfer orbit

The total ΔV obtained in Table 7-G are slightly higher than that listed in Table 3-A. This is because in that table the S/C is considered temporarily captured by the Moon. In this case a stable lunar orbit is reached. Therefore the obtained values seem to be reasonable. Anyway it is not possible to better benchmark those values, since the 3BM is the first tool able to compute this kind of trajectories and in the reference papers no detailed data about manoeuvres are available.

The final payload mass for Ares V is quite higher than the value stated in section 2.5. That is because an engine with better performance (higher I_{sp}) has been considered here, since the exact data of the engine used for the interplanetary S/C are not known yet.

Also for this kind of trajectories, Ares V is the only launcher suitable for this mission.

7.4 Halo orbits for Communication Satellites

In this last section, a transfer orbit from the Earth to the LL2 point will be computed. This orbit will allow two communication satellites to go from the Earth to a Halo orbit around the LL2 point, in order to guarantee a complete coverage of the south pole [Hamera et al., 2008]. No other options will be evaluated for this mission, since Halo orbits naturally fit within the 3BP. Besides it would be difficult to use other techniques to design a transfer trajectory towards an orbit designed only within the 3BP.

The only requirement is the period of the Halo orbit: 7.5 days (see section 2.3). Their orbital phase will be shifted by half a period.

Using mode 2 of the 3BM, the following Halo orbit has been computed:

| Ax (km) | Az (km) | Period (days) | x | z | Vy |
|----------|-----------|---------------|--------------|--------------|--------------|
| 9885.688 | 39911.907 | 7.53 | 0.9870758413 | 0.0161373370 | 1.1928894728 |

Table 7-I Halo orbit data for Earth-Moon communication satellites

The Halo orbit selected is shown:

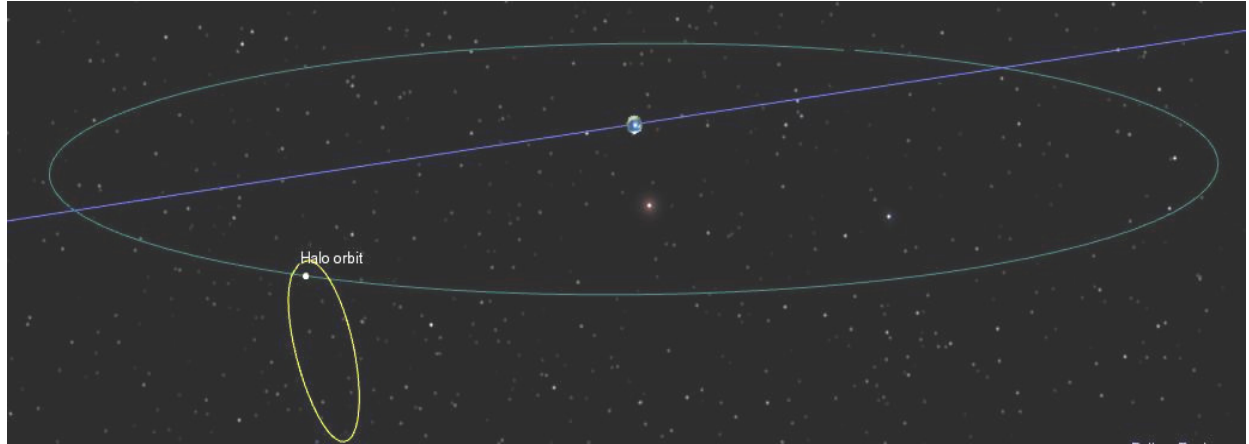


Fig 7.13 Table 7-J Halo orbit for Earth-Moon communication satellites

The transfer trajectory is computed in the same way as done previously in section 7.3, except for leg 4 of Fig 7.6: once the S/C will have reached the EM Halo orbit, the transfer is considered accomplished. For this reason the procedure used to get this transfer orbit is the same, with the following changes:

- the initial parking orbits around the Earth are the same, but a smaller launcher will be considered (Vega), since the mass of both satellites is totally 800 kg. Therefore applying the Tsiolkovsky law from the last manoeuvre (knowing the final payload mass) to the first one, the initial mass to put into a LEO orbit will be computed.
- EM Halo orbit is fixed (specified in Table 7-I), so the optimization process will not regard this orbit;
- the transfer trajectory will present only the first 3 legs of Fig 7.6.

The use of mode 3 has been not considered, even though it seems to be more suitable for this case. Actually it has been tested, but the total ΔV found is quite higher (7-8 km/s) than that found by using heteroclinic connections (about 4 km/s).

Homoclinic connections resulted to be more expansive since the energy required to go directly from the Earth to a Halo orbit around the LL2 point is higher than that one to get into a Halo orbit around the EL2 point. It can be explained by using the Jacobi's constant (actually a measurement of the energy level). Comparing (with the 3BM) the energy required to go from the Earth into the SE Halo orbit with Az-amplitude of 200,000 km and the energy required to get into the target EM Halo orbit computed in this section, the difference of energy is about 4 km²/s² per kg. It means that by using heteroclinic connections it's possible to save a lot of propellant, reducing the total ΔV .

Therefore mode 4 has been used also in this case and the results of the optimization process for this transfer orbit are summarized in the next table:

| Inclination (°) | EM Halo mass (tons) | ΔV_3 (km/s) | ΔV_2 (km/s) | ΔV_1 (km/s) | Total ΔV (km/s) | LEO mass (tons) |
|--------------------|------------------------|------------------------|------------------------|------------------------|----------------------------|--------------------|
| 5 | 0.8 | 2.111 | 1.353 | 3.356 | 6.820 | 3.491 |
| 28.5 | 0.8 | 2.111 | 1.433 | 1.040 | 4.584 | 2.154 |
| 51.6 | 0.8 | 2.111 | 1.469 | 1.108 | 4.688 | 2.203 |

Table 7-K Total ΔV and initial mass (in LEO) for the Earth-Moon communication satellites

For all three different cases, the SE Halo orbit with Az-amplitude of 200,000 km resulted to be the most suitable (best value for $\Delta V_2 + \Delta V_3$) for this transfer orbit.

The transfer orbit is shown:

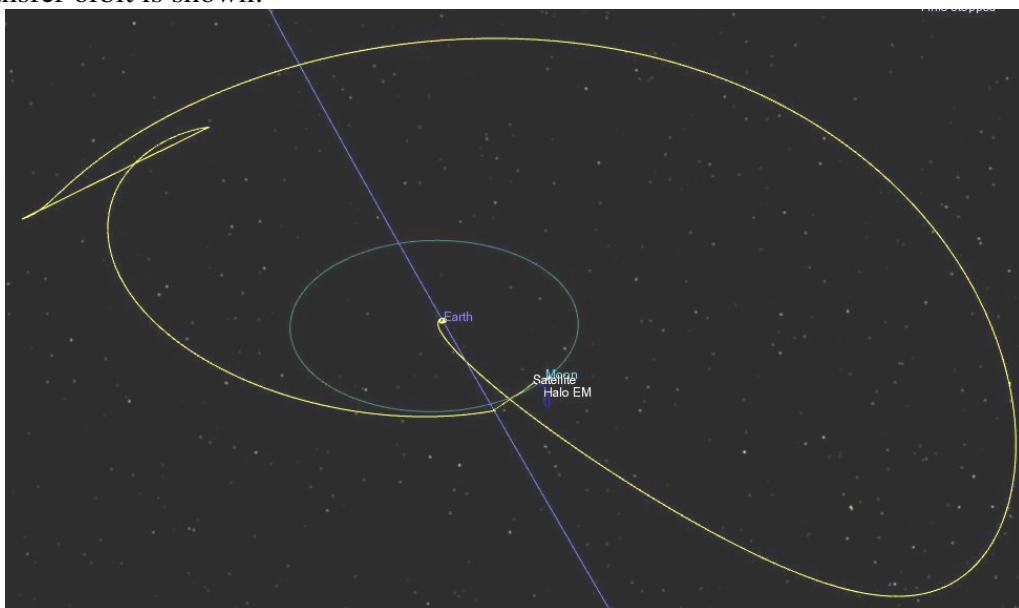


Fig 7.14 Entire trajectory for communication satellites

It is worth noticing the discontinuity present between leg 1 and leg 2. Once the SE Halo orbit has been acquired, the second leg doesn't start from that position, but from another one along the same Halo orbit (since it is assumed that the S/C can choose the proper phase angle along the Halo orbit to leave it). For this reason, there is a discontinuity in position, shown by the line crossing the Halo orbit. Avoiding that line would have been quite difficult within the STA framework, since the trajectory should have been split in two different parts.

From Table 7-K, the smallest initial mass is reached for an inclination of 28.5° . The initial mass required in LEO is 2,154 kg. Vega is able to deliver a LEO mass of circa 2,220 kg at an altitude of 300 km and at an inclination of 28.5° (see Fig 3.5). It means Vega is perfectly suitable for this mission, also because the altitude here requested is 185 km instead of the reference altitude of 300 km.

The higher ΔV required (2.111 km/s) to patch the two Halo orbits than that found in the previous section (0.189 km/s, see Table 7-G) could result “weird”, but actually it is not.

In the previous case the two sets of Halo orbits have been determined in the reference paper in such a way the energy levels were not so different. Therefore the ΔV required to switch trajectory was quite small. In this case the second Halo orbit is fixed (determined by mission requirements) and it is very stable, as it results from the analysis of the stable eigenvalue (and for this reason also the deviation ϵ has been selected almost 100 times bigger than the respective value of the previous case). For this reason a bigger ΔV is required to enter in such a Halo orbit.

CHAPTER 8

8. Low-Acceleration Trajectories: Theory

In this chapter, low-acceleration trajectories will be tackled. The STA Interplanetary Low-Thrust Module will be used for all computations. The term low-acceleration will be preferred to low-thrust (as already explained in section 3.1.3), since for this mission an engine delivering a thrust in the order of some N will be required, while usually low-thrust engines are able to deliver just a few mN. The term low-thrust will be kept for the STA module in use. First an introduction to the problem will be given and then the mathematical model in use will be discussed. Since the STA tool that is going to be used is based on the Exposins theory, developed by Petropoulos [Petropoulos et al., 1999] and adapted for the Lambert's problem [Izzo, 2006], this model will be fully explained.

The last section will regard low-thrust engines.

8.1 Introduction to low-acceleration trajectories

The mathematical model used in this section is again the 2-body problem (already explained in Chapter 4), where a satellite is moving around a main body, that generates a gravity field. The equation of motion has already been given in section 4.2, but in this case the low-acceleration term is added:

$$\ddot{\bar{r}} + \mu \frac{\bar{r}}{r^3} = \bar{a}_d \quad (8.1)$$

$$\bar{a}_d = \bar{a}_p + \bar{a}_T \quad (8.2)$$

where \bar{a}_p is the acceleration due to perturbations (gravity field asymmetry, third-body effects, solar radiation pressure and atmospheric drag, already discussed in section 4.5), \bar{a}_T is the acceleration produced by the thrust and \bar{r} is the radius vector directed from the Earth toward the spacecraft.

In this case all perturbations are neglected and the thrust term is analyzed.
It is well explained in [Betts and Erb, 2003]:

$$\bar{a}_T = \frac{g_0 T}{w} \bar{u} \quad (8.3)$$

$$\bar{a}_p = 0 \quad (8.4)$$

$$\dot{w} = -\frac{T}{I_{sp}} \quad (8.5)$$

$$\bar{u}^T = [u_x, u_y, u_z] \quad (8.6)$$

where \bar{u} is the control vector, w is the instantaneous vehicle mass, obtained by integration of the equation 8.5 and T is the thrust level.

In order to integrate such a trajectory the thrust profile (direction and magnitude) should be known. Since the optimization of the transfer trajectory is required, the trajectory design should start from a first guess of the thrust profile and then an optimizer should improve it in order to optimize the transfer orbit.

Because the main requirement of this thesis is the use of STA tools already developed, the Interplanetary Low-Thrust Module, developed by Tatiana Paulino, will be exploited. It is based on an analytical model, the Exposins, able to give good approximations of low-thrust trajectories. Actually this model would provide the first guess for the thrust-profile.

In this way it is possible to have a first approximated low-acceleration trajectory, that can be evaluated here. In case it would result into something promising, further investigations will be recommended for future works, since it would be not possible to address them here, because of the long development and implementation time required.

8.2 Exposins Theory

This technique is based on Petropoulos's work [Petropoulos et al., 1999] adapted for the Lambert's problem [Izzo, 2006].

Petropoulos proposed to approximate the solution of the equations of motion, for the low-thrust case, by using an exponential sinusoid function. This solution is based on an inverse dynamical calculation that leads to analytical expressions both for the thrusting history and for the derivative of the polar anomaly, when tangential thrust is assumed. This assumption is crucial in this kind of approach, because it substantially simplifies the problem solution.

The equations of motion, in polar coordinates, become:

$$\begin{cases} \ddot{r} - r\dot{\theta}^2 + \frac{\mu}{r^2} = F \sin \alpha \\ \ddot{\theta}r + 2\dot{\theta}\dot{r} = F \cos \alpha \end{cases} \quad (8.7)$$

The idea of Petropoulos is based on checking whether an exponential sinusoid defined by the equation:

$$r = k_0 \exp[k_1 \sin(k_2 \theta + \phi)] \quad (8.8)$$

may fit the equations of motion. It turned out that under the hypothesis of tangential thrust, i.e. $\alpha = \gamma$, the thrust history and the polar angle history are uniquely determined for each

exponential sinusoid by some analytical expressions. These expressions link $\dot{\theta}^2$ and $a = \frac{F}{\mu/r^2}$ to the four parameters [$k_0; k_1; k_2; \varphi$] defining each exponential sinusoid. They were derived by:

$$\begin{aligned}\dot{\theta}^2 &= \left(\frac{\mu}{r^3} \right) \frac{1}{\tan^2 \gamma + k_1 k_2^2 s + 1} \\ a &= \frac{\tan \gamma}{2 \cos \gamma} \left[\frac{1}{\tan^2 \gamma + k_1 k_2^2 s + 1} - \frac{k_2^2 (1 - 2k_1 s)}{\left(\tan^2 \gamma + k_1 k_2^2 s + 1 \right)^2} \right]\end{aligned}\quad (8.9)$$

(8.10)

where the flight path angle and s are defined by:

$$\tan \gamma = k_1 k_2 \cos(k_2 \theta + \varphi) \quad (8.11)$$

$$s = \sin(k_2 \theta + \varphi) \quad (8.12)$$

It has been demonstrated that these equations are meaningful whenever $|k_1 k_2| < 1$. This condition will be used later.

The shape of the trajectory is determined by the exponential sinusoid function, but the parameters are unknown yet. Therefore the velocity at the departure is considered known, which reduces the definition of the exponential spiral to one free parameter (k_2).

The Lambert's problem for this case has to be solved. Given r_1 , r_2 and the transfer angle ψ (shown in figure), all the possible exponential sinusoids, that link the two positions in a given transfer time (allowing for multiple revolutions) have to be found. Assuming k_2 to be known, the other three parameters (k_0, k_1, φ) must be determined.

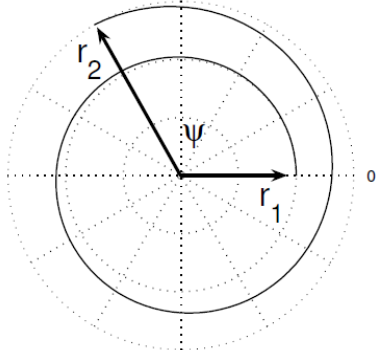


Fig 8.1 Description of the parameters involved [Vasile et al., 2006]

Without loss of generality, θ_1 is chosen equal to zero. Then it follows:

$$\tan \gamma_1 = k_1 k_2 \cos \varphi \quad (8.13)$$

Those trajectories that actually pass by the points r_1 and r_2 are interesting for our purposes, therefore the following equations can be written:

$$\begin{cases} r_1 = k_0 \exp[k_1 \sin \varphi] \\ r_2 = k_0 \exp[k_1 \sin(k_2 \bar{\theta} + \varphi)] \end{cases} \quad (8.14)$$

where $\bar{\theta} = \psi + 2\pi N$ and $N=0,1,2,\dots$, accounts for the possibility of having more than one revolution around the central body.

The other parameters are determined by:

$$k_1^2 = \left(\frac{\ln(r_1/r_2) + (\tan(\gamma_1/k_2)) \sin k_2 \bar{\theta}}{1 - \cos k_2 \bar{\theta}} \right)^2 + \frac{\tan^2 \gamma_1}{k_2^2} \quad (8.15)$$

$$\varphi = \arccos \left(\frac{\tan \gamma_1}{k_1 k_2} \right) \quad (8.16)$$

$$k_0 = \frac{r_1}{\exp(k_1 \sin \varphi)} \quad (8.17)$$

It is possible to consider the angle φ in the first two quadrants as the consideration of other possibilities would simply represent the very same exponential sinusoid, because the sign of k_1 is also changed. Given the geometry of the problem, given r_1 , r_2 and given the number of revolutions required (N), it is possible to state that $\forall k_2$ there exists a class $S_{k_2}[r_1, r_2, \psi, N]$ of exponential sinusoids passing through r_1 and r_2 and conveniently parameterized by the sole free parameter γ_1 .

Amongst all the trajectories found for specified initial and final positions, only some of them are feasible. Petropoulos showed that feasible solutions are given for those values of k_2 that satisfy the following relation:

$$1 - \frac{k_2^4}{2} \ln^2 \frac{r_1}{r_2} > \cos(k_2 \bar{\theta}) \quad (8.18)$$

[Vasile et al., 2006] states the maximum acceptable value that can meet this inequality is:

$$k_2 = \frac{2\pi}{\bar{\theta}} \quad (8.19)$$

Therefore the solution has to be found for values smaller than this one.

After having fixed the k_2 range, it is possible to determine even the acceptable range of the flight path angle:

$$\tan \gamma_{lm,M} = \frac{k_2}{2} \left[-\ln \frac{r_1}{r_2} \cot \frac{k_2 \bar{\theta}}{2} \pm \sqrt{\Delta} \right] \quad (8.20)$$

$$\text{where } \Delta = \frac{2(1 - \cos k_2 \bar{\theta})}{k_2^4} - \ln^2 \frac{r_1}{r_2}$$

Now it is possible to determine all parameters involved in this computation. Starting by k_2 , all other parameters can be calculated varying the flight path angle within its allowable range. Then k_2 has to be varied, and so on. Obviously an optimizer is required in order to obtain the

best trajectory. An example of all the feasible trajectories that can be obtained for a fixed k_2 is shown in the next figure.

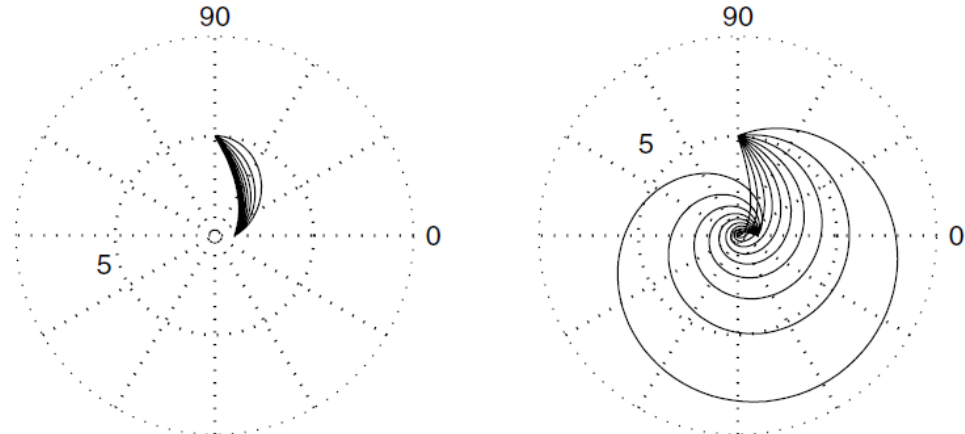


Fig 8.2 Visualization of all the feasible exponential sinusoids in the classes $S_{1/2}[1, 5, \pi/2, 0]$ and $S_{1/4}[1, 5, \pi/2, 1]$ [Izzo, 2006]

A suggestion for the function to maximize is given by [Izzo, 2006]. He suggests to use the following function:

$$J = \int_0^{\bar{\theta}} \frac{|a|}{\dot{\theta}} d\theta \quad (8.21)$$

It is possible to show that this problem is equivalent to the problem of minimizing the ratio $\frac{m_p}{m_s}$ between the mass of propellant used during the thrust arc, m_p , and the remaining spacecraft mass m_s .

The last important formula is about the TOF. It can be numerically computed by using [Vasile et al., 2006]:

$$\Delta t = \int_0^{\theta} \left(\left(\frac{\mu}{r^3} \right) \frac{1}{\tan^2 \gamma + k_1 k_2 s + 1} \right)^{-\frac{1}{2}} d\theta \quad (8.22)$$

The most important drawback of this theory is that it doesn't use anywhere the information of the final velocity. This is important, because if this velocity doesn't match the Moon's velocity, of course a manoeuvre is required in order to obtain the injection into a lunar orbit. For this reason, the auspicated condition is that the two velocities are as similar as possible, such that the manoeuvre to get into the parking orbit will be very small and cheap, in terms of propellant consumption.

Therefore, also this ΔV should be taken into account for the selection of the best trajectory.

This technique was already implemented in the Interplanetary Low-Thrust Module, therefore it will represent the model used to compute the low-acceleration trajectory.

8.3 Low-Thrust Engines

The choice of a low-acceleration engine is even more difficult and important than the choice of a high-thrust engine. Actually the low-acceleration engine will be working continuously for many days/months, therefore the specific impulse will be crucial for the performance evaluation.

An interesting overview of all the different kinds of low-thrusters is given in the next table, where the most important classes are considered with average performances.

| Type | Thrust Range (mN) | Specific Impulse (sec) | Thruster Efficiency ^b (%) | Thrust Duration | Typical Propellants | Kinetic Power per Unit Thrust (W/mN) |
|-----------------------------|-------------------|------------------------|--------------------------------------|-----------------|---|--------------------------------------|
| Resistojet (thermal) | 200–300 | 200–350 | 65–90 | Months | NH ₃ , N ₂ H ₄ , H ₂ | 0.5–6 |
| Arcjet (thermal) | 200–1000 | 400–1000 | 30–50 | Months | H ₂ , N ₂ , N ₂ H ₄ , NH ₃ | 2–3 |
| Ion engine | 0.01–200 | 1500–5000 | 60–80 | Months | Xe, Kr, Ar | 10–70 |
| Solid pulsed plasma (PPT) | 0.05–10 | 600–2000 | 10 | Years | Teflon | 10–50 |
| Magnetoplasma dynamic (MPD) | 0.001–2000 | 2000–5000 | 30–50 | Weeks | Ar, Xe, H ₂ , Li | 100 |
| Hall thruster | 0.01–2000 | 1500–2000 | 30–50 | Months | Xe, Ar | 100 |

Table 8-A Ranges of typical performances for various types of electrical propulsion systems [Sutton and Biblarz, 2001]

All these motors are based on an electric system, the difference is given by the specific energy source adopted. Actually a serious problem is given by the power required, that sometimes becomes very high (200 kW for Hall thrusters).

For the payload considered (20 tons in LEO), it is necessary to have a thrust about 20 N [Herman and Conway, 1998] in order to have a reasonable high initial acceleration. Therefore it is already possible to exclude some engines classes, as resistojet and solid pulsed plasma, that are unable to give such a thrust. Moreover the Ares V payload in LEO (130 tons) doesn't allow to use low-acceleration trajectories, since the thrust required would be too high. Therefore this technique will be used for the other cases only.

In addition, a new interesting type of engines has to be added to the previous list, the VAriable Specific Impulse Magnetoplasma Rocket (VASIMR), that will be available in few years [Ad Astra website, 2008].

Actually this last class represents the best option for this mission, as explained in [Zuccarelli, 2008]. The VASIMR motors will be able to deliver about 10-20 N of thrust, still with a high value of specific impulse.

The VASIMR is a high power magnetoplasma rocket, capable of Isp/thrust modulation at constant power. The plasma is produced by a helicon discharge. It uses radio waves to ionize a propellant and magnetic fields to accelerate the resulting plasma to generate thrust.

Two interesting thrusters are still under development: Vx-100 and Vx-200. Because of their newness, it is difficult to find the features of these engines, because the data available are very few.

The most interesting is the Vx-200. The next table summarizes its performances [Bering III et al, 2008] and [Wikipedia, 2008]:

| | Thrust (N) | Input Power (kW) | Specific Impulse (s) |
|--------|------------|------------------|----------------------|
| Vx-200 | 9.24 | 200 | 3000 |

Table 8-B Vx-200 performances

This engine is already in testing and developing phases, but even in this case the availability in the next few years is not proven. Anyway during the literature study its availability has been assumed reasonable, therefore now it will be used for the low-acceleration trajectories. Since a thrust of 20 N can be required, the use of two thrusters at the same time is considered allowable. This solution would require a conspicuous amount of electrical power (400 kW). This problem is tackled in the coming paragraph.

8.4 Electric Input Power

So far the electrical power required for S/C usually was about a couple of kW; for instance SMART-1 and Deep Space 1, that carried an electrical thruster, required just less than 2 kW, while the Space Shuttle requires 7 kW. The greatest power supply is required by the ISS, that with its solar array wings of 408 m^2 can obtain 32.8 kW (power density of circa 80 W/m^2). As already shown, previous motors require huge quantities of electrical power. It means that many problems could arise about the power supply, because maybe the required power could be supplied only by too big and too heavy array wings, indeed an unfeasible solution.

Therefore a technology able to deliver this amount of energy is required.

Actually many interesting developments are coming from many companies, in particular from Entech, that is collaborating intensely with NASA, in order to improve the solar array performances. The actual typical value for the Areal Power Density and for the Specific Power, crucial parameters in order to keep the array wing dimension feasible, don't exceed respectively 300 W/m^2 and 60 W/kg . In the next years, substantial improvements are expected. The actual available technology is the Stretched Lens Array (SLA), developed by Entech. This is based on a solar array, using triple-junction solar cells as the principle power source for a spacecraft. This is an improvement of the system that already flew on the Deep Space 1 mission, with the name SCARLET (Solar Concentrator Array using Refractive Linear Element Technology) [O'Neill et al., 2006].

The SLA is an evolved version of SCARLET. The essential power-generating elements (the silicone Fresnel lens, the multi-junction solar cells, and the composite radiator sheet) have been retained, while many of the non-power-generating elements have been changed. One of the most efficient platforms for deploying and supporting the flexible-blanket version of SLA is the SquareRigger platform (shown in the next figure), developed by ABLE Engineering.

However, with the much higher efficiencies achievable with SLA compared to thin-film photovoltaics, the combination of SLA and SquareRigger gives unprecedented performance metrics [O'Neill, 2004].



Fig 8.3 SLA on SquareRigger platform [O'Neill, 2007]

The dimensions are about 2.5 m x 5.0 m (12.5 m^2) and the deployment system is shown in the next figures.



Fig 8.4 SquareRigger platform deployment [O'Neill, 2007] Fig 8.5 SLA deployment on the SquareRigger platform [O'Neill, 2007]

In addition, a laser-receiving version of SLA is under development for space applications when or where sunlight is not available (for instance the eternally dark lunar polar craters). The laser-receiving SLA can collect and convert beamed laser power from other sources (e.g., solar-powered lasers on the permanently illuminated ridges of lunar polar craters). A combined dual-use version of SLA can produce power both from sunlight and from beamed laser light during darkness periods. It's clear that this new development could be very useful for a lunar permanent base.

The laser version of SLA uses single-junction photovoltaic cells instead of the multi-junction cells used in the solar version. For infrared laser light in the wavelength range of 0.80–0.85 microns, GaAs is an ideal photovoltaic cell. In order to verify the achievable conversion efficiency of the laser version, a number of prototype SLA modules were developed. The laser version of SLA is being developed to utilize the same deployment and support structures as the solar version.

The performances of both these systems are summarized in the following table:

| Parameter | Solar SLA | Laser SLA |
|--|-----------|-----------|
| Net Areal Power Density (W/m^2) | 309 | 690 |
| Wing Mass Density (kg/m^2) | 0.86 | 0.86 |
| Net Specific Power (W/kg) | 359 | 803 |

Table 8-C Solar and Laser SLA performances on SquareRigger platform [O'Neill et al., 2006]

Taking a look at the Entech technology roadmap, systems based on SquareRigger platforms will be able to give since 100 kW till 1 MW before 2015, that is more or less the initial date for this lunar mission, making this solution available and suitable for this mission [O'Neill, 2007]:

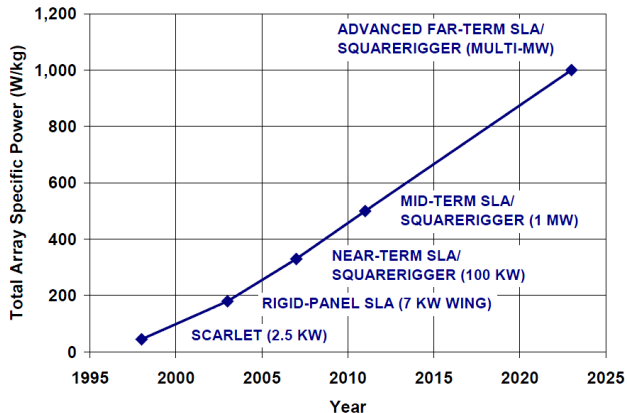


Fig 8.6 Enitech technology road-map [O'Neill, 2007]

Therefore from all these data, it is possible to conclude that the technology in order to obtain huge amounts of power will be available in a few years. Moreover the dimensions of these solar arrays will not be so big, because the deployment system allows the launcher to store the platform in a very comfortable way. As shown in one of the previous figures, the platform, before being deployed, has one relevant dimension of 2.5 m. So the use of VASIMR motors can be considered feasible also from a power supply point of view.

CHAPTER 9

9. Low-Acceleration Trajectories: Results

In this chapter, all the results regarding low-acceleration trajectories will be addressed. A brief introduction to the STA Interplanetary Low-Thrust Module will be given. This module, already developed by Tatiana Paulino [ESA Technical Note, 2009c], has been integrated in STA by the author of this work, in order to use it and to plot the final trajectory. The inputs used for the different simulations will be listed and all the results collected and discussed.

9.1 STA Interplanetary Low-Thrust Module

As already mentioned in Chapter 8, the low-acceleration trajectories will be tackled by using this STA tool. It is based on the solution of the Lambert's problem and it makes use of the Exposins theory. An optimizer (DG-MOPSO [Coello et al, 2004]) based on a Particle Swarm algorithm is used in order to minimize the total ΔV of the mission.

The inputs required are the initial and final altitudes of the orbit respectively around the Earth and the Moon (specified in section 3.2), the launch window, information about the high-thrust propulsion subsystem (given in section 4.6.6) and about the low-acceleration engine (given in section 8.3), optimization settings (used default values), the initial mass of the S/C (specified in section 3.2.1) and the relative propellant mass.

It is worth emphasizing:

- the high-thrust engine is required to escape from the orbit around the Earth in order to inject the S/C into the transfer orbit (ΔV_1) and to insert it into the final lunar orbit (ΔV_2). Therefore two high-impulsive manoeuvre are anyway executed. Between them, the low-acceleration engine will be working;
- the initial propellant mass has been assumed as the 60% of the total mass delivered in a LEO orbit (section 3.2.1). This value is reasonable, taking a look at many interplanetary missions, but anyway it is not a driving parameter, since it is used just to check the propellant mass constraint. Actually the final mass delivered around the Moon is the goal of this work, therefore by subtracting the propellant mass consumed from the total mass in LEO, the final mass delivered can be computed;

- during the low-acceleration arc the maximum acceleration required is checked by using the maximum acceleration available at each instant. This constraint is implemented in the STA Interplanetary Low-thrust Module in order to avoid unfeasible trajectories;
- the starting epoch is selected by the optimizer in such a way the arrival date is within the interval selected by the user. Therefore the starting epoch can be selected by the optimizer also some time before the starting epoch given by the user. It will not affect our computations;
- only the initial and final altitudes of the two parking orbits are considered. Since the Exposins theory is an analytical approximation of low-acceleration trajectories, no information are given about the inclination and the orientation of those orbits. For this reason, as explained in section 8.1, this module can give just a first approximation of this kind of trajectories.

The GUI of this module, with all the inputs required, is shown in the following figure:

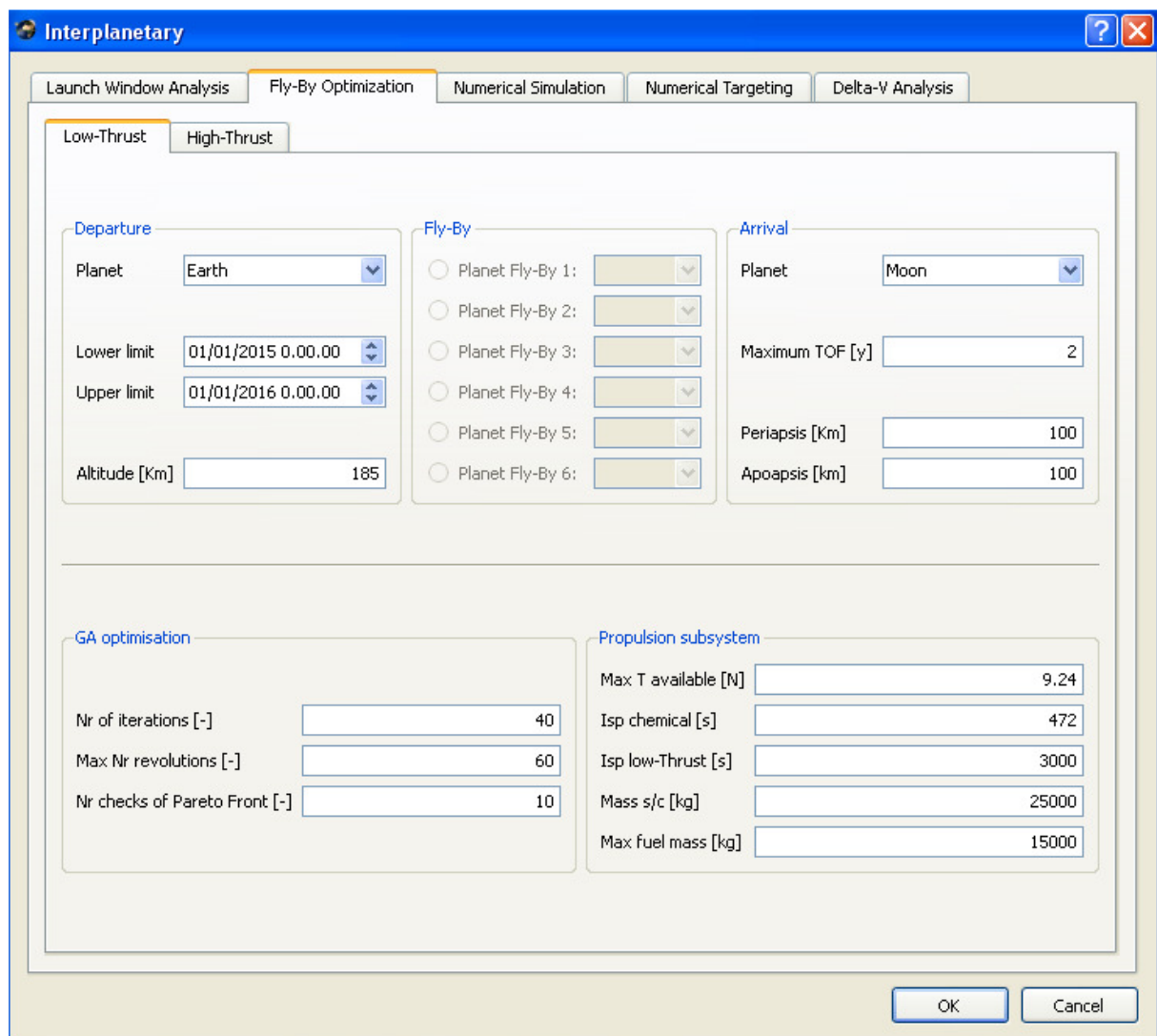


Fig 9.1 STA Low-Thrust Interplanetary module GUI

Several different simulations have been planned in order to verify how many missions per year are possible to launch by using this technique and to verify whether the performance is sensitive to the launch windows. Therefore the following simulations have been run and their results will be shown in the next paragraphs:

| Simulation | Lower Limit | Upper Limit | Mass S/C (tons) | Max TOF (y) |
|------------|-------------|-------------|-----------------|-------------|
| A | 01/01/2015 | 01/01/2016 | 25 | 2 |
| A | 01/01/2016 | 01/01/2017 | 25 | 2 |
| B | 01/01/2015 | 31/03/2015 | 25 | 0.25 |
| B | 01/04/2015 | 30/06/2015 | 25 | 0.25 |
| B | 01/07/2015 | 30/09/2015 | 25 | 0.25 |
| B | 01/10/2015 | 31/12/2015 | 25 | 0.25 |
| C | 01/01/2015 | 31/03/2015 | 25 | 0.25 |
| C | 01/01/2015 | 31/03/2015 | 22 | 0.25 |
| C | 01/01/2015 | 31/03/2015 | 21 | 0.25 |
| C | 01/01/2015 | 31/03/2015 | 20 | 0.25 |

Table 9-A Simulations plan for STA Interplanetary Low-thrust module

The aim of each simulation is briefly described:

- **Simulation A:** wants to analyze differences on performances varying the year of the launch window in order to verify if performances are strongly affected by the year selected for the mission. Moreover the TOF obtained will be used to reduce the maximum TOF for simulation B;
- **Simulation B:** wants to analyze differences on performances varying the launch window within the same year. Moreover it will be used to fix the launch window for simulation C;
- **Simulation C:** wants to analyze differences on performances varying the launcher.

9.2 Simulation A

In order to check if the transfer trajectory is affected by the selection of the year of the launch, two different simulations have been run, one for 2015 and the other one for 2016. The results follow:

| Year | TOF (y) | $\Delta V1$ (km/s) | $\Delta V2$ (km/s) | Total ΔV (km/s) | Fuel for low-acc phase (kg) | LEO mass (tons) | LLO mass (tons) |
|------|---------|--------------------|--------------------|-------------------------|-----------------------------|-----------------|-----------------|
| 2015 | 0.255 | 2.477 | 0.875 | 3.352 | 3.57 | 25 | 12.115 |
| 2016 | 0.153 | 2.476 | 0.875 | 3.351 | 3.39 | 25 | 12.117 |

Table 9-B Simulation A results

In the next figures, the two trajectories are shown.

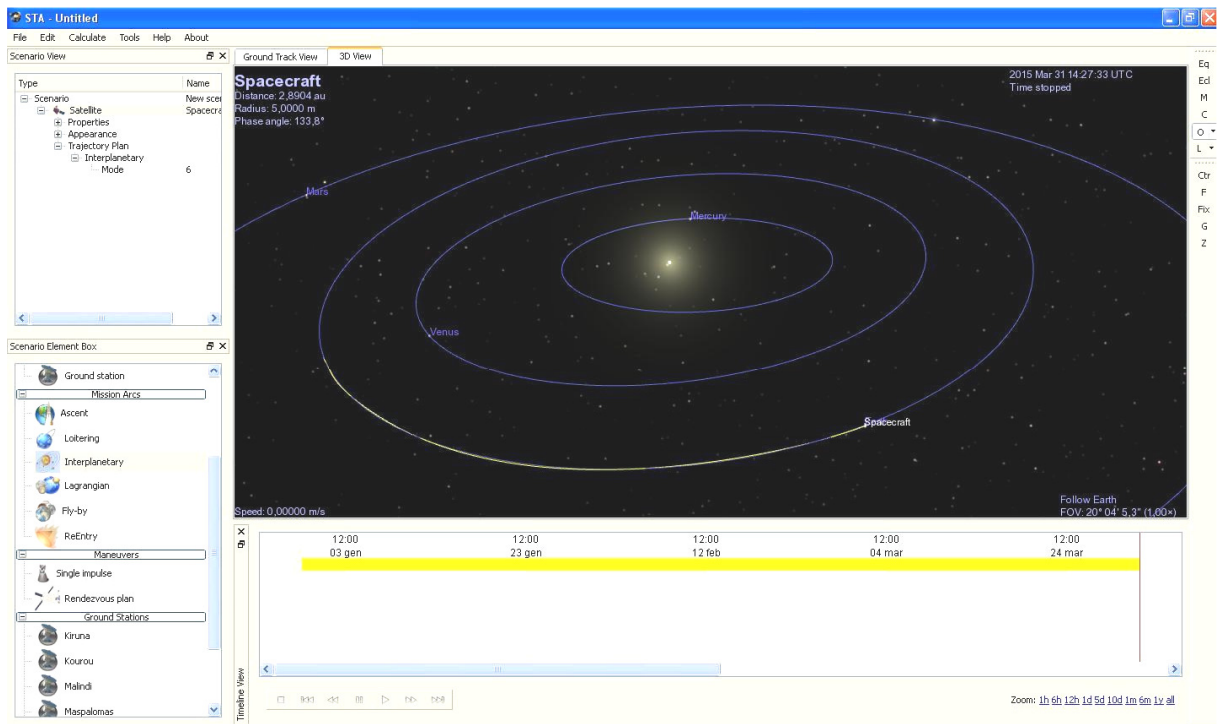


Fig 9.2 Simulation A trajectory (2015)

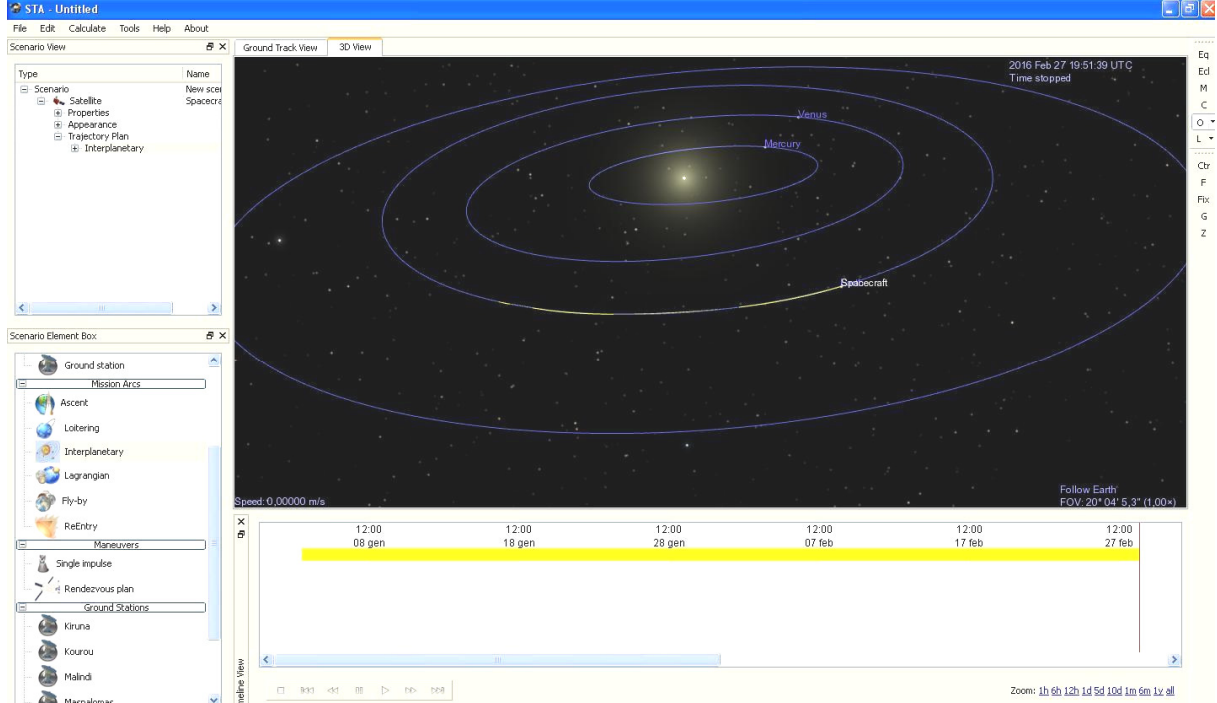


Fig 9.3 Simulation A trajectory (2016)

The two trajectories are very similar, except for the TOF, which is longer in the first case. Besides also the total ΔV and the LLO mass delivered are actually the same. It means there are no significant differences if the year of launch is changed.

From last pictures, the spiralling orbit around the Earth, as expected from an Exposins trajectory, can't be recognize, since it is plotted in the heliocentric reference frame. For this reason the first trajectory has been plotted also in the geocentric r.f. by using MATLAB.

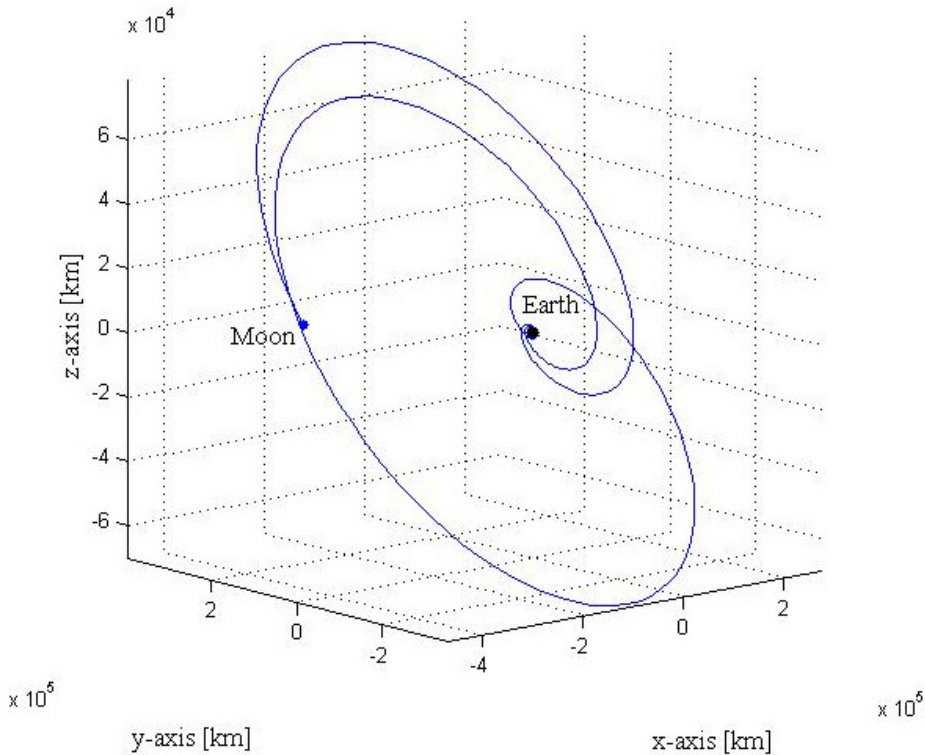


Fig 9.4 Simulation A trajectory in the geocentric r.f. (2015)

For simulation B a maximum TOF of 0.25 years will be selected, and the year selected will be 2015. In this way, it's possible to check if also during 2015 it is possible to have shorter trajectories.

This first simulation shown that one low-acceleration motor (Vx-200) is enough to go from the Earth to the Moon, since the thrust level has been selected equal to 9.24 N (only one motor).

9.3 Simulation B

Since the maximum TOF chosen for this simulation is 0.25 years, the year 2015 will be split in four trimesters, and for each of them a simulation will be run in order to compare the results. In case this technique will result very promising, a more detailed analysis will be executed in order to understand if more launchers per year would be available. Again the same initial mass is used. All the results are collected in the following table:

| Trimester | TOF (y) | ΔV_1 (km/s) | ΔV_2 (km/s) | Total ΔV (km/s) | Fuel for low-acc phase (kg) | LEO mass (tons) | LLO mass (tons) |
|-----------------|---------|---------------------|---------------------|-------------------------|-----------------------------|-----------------|-----------------|
| 1 st | 0.111 | 2.476 | 0.876 | 3.352 | 3.34 | 25 | 12.115 |
| 2 nd | 0.160 | 2.476 | 0.875 | 3.351 | 3.40 | 25 | 12.118 |
| 3 rd | 0.144 | 2.476 | 0.876 | 3.352 | 3.38 | 25 | 12.116 |
| 4 th | 0.245 | 2.476 | 0.874 | 3.350 | 3.53 | 25 | 12.118 |

Table 9-C Simulation B results

Also in this case, there are almost no differences (in the total ΔV) between the results obtained. The total mass delivered is actually the same. The TOF changes depending on the period considered, but that is because the total ΔV is the only parameter optimized. If it would be slightly increased (in the order of few m/s) it would be possible to obtain other solutions with shorter TOF, as in the first trimester. Anyway also from the previous simulation, it is possible to state that there are many different good trajectories at least every three months (most likely every month, as demonstrated by Chapter 5) not depending on the year. Actually reducing the maximum allowable TOF, it would be possible to find trajectories with the same performances also in the same trimester. It seems reasonable, because this model doesn't take into account inclinations and orientations of the parking orbits around the Earth and the Moon, that can strongly affect the magnitudes of the impulsive manoeuvres and because of the geometry of the problem. Also for this reason, the total ΔV obtained is quite smaller than that derived in chapter 5.

Anyway the availability of at least four launches per year with a TOF of 0.111-0.160 years (40-60 days) is assumed for every year. The value of 0.245 years obtained for the 4th trimester has been taken out, because, by increasing the total ΔV , the TOF can be easily decreased, as already explained.

9.4 Simulation C

Now the performances of different launchers will be evaluated. In this simulation the initial mass depends on the launcher, while the launch window is the first trimester of 2015, since this choice doesn't affect the computations. The results obtained are collected here:

| Launcher | TOF (y) | $\Delta V1$ (km/s) | $\Delta V2$ (km/s) | Total ΔV (km/s) | Fuel for low-acc phase (kg) | LEO mass (tons) | LLO mass (tons) | Moon Payload (tons) |
|----------|---------|--------------------|--------------------|-------------------------|-----------------------------|-----------------|-----------------|---------------------|
| Ariane V | 0.111 | 2.476 | 0.876 | 3.352 | 3.02 | 22.6 | 10.952 | 5.052 |
| Proton | 0.111 | 2.476 | 0.876 | 3.352 | 2.80 | 21 | 10.177 | 4.277 |
| Ares I | 0.111 | 2.476 | 0.876 | 3.352 | 3.34 | 25 | 12.115 | 6.215 |
| Atlas V | 0.111 | 2.476 | 0.876 | 3.352 | 2.70 | 20.25 | 9.813 | 3.913 |

Table 9-D Simulation C results

The TOF and the total ΔV obtained are the same for all the launchers, and this was expected since the transfer orbit doesn't depend on the initial mass and inclination. The difference on the final mass is given by the manoeuvres, that regard different masses.

The launcher with the highest total mass delivered is Ares I, due to the higher initial LEO mass. Ariane V and Ares I seem to be suitable for unmanned missions, but further discussions about them will take place in the next chapter (for this reason they are highlighted in orange and not in green), where also these results will be discussed.

It's worth emphasizing here that the small amounts of fuel consumed for the low-acceleration phase suggest that this phase is not predominant, but the interplanetary transfer is actually performed by using the two impulsive shots (this is confirmed by their high values). It means that with this module (actually with the Exposins theory) is not possible to obtain a real low-thrust trajectory within the Earth-Moon system, at least for so massive S/C's and for so short

TOF (increasing only the TOF doesn't change that behaviour). The low-acceleration phase seems to be used mainly to correct the trajectory.

However, it is impossible to benchmark this results, because a similar trajectory has been never used so far. Actually low-acceleration motors have been used only on smaller S/C's. The total ΔV obtained seems reasonable, since it doesn't take into account the inclination of the two parking orbits.

CHAPTER 10

10. Conclusions and Recommendations

In this chapter, all the results from Chapters 5, 7 and 9 will be summarized and discussed and a launch sequence (starting by that one in section 2.6) with the best trajectory selected for each launch will be determined.

Then some recommendations will be given in order to help those who wants to start from this work trying to improve the results obtained.

10.1 Conclusions

The most important results obtained in the last chapters will be summarized here and then analyzed. The following structure will be followed:

- definition of the minimum Moon payload/LLO mass;
- selection of the launchers and trajectories available;
- design of the launch sequence for the building phase;
- design of the launch sequence for the maintenance phase

From this analysis the transfer orbit for the communication satellites has been excluded, since the orbit computed in section 7.4 is the only one available for such a mission. The STA Interplanetary Module and the STA Interplanetary Low-Thrust Module, as they have been implemented, would not consent to design a transfer trajectory pointing a Halo orbit.

10.1.1 Definition of the Minimum Moon Payload/LLO Mass

As stated in section 2.4, the mass of one emergency, spaceport and lunar base module consists of 0.7 tons inflatable shell, 3 tons supporting structure, 5 tons airlock and payload mass (6.5-8 tons). Therefore the biggest part that can't be split in smaller pieces is the airlock. It represents the **minimum Moon payload** mass required to build the base. If any launchers would not be able to bring **5 tons** in a lunar parking orbit (Moon payload mass, see Table 2-G), the base can't be built.

For manned missions there are no constraints on the minimum Moon payload, since they can be performed even without bringing additional mass, as explained in the definition of Mass payload (2.3). Therefore for manned the parameter to check is the **minimum LLO mass**, that should be at least equal to **47 tons** (Table 2-F).

10.1.2 Selection of the Launchers and Trajectories Available

The results on the LLO mass (for manned missions) and on the Moon Payload mass (for unmanned missions) have been summarized in the next tables. Those options (not) matching the requirement of the mass to deliver have been written in green (red). Those other options requiring further considerations have been written in orange.

| Launcher | LLO mass High-Thrust (tons) | LLO mass 3BP (tons) | LLO mass <u>required</u> (tons) |
|----------|-----------------------------------|---------------------------|------------------------------------|
| Ares V | 49.341 | 51.866 | 47 |

Table 10-A Check on the mass delivered for manned mission

For manned missions low-accelerations trajectories have not been considered, because the thrust required for such a massive S/C is not allowed by any motor.

From Table 10-A some conclusions can be derived for manned missions:

- for both the trajectories (based on high-thrust and the 3BP), the LLO mass delivered matches the minimum mass to deliver (defined in section 2.5) in order to transport astronauts to the Moon;
- for manned mission an important parameter is the total TOF, since men shouldn't travel for too long through the space. For the high-thrust trajectories the TOF is in the order of days, while for the 3BP trajectories the TOF is in the order of months. Therefore this second option should be discarded;
- for High-Thrust trajectories the Moon payload is “only” 2.523 tons (Table 5-G), therefore most likely it will be not used to bring any additional payload to the Moon.

For manned missions the only available option is an Ares V mission based on a high-thrust trajectory. It is able to bring astronauts to the Moon with a smaller additional payload than that previously stated in section 2.5.

| Launcher | Moon payload High-Thrust (tons) | Moon payload 3BP (tons) | Moon payload Low-Acceleration (tons) | Moon payload <u>required</u> (tons) |
|----------|---------------------------------------|-------------------------------|--|--|
| Ariane V | 2.289 | 2.152 | 5.052 | 5 |
| Proton | 0 | 3.094 | 4.277 | 5 |
| Ares V | 29.341 | 31.896 | - | 5 |
| Ares I | 3.589 | 4.074 | 6.215 | 5 |
| Atlas V | 1.786 | 2.179 | 3.913 | 5 |

Table 10-B Check on the Moon payload mass delivered for cargo missions

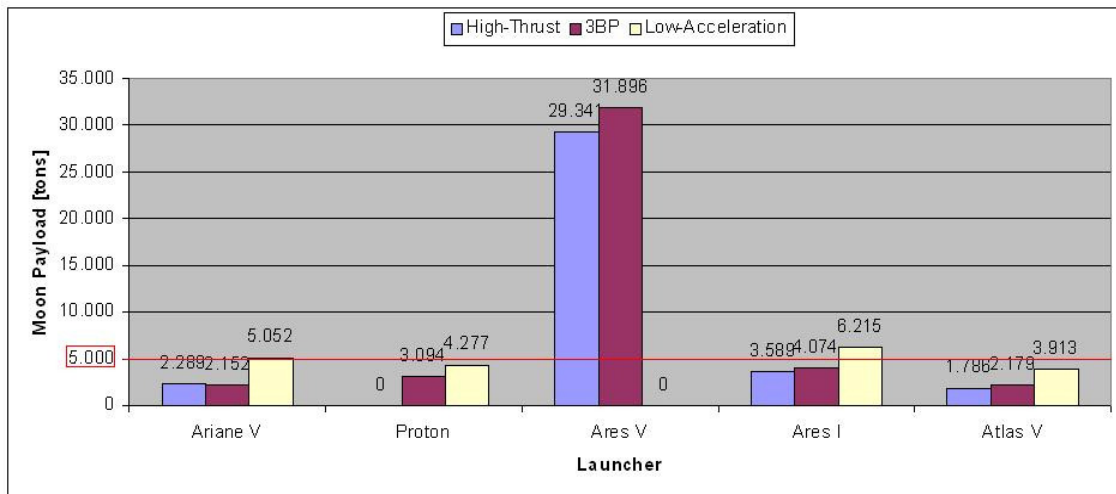


Fig 10.1 Moon payload mass plot for cargo missions

From Table 10-B and **Fig 10.1** some conclusions can be derived for cargo missions:

- high-thrust and 3-body trajectories allow only Ares V missions. The other launchers can be used to bring to the Moon smaller payload: 3.5-4 tons for Ares I (respectively by means of high-thrust and 3BP trajectories), 3 tons for Proton and 2 tons for Atlas V (by means of 3BP trajectories) and 2 tons for Ariane V (by means of both techniques);
- since for Ariane V high-thrust and 3-body trajectories give almost the same Moon payload, the first ones are preferred, due to the shorter TOF;
- low-acceleration trajectories allow Ariane V and Ares I missions. This kind of orbits didn't take into account the inclination of the initial and final orbits. Therefore a certain amount of propellant should be considered for additional manoeuvres. Since the surplus of mass for Ariane V and Ares I (respectively 52 kg and 1215 kg) are not sufficient to cover them (they would allow an additional ΔV respectively of 0.022 km/s and 0.489 km/s, computed by using the Tsiolkovsky law), these launchers should be considered not allowable;
- for the same reason explained before, low-thrust trajectories for Ariane V, Proton and Ares I can't be considered for missions with smaller payload. For instance, in case a Moon payload of 4 tons would be considered for Ares I missions, the total ΔV available for manoeuvres would be 0.935 km/s (corresponding to 2,215 kg of propellant by using the Tsiolkovsky law). Since it's difficult to understand if that value could be sufficient or not, in case of smaller payload it seems logical to use 3BP trajectories for them;
- only Ares V missions allow to bring modules of the base to the Moon. The Moon payload obtained is 29.341 tons for high-thrust trajectories and 31.896 tons for 3-body trajectories;
- since for Ares V two different trajectories are available, for those missions the Moon payload required is below 29.341 tons a high-thrust trajectory will be selected, because of the shorter TOF, while if the Moon payload required will exceed 29.341 tons (until 31.896 tons) a 3-body trajectory will be selected.

For cargo missions, the only launcher able to bring on the Moon modules of the lunar base is Ares V. No back-up launchers have been identified, therefore the availability and the reliability of Ares V will be crucial in order to build this base. Ares I, Proton, Atlas V and Ariane V missions will be considered for smaller payloads (up to respectively 4 tons, 3 tons, 2 tons and 2 tons) by means of 3BP trajectories (high-thrust trajectories for Ariane V).

The results are summarized in the next table:

| Mission | Launcher | Trajectory | TOF (days) | Moon payload (tons) |
|---------|----------|-------------|------------|---------------------|
| Manned | Ares V | High-thrust | 5-6 | 0 |
| Cargo | Ares V | 3-body | *100 | 31.896 |
| Cargo | Ares V | High-thrust | 5-6 | 29.341 |
| Cargo | Ares I | 3-body | *100 | 4 |
| Cargo | Proton | 3-body | *100 | 3 |
| Cargo | Ariane V | High-thrust | *100 | 2 |
| Cargo | Atlas V | 3-body | 5-6 | 2 |

Table 10-C Launchers and trajectories selected depending on the maximum payload

* based on reference data, since here the TOF has not been considered for the 3BM [Belbruno and Carrico, 2000] and [Parker and Lo, 2006].

10.1.3 Design of the Launch Sequence for the Building Phase

The first launch sequence designed in section 2.6 for the building phase (reported in Table 10-D) will be now reworked taking into account the results summarized in Table 10-C.

| Year | Number of launch | Payload type | Moon Payload (tons) | Manned/ Unmanned |
|------|------------------|--|---------------------|------------------|
| 1 | 1 | Two comm. satellites in L2 | 0.8 | U |
| 1 | 2 | Base module 1+payload | 16.7 | U |
| 1 | 3 | Base module 2+payload | 16.7 | U |
| 1 | 4 | Base module 3+payload | 16.7 | U |
| 1 | 5 | Base module 4+payload | 16.7 | U |
| 1 | 6 | Emergency base+payload + cargo rover | 15.7 | U |
| 2,3 | 7-16 | Astronauts | - | M |
| 4 | 17 | Spaceport module 1 + payload + unpressurized rover + telescope | 16.6 | U |
| 4 | 18 | Spaceport module 2+payload | 15.2 | U |
| 4 | 19-22 | Astronauts | - | M |

Table 10-D First launch sequence for the building phase (see Table 2-H)

In the new launch sequence, also the launcher and the trajectory to use are specified:

| Year | Nr. of launch | Launcher | Trajectory | TOF (days) | Payload type | Moon Payload (tons) | Manned/Unmanned |
|------|---------------|----------|-------------|------------|---|---------------------|-----------------|
| 1 | 1 | Vega | 3-body | **100 | Two comm. satellites in L2 | 0.8 | U |
| 1 | 2 | Ares V | 3-body | **100 | Base module 1+ ***Base 2 module (-2 tons of pay) | 31.4 | U |
| 1 | 3 | Ares V | High-thrust | 5-6 | Base module 2(2 tons of pay) + Base module 3 + Base module 4 (struc) | 27.4 | U |
| 1 | 4 | Ares V | 3-body | **100 | Base module 4 (pay) + Emergency base +Spaceport module 1(pay) + rovers | 30.4 | U |
| 2-3 | 5-14 | Ares V | High-thrust | 5-6 | Astronauts | - | M |
| 4 | 15 | Ares V | High-thrust | 5-6 | Spaceport module 1(struc) + Spaceport module 2 + telescope | 25.1 | U |
| 4 | 16-19 | Ares V | High-thrust | 5-6 | Astronauts | - | M |

*Table 10-E Final launch sequence for the building phase

*a module can be decomposed in payload (pay) of 8,000-6,500 kg and structure (struc). The structure can be further divided in: inflatable shell (shell) of 700 kg, supporting structure (supp) of 3,000 kg, airlock (air) of 5,000 kg; only the payload mass can be split in smaller pieces (as explained in section 2.4).

** based on reference data, since here the TOF has not been considered for the 3BM [Belbruno and Carrico, 2000] and [Parker and Lo, 2006].

*** - means that all the module has been carried except for the part specified.

By means of the 3-body trajectories three launches less are required to build the base. Since 4 years are required to build the base, it seems reasonable to start the building phase in 2015 or 2016 in order to have a certain safety margin to deliver the base in time.

It has been explained already that no back-up launchers are available for Ares V. It means in case of technical problems, the building phase should be stopped.

10.1.4 Design of the Launch Sequence for the Maintenance Phase

The first launch sequence designed in section 2.6 for the maintenance phase (reported in Table 10-F) will be now reworked taking into account the results summarized in Table 10-C.

| Number of launch per year | Payload type | Moon Payload (tons) | Manned/ Unmanned |
|---------------------------|---------------------------------------|---------------------|------------------|
| 1 | Astronauts/Cargo supply (maintenance) | 4 | M |
| 2 | Cargo supply | 8 | U |
| 3 | Astronauts | - | M |

Table 10-F First launch sequence for the maintenance phase (see Table 2-I)

In the new launch sequence, also the launcher and the trajectory to use are specified:

| Number of launch per year | Launcher | Trajectory | TOF | Payload type | Moon Payload (tons) | Manned/ Unmanned |
|---------------------------|----------|-------------|------|---------------------------------------|---------------------|------------------|
| 1 | Ares | 3-body | *100 | Astronauts/Cargo supply (maintenance) | 4 | M |
| 2-3 | Ares I | 3-body | *100 | Cargo supply | 4 (2x) | U |
| 4 | Ares V | High-thrust | 5-6 | Astronauts | - | M |

Table 10-G Final launch sequence for the maintenance phase

* based on reference data, since here the TOF has not been considered for the 3BM [Belbruno and Carrico, 2000] and [Parker and Lo, 2006].

The use of Ares V for “only” 8 tons is not justified, therefore two launches of a smaller launcher are preferred. They can be Ares I, Proton, Atlas V or Ariane V, depending on the real dimensions of the cargo supplies. Actually during the literature study they have been quantified equal to 8 tons and 4 tons respectively for food/water/oxygen/etc. supply and for maintenance supply; in that case Ares I will be used. In case a different mass is required, depending on the specific needs that can change from year to year, the best combinations of launchers can be used.

It is very important to have back-up launchers, because in case of technical problems, cargo supplies can be sent to the base always. In this way the astronauts will not remain without supplies.

10.2 Recommendations

In this subsection, a list of recommendations and suggestions for future developments of this work are given.

Since more than one year has been spent on this project and since the complexity of this work easily came up during this period, some recommendations will be given in order to further improved it and to give some guidelines for future works.

- The inputs coming from the ascent and landing phases should be taken into account for the determination of the initial and final orbits, respectively around the Earth and the Moon, instead of assuming them, as done in this work.
- Developments of new S/C as well as new motors (both high or low-thrust) should be considered to improve the mission performance.
- An extensive use of perturbations (solar radiation pressure, lunar third-body effect, etc.) will improve the accuracy of the computations and it is strongly suggested for all the three different kinds of trajectories here considered, but maybe it will not change so much the performances obtained.
- The efficiency of the numerical targeting mode of the STA Interplanetary Module should be strongly improved. The computational time required is very high (from 8 to 48 hours). Furthermore sometimes the results lack of robustness (differences of 20-40° on the inclination of the initial parking orbit around the Earth).
- The use of Lissajous orbits along with Halo orbits should be explored.
- The use of ballistic captures, even though very difficult to implement, could give more accurate results. In this way the computation of the TOF could be more reliable as well as the complete transfer orbit, since the injection into Halo orbits will be avoided, saving time.
- The use of a complete ephemerides model in order to nullify the patching ΔV is suggested.
- A less stable Halo orbit with the same period required (7.5 days) might be found. In this way the patching ΔV might be slightly reduced.
- The optimization tunings for the 3BM should be further improved. Since the complexity of the problem, it's not easy to defined properly the optimization parameters and their ranges. For this reason a refinement of them is suggested.
- A numerical integration for the low-acceleration trajectory is required to check the results coming from the analytical model adopted here.

- The inclinations of the initial and final orbits should be considered in the low-acceleration model in order to understand how expansive the correcting manoeuvres would be.

REFERENCES

- Ad Astra Rocket Company website, *Vasimr Advantages*,
<http://www.adastrarocket.com/Advantages.html>, Last accessed: November 25, 2008
- Astronautix website, *RD-0126E performances*, <http://www.astronautix.com/engines/rd0126.htm#RD-0126>, 2008, Last accessed: November 25, 2008
- Baker J. D. and Eichstadt F., *Commercial Cargo Transport Service for ISS*,
Acta Astronautica, Vol. 57, Issue 2-8, pages 257 – 265, 2005
- Battin R.H., An Introduction to the Mathematics and Methods of Astrodynamics, second edition, American Institute of Aeronautics and Astronautics, New York, USA, 1987
- BBC website, *Bush Proposal to Send Man to Mars*, <http://news.bbc.co.uk/2/hi/science/nature/3381531.stm>, Last accessed: November 25, 2009
- Belbruno E. A. and Carrico J. P., *Calculation of Weak Stability Boundary Ballistic Lunar Transfer Trajectories*, AIAA/AAS Astrodynamics and Specialist Conference, Denver (Colorado), 14-17 August 2000
- Bering III E., Longmier B., Glover T., Chang-Diaz F., Suire J. and Brukardt M.,
High Power Electric Propulsion Using The VASIMRTM VX-200: A Flight Technology Prototype, abstract from 50th Annual Meeting of the Division of Plasma Physics Dallas, Texas, <http://www.aps.org/meetings/unit/dpp/index.cfm>, November 20, 2008
- Betts J. T. and Erb S., *Optimal Low Thrust Trajectories to the Moon*, Siam Journal Applied Dynamical Systems, Vol. 2, No 2, Pages 144-170, 2003
- Camino O., Alonso M., Gestal D., de Bruin J., Rathsmann P., Kugelberge J., Bodine P., Rickenc S., Blakeb R., Voss P. P. and Stagnaro L., *SMART-1 operations experience and lessons learnt*, *Acta Astronautica*, 2007
- Canalias E. and Masdemont J. J., *Computing natural transfers between Sun–Earth and Earth–Moon Lissajous libration point orbits*, *Acta Astronautica* Vol 63, Issues 1-4, Pages 238-248, July-August 2008
- Coello C. A. C., Pulido G. T. and Lechuga M. S., *Handling multiple objectives with particle swarm optimization*, *Evolutionary Computation, IEEE Transactions on*, Volume 8, Issue 3, Pages 256- 279, 2004
- Cornelisse J. W., Schoyer H. F. R. and Wakker K. F., *Rocket Propulsion and Spaceflight Dynamics*, Pitman, London, 1979

- Correa, Gómez G. and Stuchi T. J., *Transfer Orbits Guided by the Unstable/Stable Manifolds of the Lagrangian Points*, Congreso Brasileño de Dinamica Orbital, 2004.
- Discovery Science website, *Water Found on the Moon*, <http://dsc.discovery.com/news/2009/09/23/moon-water.html>, Last accessed : November 25, 2009
- Donahue B.B., Caplin G.N., Smith D.B., Behrens J. and Maulsby, *Lunar lander concepts for human exploration*, Journal of spacecraft and rockets, Vol 45, Num 2, 2008
- EADS Astrium website, *Rendez-Vous in Space : ATV Jules Verne reaches its destination*, <http://www.astrium.eads.net/en/press-center/press-releases/2008/Rendez-Vous-Space-ATV-Jules-Verne-ISS-international-space-station>, Last accessed: October 14, 2009
- ESA Technical Note, STA 3BM: *TEC-ECM-TUD-VVD-0902*, 3BM Verification & Validation Document, 2009a
- ESA Technical Note, *STA Interplanetary Module: TEC-ECM-BN-SDD-0801*, Interplanetary Module Software Design Document, 2009b
- ESA Technical Note, *STA Interplanetary Low-Thrust Module: TEC-ECM--ADD-0801*, Interplanetary Module Software Design Document, 2009c
- ESA User's Manual, *Vega User's Manual*, ArianeSpace, 2006
- Gooding R.H., *A procedure for the solution of Lambert's orbital boundary value problem*, Celestial Mechanics and Dynamical Astronomy 48, pp. 145–165, January 1990.
- Hamera K. E., Mosher T., Gefreh M., Paul R., Slavkin L. and Trojan J., *An Evolvable Lunar Communication and Navigation Constellation Architecture*, AIAA 2008-5480, 2008
- Herman A. L. and Conway B. A., *Optimal, Low-Thrust, Earth-Moon Orbit Transfer*, Journal of Guidance Control and Dynamics, Vol. 21, No. 1, 1998
- Howell K. C., *Three Dimensional Periodic Halo Orbits in the Restricted Three-Body Problem*, Ph.D. dissertation, Stanford University, 1983
- Howell K. C. and Kakoi M., *Transfers between the Earth–Moon and Sun–Earth systems using manifolds and transit orbits*, Acta Astronautica, 2006
- Isakowitz S. J., Hopkins J. B. and Hopkins J. P. Jr., *International ReferenceGuide to Space Launch Systems*, American Institute of Aeronautics and Astronautics (AIAA), Washington DC, 2004
- Izzo D., *Lambert's Problem for Exponential Sinusoids*, Journal of Guidance Control and Dynamics, Vol. 29, No. 5, 2006
- JAXA website, *International Space Station*, http://www.jaxa.jp/projects/iss_human/iss/index_e.html, Last accessed: October 14, 2009
- JPL robotics: <http://www-robotics.jpl.nasa.gov/index.cfm>. Last accessed: November 29, 2008.

Koon W.S., Lo M. W., Marsden J. E. and Ross S. D., *Dynamical Systems, the Three-Body Problem and Space Mission Design*, 2006

Koon W. S., Martin W., Lo M. W., Marsden J. E., Ross S. D., *Shoot the Moon*, AAS/AIAA Astrodynamics Specialist Conference, 2000

Kumar K., *Weak Capture and Weak Stability Boundary*, MSc Thesis, TU Delft, 2008

Loucks M., Carrico J., Carrico T. and Deiterich C., *A Comparison Of Lunar Landing Trajectory Strategies Using Numerical Simulations*, International Lunar Conference, Toronto, CA, 2005

Lunar and Planetary Institute, Lunar Mission Summaries, 2008,
<http://www.lpi.usra.edu/lunar/missions/> Last accessed: October 22, 2008

Manzella D., Jankovsky R. and Hofer R., *Laboratory Model 50 KW Hall Thruster*, NASA/TM—2002-211887, 38th Joint Propulsion Conference and Exhibit cosponsored by the AIAA, ASME, SAE, and ASEE, 2002

Miller J. K., *Targeting an Optimal Lunar Transfer Trajectory Using Ballistic Capture*, JPL Technical Report, 1992

Montenbruck O. and Gill E., *Satellite Orbits*, Springer, 2005

MSU Polar Phisyscs website, Preparing for our second transit of Mercury,
<http://solar.physics.montana.edu/nuggets/1999/991112/991112.html>
Last accessed: December 16, 2009

NASA, International Space Station, 2008, http://www.nasa.gov/mission_pages/station/structure/isstodate.html, Last accessed: December 16, 2008

NASA, *Apollo 11*, 2004, http://history.nasa.gov/SP-4029/Apollo_11a_Summary.htm,
Last accessed: November 20, 2008

NASA, *Lunar Prospector*, 2001, <http://lunar.arc.nasa.gov/>, Last accessed: October 22, 2008

NASA Study, *Exploration Systems Architecture Study*, pp. 1-752, 2005

NASA/GSFC, *Hiten*, <http://nssdc.gsfc.nasa.gov/nmc/masterCatalog.do?sc=1990-007A>, 2008
Last accessed: October 22, 2008

O'Neill M. J., *Advances In Color-Mixing Lens/Multi-Junction Cell (CML/MJC) Concentrators for Space and Ground Power*, 4th International Conference on Solar Concentrators (ICSC-4), 2007

O'Neill M. J., Howell J., Fikes J., Fork R., Phillips D., Aiken D. and McDanal A.J., *Stretched Lens Array (SLA) for Collection and Conversion of Infrared Laser Light:45% Efficiency Demonstrated for Near-Term 800 W/kg Space Power System*, Presented at the 4th World Conference on Photovoltaic Energy Conversion, Waikoloa, Hawaii, May 7-12, 2006

- O'Neill M. J., *1,000 W/kg Solar Concentrator Arrays for Far-Term Space Missions*, AIP Conference Proceedings, Vol. 699, pp. 875-882, 2004
- Ortega G., *STA Mission for a Moon Base*, ESA-ESTEC, 2008
- Parker J. S., *Family of Low-Energy Lunar Halo Transfer*, Advances in the Astronautical Sciences, AAS 06-132, 2006
- Parker J. S. and Lo M. W., *Shoot the Moon 3D*, Advances in the Astronautical Sciences, AAS 05-383, 2006
- Petropoulos A.E., Longuski J. M. and Vinh N. X., *Shape-Based Analytic Representations of Low-Thrust Trajectories for Gravity-Assist Applications*, AAS Paper 99-337, Aug. 1999.
- Relativity Calculator website, *Kepler 1st Law*, http://www.relativitycalculator.com/Kepler_1st_Law.shtml, Last accessed: 26 October, 2009a
- Roberts C. E., *The SOHO Mission L1 Halo Orbit Recovery From the Attitude Control Anomalies of 1998*, Libration Point Orbits and Applications Conference, Parador d'Aiguablava, Girona, Spain, 10–14 June 2002
- Roberts M., *Inflatable habitation for the lunar base*, 2nd Conference on lunar bases and space activities, pages 249-253, 1998
- Rocket and Space Technology website, *Orbital Mechanics*, <http://www.braeunig.us/space/orbmech.htm>, Last accessed: 27 November, 2009
- Russell R. P., *Global Search for Planar and Three-Dimensional Periodic Orbits near Europa*, AAS 05-290, 2006
- Russianspaceweb, *A complete chronology of ISS missions*, http://www.russianspaceweb.com/iss_chronology_flights.html, Last accessed: 26 November, 2009
- Schouten G., The Space Trajectory Analysis tool and the development of its interplanetary module, Master's thesis, Delft University of Technology, Faculty of Aerospace Engineering, October 2006.
- Srinivas N. and Deb K., *Multiojective Optimization Using Nondominated Sorting in Genetic Algorithms*, Evolutionary Computation, MIT Press, 1994
- Sutherland T., Cunio P. and Khan Z., *ATA-01-1003 – Lunar Telescope Facility*, IDAC3 Results Presentation to the CxAWG, MIT, July, 2007
- Sutton G. P. and Biblarz O., *Rocket Propulsion Elements*, A Wiley-Interscience Publication, John Wiley & Sons Inc., 2001
- Tallgeorge website, *A Visual History of NASA's Project Constellation*, <http://www.tallgeorge.com/projectconstellation.php>, Last accessed: October 14, 2009

Uesugi k., *Results of the Muses-A “Hiten” Mission*, Advances in Space Research, 1996

Univ. of Oregon, Lecture 15, <http://abyss.uoregon.edu/~js/space/lectures/lec15.html>,
2008-10-22, Last accessed: October 22, 2008

Vasile M., Schütze O., Junge O., Radice G. and Dellnitz M., *Spiral Trajectories in Global Optimisation of Interplanetary and Orbital Transfers*, ESA Final Report, 2006

Vallado D. A. and McClain W. D., *Fundamentals of Astrodynamics and Applications*, 2001

Wakker K. F., *Astrodynamic I*, Delft University of Technology, 2007a. Faculty of Aerospace Engineering, Lecture notes AE4-874

Wakker K. F., *Astrodynamic II*, Delft University of Technology, 2007b. Faculty of Aerospace Engineering, Lecture notes AE4-874

Wertz J. R., *Mission Geometry: Orbit and Constellation Design and Management*, Kluwer Academic Publishers, 2001

Wiesel W. E., *Spaceflight Dynamics*, McGraw-Hill, New York, 1989

Wikipedia website, *Hohmann Transfer*, http://en.wikipedia.org/wiki/Hohmann_transfer_orbit,
Last accessed: October 26, 2009a

Wikipedia website, *Moon*, <http://en.wikipedia.org/wiki/Moon>, Last accessed: November 03, 2009b

Wikipedia website, *Rotation Matrix*, http://en.wikipedia.org/wiki/Rotation_matrix,
Last accessed: November 06, 2009c

Wikipedia website, *Sphere of Influence*, http://en.wikipedia.org/wiki/Sphere_of_influence_%28astrodynamics%29, Last accessed: November 26, 2009d

Wikipedia website, *Variable specific impulse magnetoplasma rocket*,
http://en.wikipedia.org/wiki/Variable_specific_impulse_magnetoplasma_rocket,
Last accessed: 25 November, 2008

Woytach J. M., Zakrajsek J. F., Oswald F. B., McEntire K. J., Hill G. M., Abel P.,
Eichenberg D. J., Goodnight T. W., Zakrajsek J. J. and McKissock D. B.,
Exploration rover concepts and development challenges, NASA. Glenn Technical Reports Server, 2005

Zuccarelli V., *Earth-Moon Transfer Orbits*, Literature study, TU Delft, December 2008